STRUCTURAL ENGINEERING ASPECTS

OF PRESTRESSED CONCRETE REACTOR VESSELS

by

Bruce Ira Goldman

BS, Swarthmore College

(1973)

Submitted in partial fulfillment of
the requirements for the degree of
Master of Science in Civil Engineering

at the

Massachusetts Institute of Technology

(May, 1975)

Signature of Author .....
Department of Civil Engineering, May 9, 1975

Certified by .....
Thesis Supervisor

Accepted by .....
Chairman, Departmental Committee on Graduate
Students of the Department of Civil Engineering

ABSTRACT

STRUCTURAL ENGINEERING ASPECTS OF

PRESTRESSED CONCRETE REACTOR VESSELS

by

BRUCE IRA GOLDMAN

Submitted to the Department of Civil Engineering on May 9,1975

in partial fulfillment of the requirements for the degree of Master

of Science in Civil Engineering.

The utilization of prestressed concrete pressure vessels for high temperature gas cooled reactors has developed rapidly during the last ten years. In this study, we first review the evolution in vessel geometries and enumerate the advantages and disadvantages of concrete vessels. Attention is then directed at methods of analysis. Mathematical models for linear elastic analysis, visco-elastic material models for creep analysis, and nonlinear models for ultimate analysis are reviewed, and comparisons for actual vessels and scale models are presented. Material models for concrete and steel nonlinearities, and nonlinear finite element solution techniques are also described.

Finally, a three dimensional nonlinear finite element analysis for an actual vessel is presented. The assumptions made in constructing a model for the vessel and the loading strategy are discussed in depth. Also, results showing the cracking patterns and the influence of temperature induced creep are included.

Thesis Supervisor: Jerome J. Connor

Title: Professor of Civil Engineering

Acknowledgements

I wish to express my deepest gratitude to Professor J.J. Connor for all his guidance and assistance. Also, special thanks to Y. Sarne for all his aid; C. Reeves of Stone & Webster Engineering Corporation for his support of the Engineering Residency Program which made this work possible; W. Pananos and J. Roberts for their contributions, and A. Hunter for her patience in typing this manuscript.

TABLE OF CONTENTS

INTRODUCTION

The high temperature gas cooled reactor is the latest development in the production of electricity from nuclear energy. Its many advantages over light water reactors, and the fact that more advanced types such as the liquid metal fast breeder reactor and the gas cooled fast reactor are many years off, make it the probable workhorse of the near future.

Today, several experimental stations have been built throughout the world, and have been operating for several years. Larger prototype plants have been built at Fort St. Vrain in Colorado, U.S.A., and at Schmehausen, Germany. The Fort St. Vrain reactor became critical on January 31, 1974. (ref. 45) The plant is capable of producing 330 MWe. The German plant is rated at 300 MWe and is scheduled to become critical in May, 1975.

Today, larger commercial reactors capable of producing over 1000 MWe are being designed, and will be producing electricity by the next decade.

Four basic features of the high temperature gas reactor are:

1) The helium coolant

2) The graphite core

3) The carbon coated fuel particles

4) The prestressed concrete reactor vessel.

To the structural engineer, the last is the most interesting. The complicated states of stress and the nonlinear properties of the materials used make analysis of the pressure vessel extremely difficult. It has

become necessary for the engineer to develop mathematical modeling techniques capable of giving acceptable results. These analytical tools include finite difference, dynamic relaxation, and finite element methods.

The latter is generally recognized as the most convenient technique for analyzing complex structures. (ref. 55). Today, the finite element method is capable of analyzing the three dimensional states of stress, and modeling the nonlinear material properties which are found in prestressed concrete vessels.

In Chapter One, the development of the use of concrete pressure vessels for gas cooled reactors is presented, and the advantages and disadvantages of the high temperature gas cooled reactor and its prestressed concrete pressure vessels are given.

In Chapter Two, the analysis of concrete pressure vessels is reviewed. This is done in three parts:

1) Elastic Analysis

2) Analysis for Time Effects

3) Ultimate Analysis.

Methods used in the past are given, and the present state of the art is described.

The finite element method is presented in Chapter Three. Nonlinear solution techniques, and material modeling of concrete and steel properties beyond the elastic range are presented.

Finally, an analysis of the prestressed concrete reactor vessel for the General Atomic 1160 MWe reactor using the nonlinear finite element method is shown. Finite element models, assumptions, and results are given.

Chapter 1

The High Temperature Gas Reactor and Its Concrete Pressure Vessel

1.1 Introduction

The future trend to very large reactor unit sizes because of economic considerations is limited by technological difficulties present in the construction of steel pressure vessels. (ref. 33) Prestressed concrete vessels, however, overcome those problems, and their use for nuclear reactors is expanding. Today, designs are being made for concrete pressure vessels for light water and fast breeder reactors.

The development of concrete pressure vessels closely follows that of the gas cooled reactor. Limitations imposed upon the outlet gas temperature by the carbon dioxide coolant and Magnox cladding of the earlier reactors were overcome by the use of helium as a coolant, a graphite moderator, and non-metallic fuel particle coatings.

The new high temperature reactor uses fuel particles which consist of a uranium-thorium mixture coated with carbon. The particles, 200M-400M inches in diameter, are embedded in graphite fuel elements. (ref. 47)

In this chapter, the development of the gas reactor and its pressure vessel is presented. It is followed by a description of the advantages and disadvantages of the high temperature gas reactor and the prestressed concrete pressure vessel.

1.2 Development of High Temperature Gas Reactors

The basic concept of the high temperature gas reactor (HTGR) first

emerged in the early fifties, with its development beginning independently in Great Britain, France, the United States, and Germany by the early sixties.

The first generation of experimental gas cooled reactors began with the 20 MWe Dragon reactor in the United Kingdom. Others included the 30 MWe reactor at Marcoule, France, the 15 MWe AVR station in Germany, and the Peach Bottom 40 MWe plant in the United States. (ref. 19) All had steel pressure vessels housing the reactor, with the AVR having the heat exchangers inside the vessel.

The move to concrete pressure vessels began in France. At the nuclear power plants EDF3 and EDF4, a concrete vessel was substituted for the steel vessel.

The next step in the development of prestressed concrete reactor vessels (PCRV) came in the United Kingdom where use of PCRV's led to the use of integral design. The integral design concept includes the whole gas pressure circuit of reactor core, heat exchangers and gas circulators within the single vessel. Three power plants were designed and built using integral design. In all of them, carbon dioxide is used as a coolant. Also, the heat exchangers, and the gas circulator penetrations which pass through the lower part of the vessels, are arranged radially around the reactor.

The first plant completed was the Oldbury Power Station (ref. 9) with a total output of 600 MWe from its two reactors. It has a cylindrical pressure vessel housing each of the reactors which use uranium fuel cans. The internal dimensions are 77 feet in diameter by 60 feet in height. The prestressing system consists of a helical arrangement at 45° in the walls

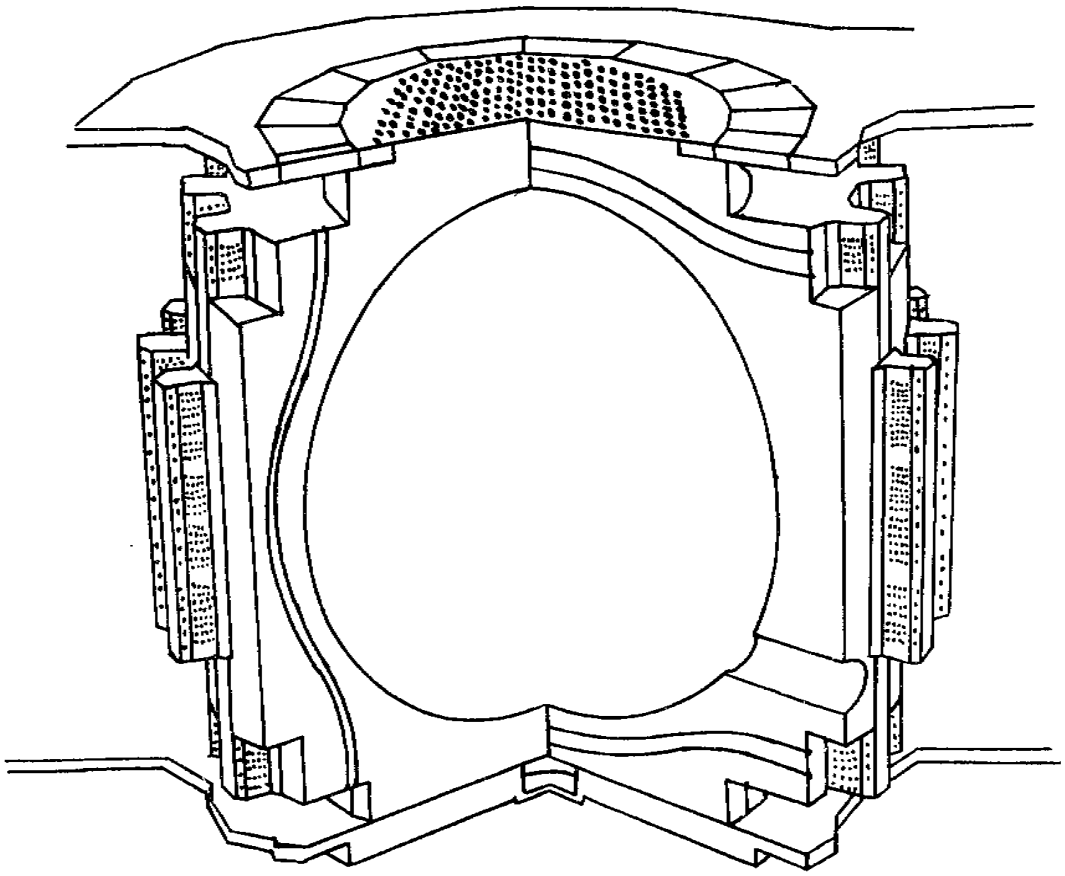

WYLFA PRESSURE VESSEL

FIG. 1.1

and horizontal tendons in the top and bottom heads.

The 1180 MWe Wylfa power station (ref. 61) has two identical spherical pressure vessels with cylindrical external shapes. (figure 1.1) The internal diameter is 96 feet. Like the Oldbury power plant,Magnox fuel is used. The prestressing system consists of tendons which pass horizontally through the top and bottom of the vessel, and vertically through the sides. Also horizontal tendons are arranged around the sides, and anchored in ribs which extend out from the vessel. It should be noted that construction of this spherical vessel had considerable problems, and none have been designed since.

The cylindrical vessels for the two reactors of the 1200 MWe Dungeness B power station (ref. 64) were the first designed for the advanced gas reactor (AGR). The fuel used is uranium oxide in a stainless steel casing which permits higher temperatures. Thus, less heat exchanger surface area is needed, and a smaller pressure vessel is possible. The cylindrical vessels have internal dimensions of 65.5 feet in diameter by 58 feet in height. The prestressing system consists of vertical tendons which extend the height of the vessels, and horizontal tendons which run in a tight curve which just misses the standpipe region. This is necessary because the close spacing of the standpipes does not permit cables to be placed across the top head.

The French integral design vessels for St. Laurent II, Bugey I, and Fessenheim I power stations (ref. 38) use an alternative cylindrical design with the heat exchangers below the reactors (figure 1.2). All the reactors use a uranium fuel with a carbon dioxide coolant. The internal dimensions of the Bugey I vessel are 56 feet in diameter and 125.5 feet

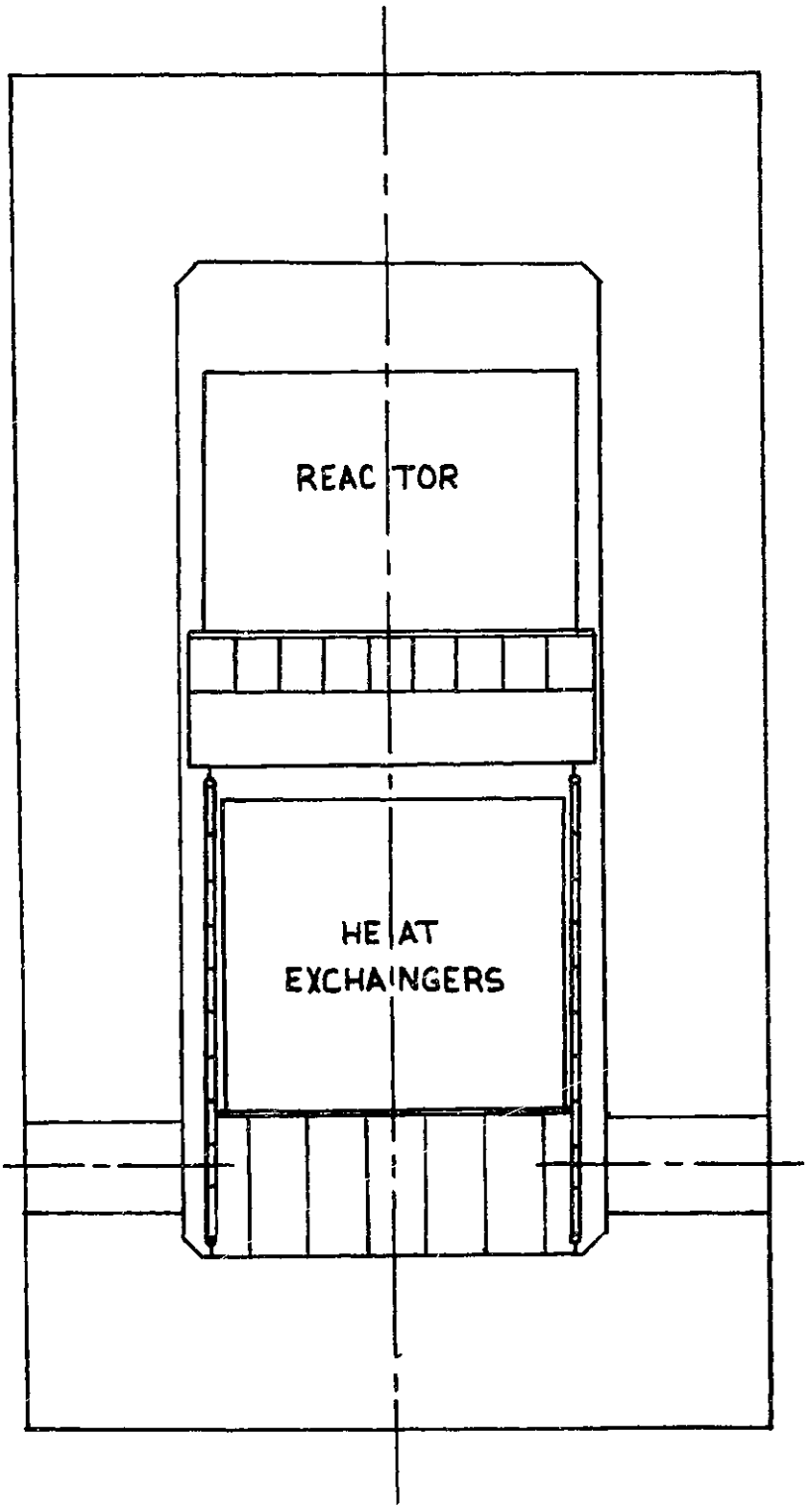

BUGEY 1 POWER STATION

Fig. 1.2

in height. The horizontal prestressing consists of 2200 hoop tendons, each traversing two thirds of a circle. The vertical prestressing system consists of 1300 cables.

A major drawback of these integral design systems is the need of the large heat exchangers for in-place maintenance and repair. Because of this, adequate working space and shielding from the core increase the internal size of the vessel.

Further developments led to the reduction of heat exchange surface areas to 1/10. (ref. 33) This permitted putting the heat exchangers in the side walls of the concrete pressure vessels.

Design of such a vessel is used for the Hartlepool nuclear power station. (ref. 40) The vessel has eight heat exchangers in the wall connected to the reactor cavity by cross ducts. (figure 1.3) This permits removal of the heat exchangers for necessary work.

In the United States, the development has been aimed at using a completely ceramic core and helium as a coolant. After the initial experimental plant built at Peach Bottom, a larger 300 MWe prototype was built at Fort St. Vrain. It was the first in the United States to use a PCRV, and was built using an integral design with the reactor above the steam generators. It uses graphite fuel elements with uranium-TH dicarbide fuel particles with pyrolytic-carbon and silicon-carbide coatings. (ref. 45) The concrete vessel has internal dimensions of 31 feet diameter by 75 feet height.

The final step in the development of HTGR's and PCRV's in the United States is the commercial 1160 MWe reactor. (ref. 8, 45, 60) It has six steam generators and three auxiliary heat exchangers housed in the

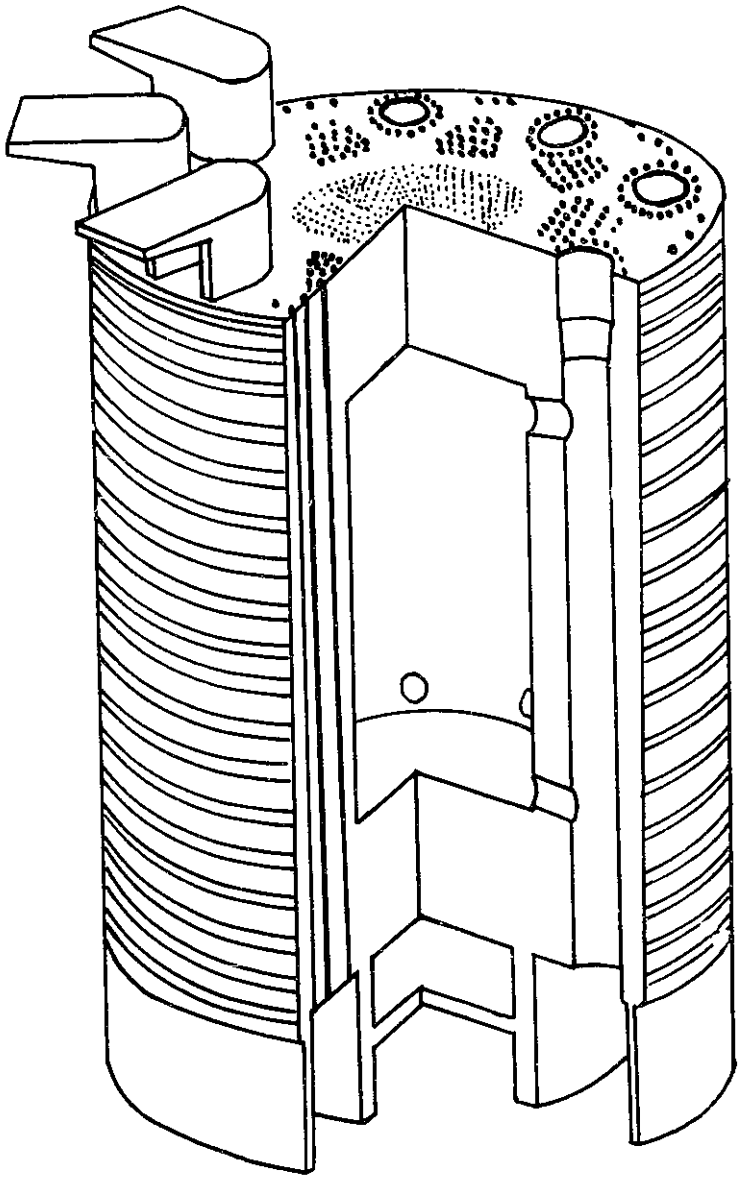

THE HARTLEPOOL PRESSURE VESSEL

FIG. 1.3

vessel walls. (figure 1.4) The reactor cavity is 37 feet in diameter by 44 feet high. The prestressing system consists of vertical tendons passing through the height of the vessel and a circumferential system of wire wound around the outside of the vessel.

The initial experimental plant in Germany led to the design of a 300 MWe THTR plant scheduled to go critical in May, 1975. An outstanding feature of this plant, and the 15 MWe AVR power station is the pebble bed reactor. In this reactor, the fuel, absorber, and moderator spheres are continuously injected into the core, and checked upon leaving for damage and burnup. The THTR uses an integral design with the heat exchanger an annular arrangement around the reactor.

The future sees further advances in the use of HTGR's and their PCRV's. These include the single circuit gas turbine system, gas cooled fast breeder reactors, and process heat plants. (ref. 19)

Interest by other energy consumers in the high temperature heat gives rise to uses of the HTGR other than to produce electricity. These include coal gasification, tar sands recovery, and steelmaking.(ref. 45)

The move towards gas-cooled fast breeder reactors with their higher working pressures has made the use of PCRV's almost a necessity. A concrete vessel can be made more secure from fast depressurization than any steel system of vessels and pipes through the use of multiple strength measures and closures.

1.3 Advantages and Disadvantages of the HTGR and the PCRV

The reason for the rapid development of the HTGR is its many advantages over the pressurized water and boiling water reactors. The higher reactor coolant outlet temperature makes it possible to link the

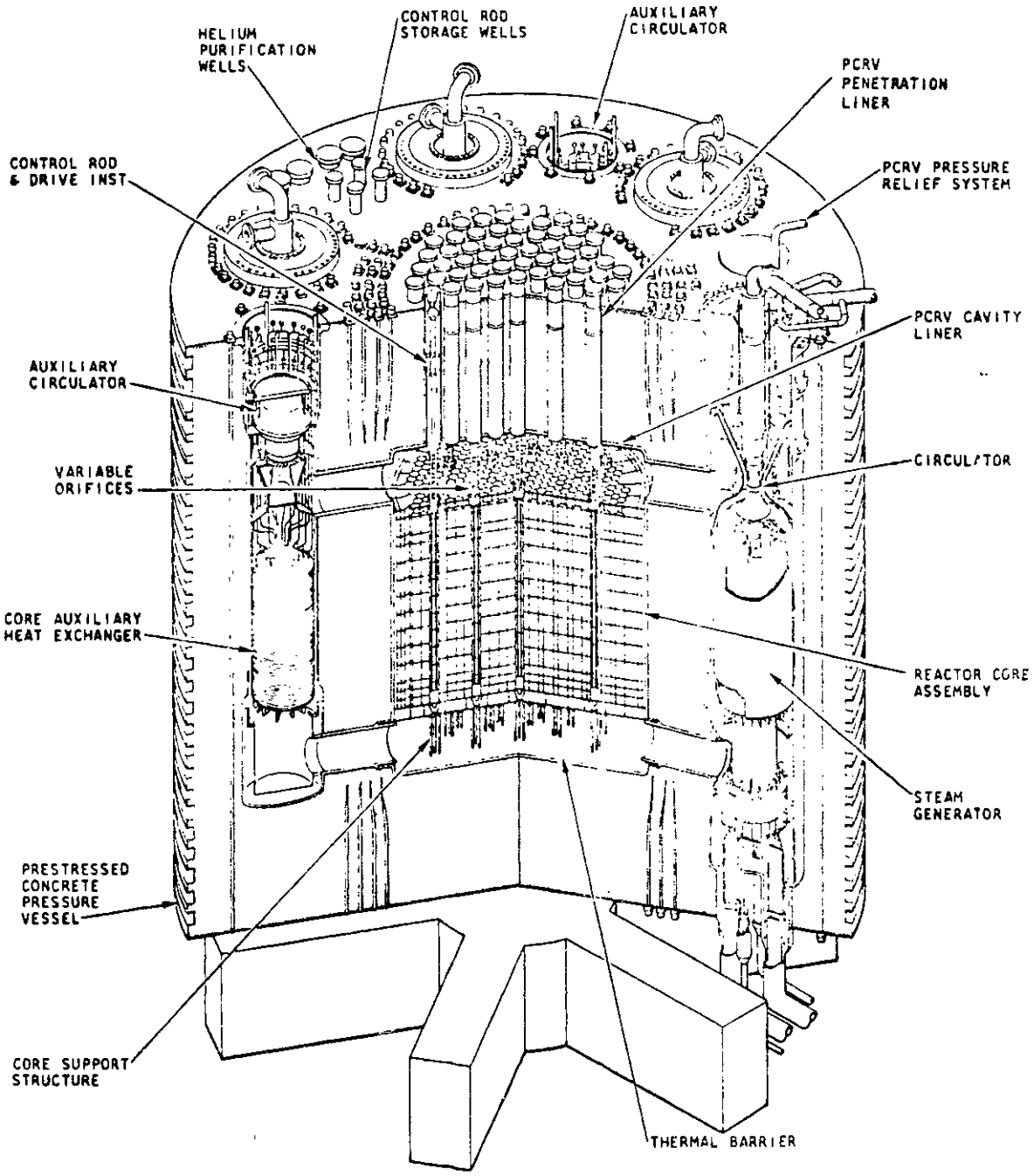

Fig. 1.4
PRESTRESSED CONCRETE REACTOR VESSEL
1160 MWe

HTGR with conventional non-nuclear energy conversion cycles. Higher temperatures also permit higher thermal conversion efficiency. For the HTGR it is about 39% vs about 32% for the other reactors. As a result, less waste heat is discharged into the environment, less make up water is necessary, and smaller cooling towers or cooling ponds are required.

The use of a graphite core structure and moderator also adds several advantages. These include high specific heat, excellent thermal conductivity, low neutron capture, and a negative coefficient of reactivity at all temperatures of interest. Also, all metal is removed from the core, and is replaced by the graphite which has excellent high temperature strength.

The helium coolant, being a gas to start, undergoes no phase change. Thus a catastrophic loss-of-coolant accident is a physical impossibility. Circulation of helium at atmospheric pressure is sufficient to remove the radioactive decay heat given off by the core during shutdown periods. (ref. 27) Helium, because it is inert, minimizes the possibility of corrosion of equipment. Also, it absorbs essentially no neutrons and has zero reactivity.

The advantages of the concrete pressure vessel are also manifold. The multiplicity of prestressing tendons makes the vessel immune to catastrophic failure. The integral design makes it unnecessary for radioactive gases to pass outside the vessel, eliminating the need for piping and possible accidents. The vessel is field erected, and the concrete walls give sufficient biological shielding to permit ready access to the reactor containment building.

Because the vessel is under large compressive forces after pre-

stressing, the load during its life history is not of a cyclic nature. This eliminates the fatigue problems which are present in steel vessels.

There are also several disadvantages to the HTGR. One major item is the high initial cost associated with it. The reactor and boiler plant costs for the HTGR comprise 45% of the total cost versus 32% for the light water reactor. (ref. 47) Also, the possibility of the entry of steam or water into the primary coolant system from the failure of a boiler tube would permit graphite corrosion to take place.

1.4 Conclusion

The rapid development of gas cooled reactors since the original work began in the 1950's has produced the multicavity, or podded boiler pressure vessel of today. The use of new materials for the coolant,fuel, and core made the increase in operating temperatures possible. The prestressed concrete pressure vessel helped overcome the problems of large steel vessels, adding to the many advantages of the high temperature gas cooled reactor. In the chapters that follow, the analysis of the concrete pressure vessels is reviewed, and results presented.

Chapter II

Analysis of Concrete Pressure Vessels

2.1 Introduction

The pressure vessel of a high temperature gas cooled reactor is a massive concrete structure which must satisfy three design requirements. First, it must remain elastic for all possible loads during the operational life. Second, it must have an ultimate load capacity, or margin of safety, to account for possible overload conditions, and third, it must have a gradual mode of failure.

These three conditions are best represented by a load-deformation curve for the radial deflection of the side wall due to internal pressure. (figure 2.1) In phase I the vessel has an elastic behavior. There is no cracking of concrete, and no steel components have yielded. In phase II, cracks gradually develop and widen until phase III begins. At this point the structure can be considered to act as a mechanism. The structure is broken up into sections which can rotate about the concrete hinges formed by cracks extending through the side wall or head thickness.

Traditionally, the final analysis of the pressure vessel is done in two steps, elastic and ultimate analysis. Because of the complex geometry, mathematical modeling techniques are used to perform the elastic analysis for pressure and temperature loads, and time effects, or creep, of concrete. The ultimate strength was initially determined by assuming failure mechanisms, but development of mathematical material models for concrete cracking and liner yielding criteria, and the advance of

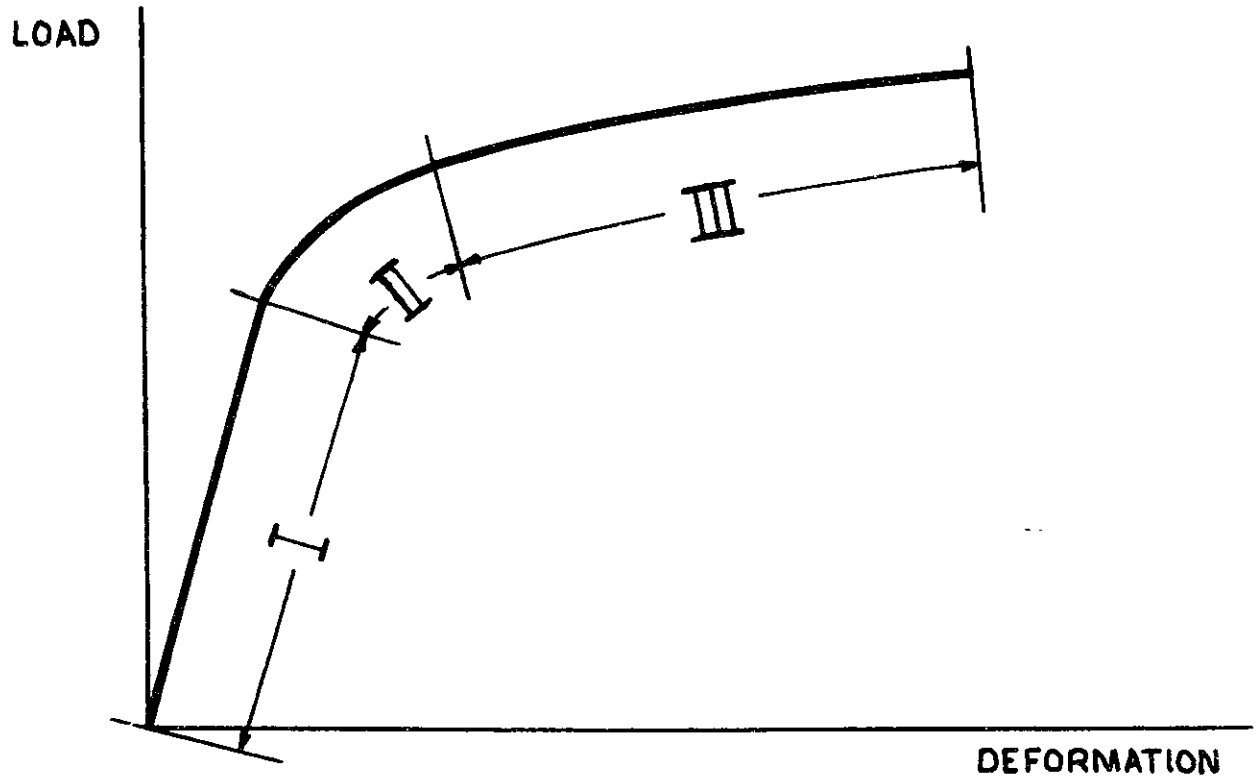

FIG. 2.1

LOAD-DEFORMATION CURVE
RADIAL DEFLECTION OF SIDE WALL

computer capabilities have made it possible to use the same mathematical methods to determine the vessel's margin of safety.

In the sections that follow, the elastic and ultimate load analysis methods are reviewed. Results are compared to measurements from actual vessel and model tests performed throughout the world. The effect of loading of concrete for a sustained period is described, along with the mathematical models used to represent this creep behavior. Analysis results are presented which illustrate the importance of considering time effects when performing the elastic analysis.

2.2 Elastic Analysis

The analysis procedure must be capable of simulating the vessel's deflections, stresses, and strains for all loading conditions. Physical assumptions made for the elastic analysis include linear strain-displacement relations, and linear stress-strain relations. It is necessary that these assumptions hold for all expected loading conditions during the operational life of the vessel. These loading cases include prestressing, proof pressure tests, and operating loads, with time effects included. The procedure must be able to model not only material and geometric properties, but loading and boundary conditions as well.

The development of the analysis of pressure vessels has closely followed that of mathematical modeling methods and computer capabilities. Earlier methods included finite difference and dynamic relaxation techniques for axisymmetric structures. Because of the inclusion of penetrations in the side wall of the vessel, a three dimensional analysis has become necessary. The finite element procedure has been generally accepted as the most powerful method to perform this analysis. (ref. 69)

One of the first vessels designed and built was the Oldbury #1 vessel. It has a cylindrical shape, and the analysis used an axisymmetric finite difference solution of the equilibrium equations. Prestress forces were applied as smeared body forces, with frictional losses applied where the cable contacted the tendon ducts. A comparison with measured results taken during prestressing and the proof pressure test showed good correlation between predicted and measured values. Reasons for error included differential thermal strains, and the fact that the prestressing operation took nine months to complete.

Two important results were found from the test on the actual vessel. Firstly, the vessel remained elastic during the proof pressure test, and secondly, no significant shrinkage occurred. The first was shown when gauges returned to their original values after the pressure test, and the second, by moisture content readings which revealed no reduction of concrete moisture six inches inside the surface three years after construction was completed. (ref. 20)

An axisymmetric finite element analysis modeling the top half of the vessel also showed good correlation. (ref. 43) This analysis used a reduced Young's modulus for the standpipe region, but comparisons to other analytical results showed that a reduction of stiffness of the top head to 80 or 90% of the original for vessels with widely spaced standpipes is not necessary. This is not true for the advanced gas reactors where standpipes are closer spaced, and the stiffness might be 50% or lower of that of the main vessel.

The spherical vessels for the Wylfa power station were first analyzed by dividing the vessel into a series of ring elements. (ref. 30)

Flexibility coefficients were then calculated for forces acting on each element, and the elements were allowed to deflect independently of one another. The equations of compatibility for the elements were then solved simultaneously.

A second analysis was made later using dynamic relaxation. (ref. 15) The analysis for the axisymmetric structure was performed using cartesian and polar coordinates, and a plane stress analysis was used for the equatorial region where the circulator penetrations are located. Comparisons with results measured from the vessel during prestressing, proof pressure test, and commissioning were acceptable, except in regions of stress concentrations. These include the standpipe and penetration areas. Possible reasons for discrepancies between measured and predicted results are the accuracy of measurement techniques, limitation of analysis in describing geometry and loadings, and material modeling in the analysis.

The effect of creep was analyzed using an effective modulus for a given load condition, with the results superimposed on the elastic analysis. Creep will be discussed later, along with mathematical techniques for modeling its behavior.

The Dungeness B vessel was also considered a body of revolution, and analyzed by finite difference. (ref. 62) The effect of creep on thermal stresses was found using a reduced modulus, though the rate of creep method could have better represented the sequence of loads during the design life. However, a practical analytical method was not available at the time and the reduced modulus method was used.

With the development of podded boiler vessels, two-dimensional techniques were no longer acceptable. For the final analysis, the three-

dimensional finite element method became the most widely used. Dynamic relaxation is still used for preliminary design checks, such as for the Hartlepool vessel, where plane stress and strain, and three dimensional analyses were performed using this method. (ref.40)

The use of the finite element method for the analysis of prestressed concrete pressure vessels has become an established procedure. An axisymmetric analysis of pressure vessels has been presented by Rashid (ref. 52) in 1965, and the need for three dimensional applications to predict stresses close to large penetrations is well known. One earlier problem which has been overcome is the cost of solution with available computer hardware. With increased computer capabilities, three dimensional analysis, the prediction of creep behavior, and non-linear material modeling have become possible. Creep and non-linear effects will be discussed later.

Finite Element developments applicable to the analysis of prestressed concrete pressure vessels have been the modeling of steel components which include the vessel liner, bonded reinforcing,and prestress tendons (ref. 53,69), and the introduction of iso-parametric finite elements.

The use of higher order elements has made it possible to increase the accuracy of the results for a given number of degrees of freedom. (ref. 69) Iso-parametric elements permit better representation of the structure's geometry because the same shape function which is used to describe the element displacements is used to define the element geometry. A comparison made by Carmichael (ref. 16) showed that a relatively coarse grid of 41 elements (figure 2.2) gave good results compared to a much finer grid

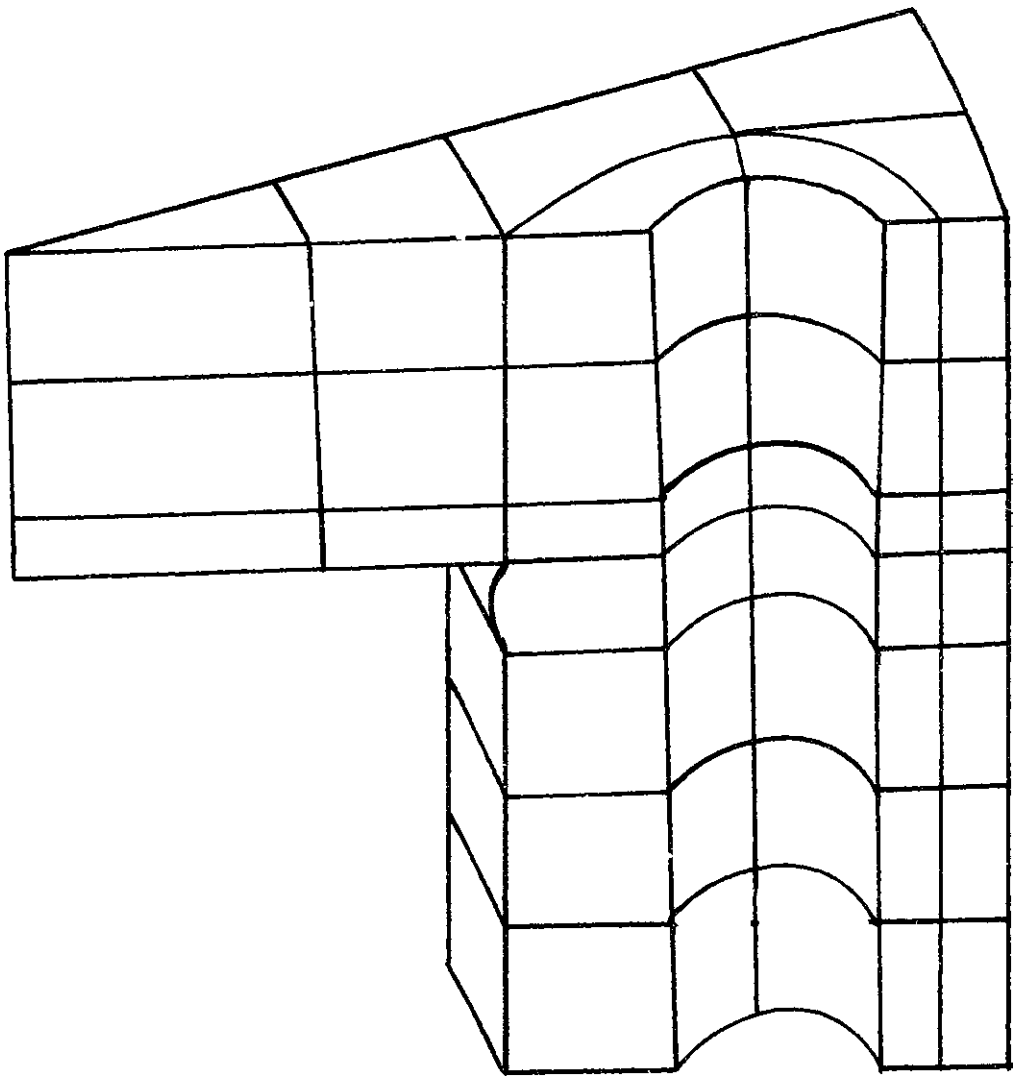

CARMICHAEL 41 ELEMENT MODEL

FIG. 2.2

of 177 elements. Results were compared to predicted values of a 1/10 scale model of the Hartlepool vessel. Analysis of time effects was considered unnecessary as test loads were short in duration and no temperature load was applied. Creep strains were considered insignificant compared to elastic strains. Because of the close spacing of standpipes in the top head, a reduced modulus of 69% was used. Measured and predicted deflections and strains agreed closely.

Other three dimensional finite element elastic analyses (ref. 3, 63) also showed good correlation. These were performed for a 1/10 scale model of the Hinckley Point B power station pressure vessel, and a 1/20 scale model test. For both cases, the vessel was found to be elastic up to the design pressure by comparing results of the tests and the analyses, and for the 1/10 scale model, by cycling of the design pressure load.

The design requirement of elastic behavior has been demonstrated to be reasonable by analysis techniques, model tests, and data available from actual vessels. Accuracy between measured and calculated data will increase with the improvement of material behavior knowledge and modeling. It is in this area that the elastic analysis must look for further improvement.

2.3 Creep

Consideration of the effect of time on non-uniform stress distributions through a concrete pressure vessel has now become the major analysis problem. The phenomenon of creep in concrete is not yet totally explained and can cause considerable damage to the vessel if not properly accounted for.

The problem is illustrated by looking at the effect of time on

the vertical stress distribution through the wall due to a slight warming of the vessel. Figure 2.4 shows the stress distribution caused by the variable temperature distribution shown in figure 2.3. Figure 2.4 also shows the new stress distribution after 75 days. The cooling of the pressure vessel can cause cracks at the inner face of the wall due to the stress reversal.

There are several theories which attempt to explain creep. (ref. 46) These include:

1) Plastic theories which suggest that creep is caused by the slippage of planes within the crystal lattice;
2) Viscous flow theories which maintain concrete consists of two parts: cementitious material and aggregate. When the concrete is loaded, the aggregate becomes more stressed while the stress on the cement decreases with time;
3) Seepage theories, or loss of water from the cement gel.

At stresses below about 40% of ultimate strength, creep is considered to be linear with respect to compressive stress.(ref. 5,11,55) Seepage and viscous flow are some of the mechanisms involved. At higher stresses, where the relationship becomes non-linear, plastic theories contribute.

Material properties affecting the magnitude of creep include moisture content, aggregates, cement, and mixture ratios. (ref. 34) Physical properties include age, temperature and dimensions.

Because of the large number of factors affecting creep, it is impossible to make a mathematical model which accounts for all of them. Material properties can be included by varying fixed parameters in the creep

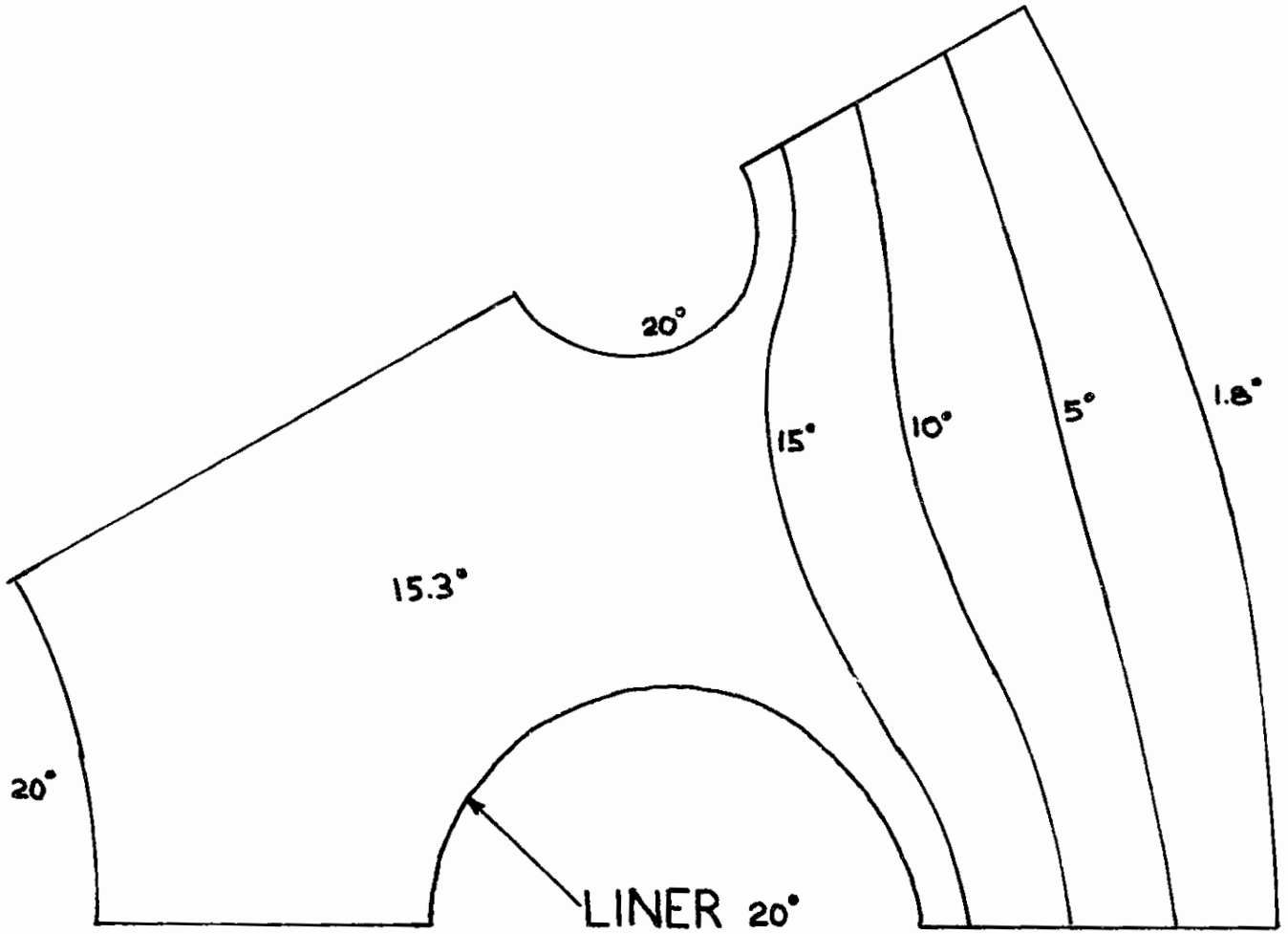

FIG. 2.3

TEMPERATURE DISTRIBUTION °F

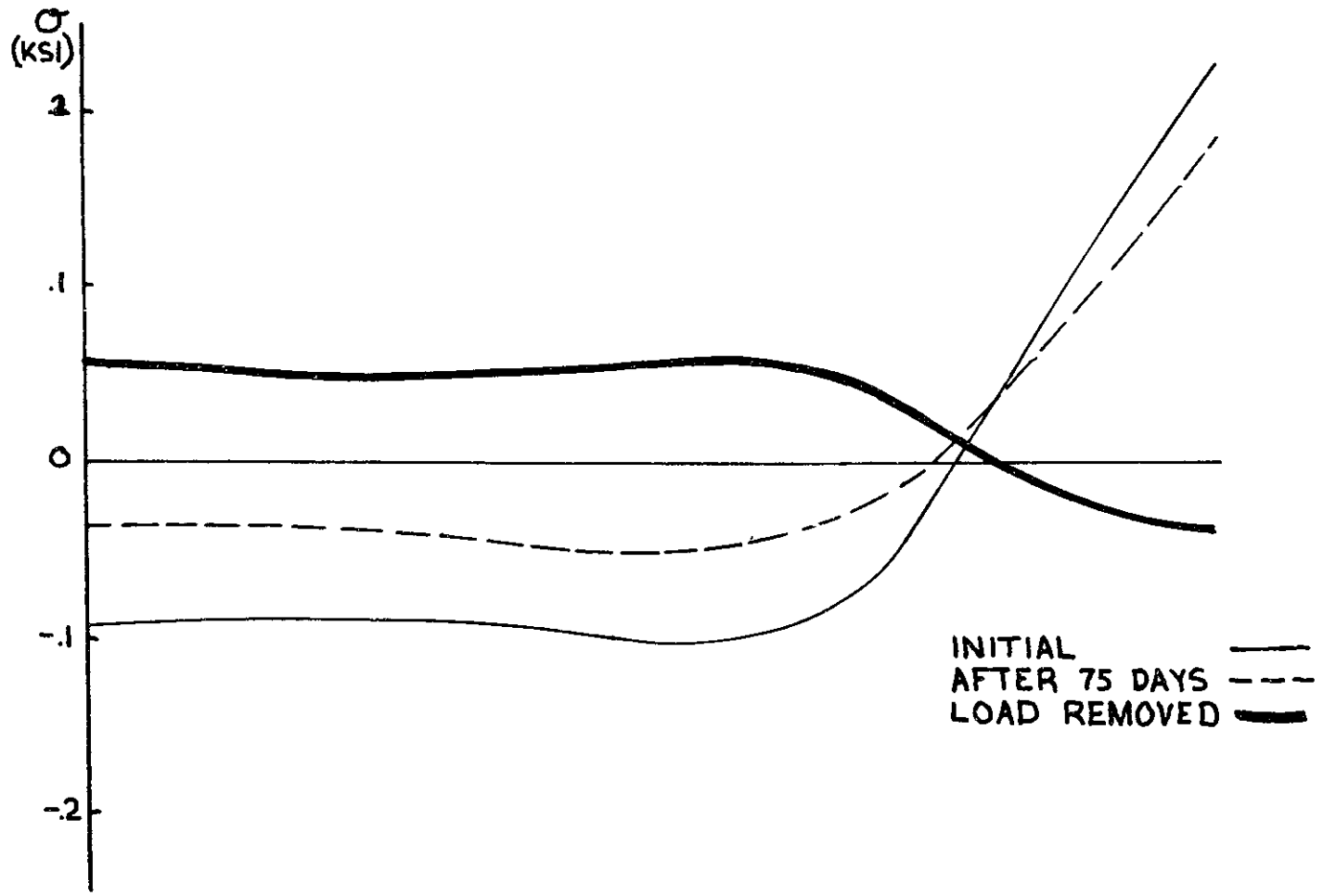

FIG. 2.4

STRESS DISTRIBUTION

equation to fit results from the laboratory. Time, age, and temperature, whose effect on creep strain is non-linear (ref. 5), should be kept as variables.

The effect of temperature on creep was extensively studied by Hannah. (ref. 28) In the tests performed, the temperature of the concrete was varied from 27°C to 93°C under several loading conditions. Results showed that the creep strain varied linearly up to 77°C, and non-linearly above that point. The creep at 77°C was about 4.5 times that at 23°C. Though no relationships can be concluded, it is obvious that the effect of temperature must be determined in the laboratory for the particular concrete to be used.

The response of concrete at a given instant is a function of the load history. For stress values less than approximately 50% of the ultimate strength, linear viscoelastic material models adequately predict creep behavior. (ref. 5) This model is represented by a physical system consisting of a number of springs and dashpots arranged in suitable combinations. (ref. 68)

The two basic arrangements are a spring and a dashpot in series or parallel. (ref. 49) The first is known as the Maxwell element, and the latter, as the Voigt-Kelvin element. (fig. 2.7) All linear viscoelatic models are made up of one or more of these elements.

The Maxwell element, which represents stress relaxation under constant initial strain (fig. 2.8), was described by Lewis et. al. (ref. 43) It was shown to give good agreement with results measured from the Oldbury vessel. Errors included overestimation of strains occurring between prestressing and first start up, and underestimation during normal operation.

MAXWELL ELEMENT

$$\frac{\partial \varepsilon}{\partial t} = \frac{\partial \sigma}{\partial t}\cdot\frac{1}{E} + \frac{1}{\eta}\sigma$$

$$\sigma = Ae^{-(E/\eta)t}$$

KELVIN ELEMENT

$$\sigma = E\varepsilon + \eta\frac{\partial \varepsilon}{\partial t}$$

$$\varepsilon = (1-e^{-(E/\eta)t})\frac{\sigma_0}{E}$$

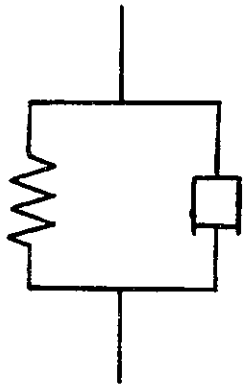

FIG. 2.7

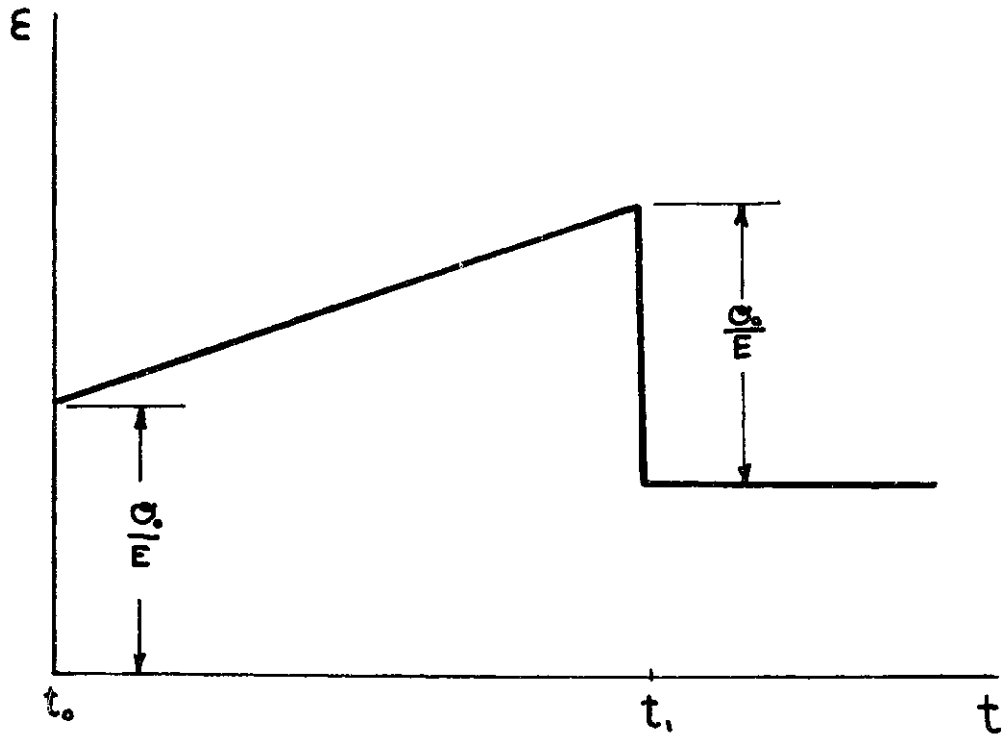

RESPONSE OF MAXWELL ELEMENT TO σ_0 APPLIED AT t_0 AND REMOVED AT t_1

FIG. 2.8

This was attributed mostly to the fact that the prestress load was applied instantaneously in the analysis, thereby causing creep rates to be higher.

Most creep strains were shown to occur early in the vessel's life, prior to start up, and most stress changes that do occur are caused by thermo-elastic strains. Stresses induced by internal straining will reduce to zero given enough time, while stresses due to mechanical loads will be redistributed. Results will be affected by the presence of non-creeping steel reinforcing, and the varying creep rates caused by non-uniform temperature distribution.

Maxwell models represent initial elastic response, plus permanent creep. They do not allow for creep recovery after load reversal. This can be a problem when analyzing a pressure vessel which has a cyclic load history caused by annual shut down for refueling. One possibility is to use a percentage of the instantaneous elastic strain for creep recovery (ref. 5), or a percentage of the creep strain. (ref. 55). Also, a linear function of time under load can be used to calculate the non-recoverable part, as suggested by the creep equation presented by Argyris et. al. (ref. 5)

The use of a series of Kelvin elements was described by Zienkiewicz et. al. (ref. 71) The creep equation is of the form:

$$\dot{\varepsilon}_c = a\sigma - b\varepsilon_c \qquad (2.1)$$

or, for several elements:

$$\Delta\varepsilon_c = \left[\sum_{i=1}^{n}(a_i\sigma - b_i\varepsilon_c^i)\right]\Delta t \qquad (2.2)$$

The degree of accuracy of the model depends on the number of elements used in series. Two elements have been suggested as being satisfactory. The number of elements is also dependent upon the available computer storage area.

The Kelvin element is a creep formulation which exhibits delayed elastic response, which, under a constant stress state, is totally recoverable when the load is removed. (ref. 49) (figure 2.9) It cannot be used to represent initial elastic response, but results can be added to that of an elastic analysis. Results using Kelvin elements have shown good correlations with those of other creep models.

A joint model which includes one Maxwell element in series with a number of Kelvin elements, or Burgess body, has been proposed by Argyris et. al. (ref. 5) Its equation is of the form:

$$\varepsilon(t) = \frac{\sigma(t)}{E(t,\tau)} + B_1^2 \int_0^t \Psi[T(\tau),t]\,\sigma(\tau)\,d\tau + \sum_{\alpha=2}^{n} B_\alpha^2 \int_0^t \Phi[T(t),\tau]\, e^{-C_\alpha[S(t)-S(\tau)]}\,\sigma(\tau)\,d\tau \qquad (2.3)$$

The first part corresponds to the instantaneous elastic response, the second to permanent flow, and the third term to delayed elastic strain which is recoverable. The equation includes functions of age and temperature in the expression. If delayed elasticity and permanent flow are affected by age and temperature in the same manner, then:

$$\Phi(T(t),\tau) = \Psi(T(\tau),t) \qquad (2.4)$$

This term can be expressed as the product of two functions:

$$\Phi = \Psi(T(t)) \times \Psi(T(t),\tau) \qquad (2.5)$$

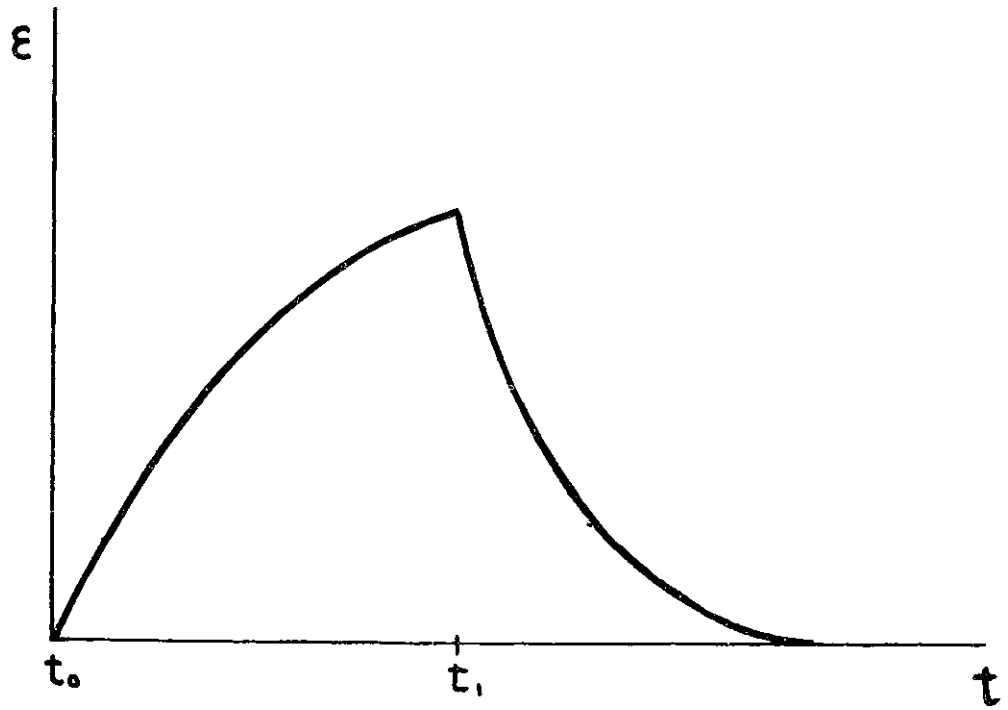

RESPONSE OF KELVIN ELEMENT

FIG. 2.9

one of which is dependent only on temperature. Φ cannot be expressed as the product of a function of temperature and a function of age.

A comparison of results to those from Wylfa concrete tests indicate satisfactory agreement during loading. However, these results only confirm the effectiveness of curve fitting to experimental data, not the creep law itself.

Several other linear equations have been presented to represent creep. These have been developed by experimentation, instead of by trying to explain creep as a viscoelastic material.

A study done by Lewis et. al. (ref. 42) in 1969 used a creep law proposed by Hanson of the form:

$$\varepsilon_t = \frac{\sigma}{E} + \sigma \cdot F(K) \log_e (1+t) \qquad (2.6)$$

where F(K) is a function of age and temperature. The study used a finite difference technique to solve for the stresses through the side wall due to temperature. The variation of temperature during shutdown and start up were included.

The study showed that the area at the inner face where tensile stresses are produced during shutdown could not be eliminated, but the area could be kept at a minimum by cutting off the flow of cooling water. An optimum time of cut off was placed at 5 hours after the beginning of the concrete temperature decrease. Also, there was little difference between thermal stresses with creep at one year and at 20 years.

An equation of this form was used to compare analytical results to measurements taken from the Oldbury pressure vessel. (ref. 20) The calculated strains illustrated the behavior of the vessel, and they gave an

upper bound to the measured values. When a load cycling was not considered, the change of internal stresses due to constant applied loads during the life of the vessel gave a lower bound.

Another creep equation which has been used is of the form:

$$\varepsilon_s = at^n \tag{2.7}$$

where ε_s is the specific creep strain with regard to stress, and a and n are functions of age and temperature. An equation of this sort was used in the analysis of the Wylfa pressure vessel. Acceptable correlation was achieved for stresses measured during the commissioning. (ref. 2)

A slightly different equation used by Greenbaum and Rubenstein (ref. 25) was

$$\varepsilon_c = a\sigma^b t^c \tag{2.8}$$

where a, b, and c are constants. Results were compared to closed form solutions, and showed good agreement. A study comparing stress values of thick-walled pressure vessels with 3 types of end closures (spherical, elliptical, and flat-end) loaded under internal pressure was presented. Results showed that initial high stress concentrations at the corners of the flat-ended vessel will redistribute and be greatly reduced due to creep.

B. Saugy (ref. 58) performed a nonlinear analysis of a podded-boiler pressure vessel using a creep equation of the form:

$$\varepsilon = \varepsilon_i(1 + a(t-\tau)^n) \tag{2.9}$$

where a and n are functions of temperature and age, and ε_i is the strain for the present loading. The analysis was performed by the finite element

method, but did not incorporate steel elements (liner, reinforcing). The additional stiffness was added to the concrete in the analysis. Results showed that creep redistributed stresses caused by an internal pressure, aiding the integrity of the vessel up to a value of about 1.5 times the design pressure, with a reverse effect above this level. This was due to the redistribution of stresses which tended to load the structure uniformly, causing a rupture condition to be reached simultaneously in relatively large regions. It should be pointed out that the analysis did not converge above a value of 2.0 times the design pressure. The redistribution of stresses of most vessels should aid its integrity beyond a value of 1.5 times the design pressure as most vessels have a factor of safety higher than 2.0.

Several methods of numerical solution of the creep equation have been presented. (ref. 43) The steady-state stress solution will give a stationary state of stress which would be achieved after a long period of time, and results will be a bound to stresses in the vessel during operation. A drawback to this method is that in reality creep strains attained in the vessel during the operating life may not be large enough to permit stresses to approach a steady-state condition. The steady-state bound could lead to tensile values that are too high when assessing the stress reversal due to shutdown. This might cause adverse opinions of the acceptability of design, or lead to restrictions on the operating temperature. (ref. 32)

A more commonly used method is the effective modulus solution. Here, a modified Young's modulus is used to calculate the creep strains for a given stress:

$$\varepsilon_c = \frac{1}{E_{eff}} \cdot \sigma \qquad (2.10)$$

Zienkiewicz (ref. 10) gives $1/E_{EFF}$ as equal to:

$$\frac{1}{E(T)} + \int_0^t C(T,t,\tau)\frac{\partial}{\partial\tau}(\sigma)\,d\tau \qquad (2.11)$$

where: $C(T,t,\tau) = (1 - e^{a(t-\tau)})\frac{1}{E_1(T)}$

For a load applied for a long time:

$$\frac{1}{E} = \frac{1}{E_0(T)} + \frac{1}{E_1(T)} \qquad (2.12)$$

The effective modulus was used in the design of the Hartlepool pressure vessel with E equal to the inverse of the specific strain, and in the analysis of the Wylfa vessel.

This method has the advantage that only one elastic solution is necessary to calculate strains. Its disadvantage is that the assumption that stresses remain constant leads to an error when stress variations actually occur. Under pressure loads where stress changes are usually small, this method can give acceptable answers. However, for temperature loads where the stress changes can be more than 30% of the initial values. (ref. 50) the error will be greater. In an analysis which includes steel components, the error will increase.

An incremental procedure, or rate of creep method, has the advantage that boundary conditions, body forces, thermal strains, and material properties can change at each time increment. The solution technique assumes that for each time step, the change in stresses is small compared to the previous stresses. The steps used for solution are:

1) An elastic solution is obtained for the applied load.
2) Using the stresses from the elastic solution, the creep strains are calculated from the creep law.
3) These strains are then applied to the structure using equivalent body forces.
4) New displacements strains, and stresses are found.

Step 2 is then repeated using the new stress values. This method will not diverge if the incremental creep strains are less than the total elastic strains.

Two methods of accumulating creep strains are commonly used. (ref. 25) The time hardening law assumes the creep rate depends on the instantaneous stress and temperature, and the time from when the load was applied. The strain hardening law assumes the creep rate depends upon the instantaneous stress, temperature and accumulated creep strain. Both laws will give about the same results, but the strain hardening law will give slower relaxation of stresses.

For large deformation problems, the number of time steps necessary might make the rate of creep method impractical because of the number of time increments necessary. When working with this method, the allowable size of time increments should be studied. A typical study made for creep under load for 64 days is shown in figure 2.10. Assuming the maximum number of steps gives the most accurate solution, acceptable time increments where found. Notice that after the first initial days, time increments can increase at a rapid rate. Another disadvantage which must be considered is the large storage space needed to use this method.

The rate of creep approach was used by Stefanou et. al. (ref.59) to analyze perforated end caps. Results showed good correlation with measured data. A three dimensional nonlinear finite element analysis of a concrete pressure vessel presented by Sarne (ref. 55) using the rate of creep method showed the cracking caused by the unloading of temperature after an extended period.

Because of the changes of load which the pressure vessel is subjected

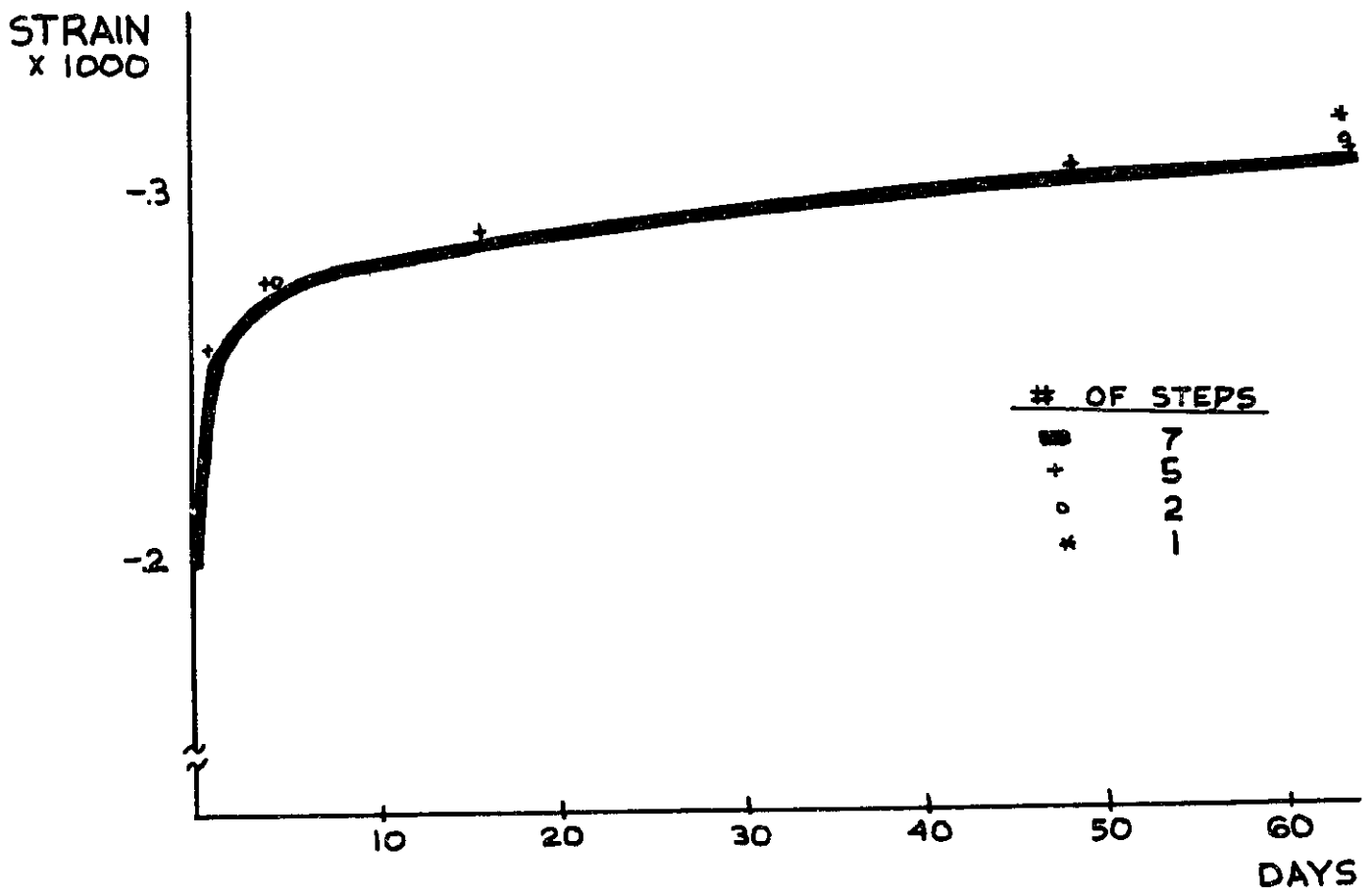

COMPARISON OF NUMBER OF CREEP STEPS

FIG. 2.10

to, the principle of superposition must be heavily relied upon. McHenry has developed a superposition law which provides reasonable prediction of strain variation with time, provided the concrete stress does not exceed about 50% of its ultimate strength.

The principle of superposition can best be described by an example. See figure 2.11. A load applied to a specimen at time t_1 will cause an initial stress, σ, and the creep curve A. A second load applied at t_2, also to an initial stress of σ, will cause creep curve B, different than A because of the effect of aging of the concrete. If a load is applied at t_1 causing the stress σ, and removed at t_2, the creep curve should be A - B. A similar principle for temperature superposition is reported by Brown et. al. (ref. 11)

The superposition model has a tendency to overestimate creep recovery, the average error being about 12%. (ref. 11) A major advantage is that once the creep under a load has been calculated to the point where additional calculations will give little change, there is no need to store the particular creep history. This method will only cause problems for short term loads with a duration of less than about 90 days. It is up to the analyst to determine if creep of the load removal will give under or over-conservative results. The problem could possibly be overcome by using a longer time under load for the initial load, or a shorter creep recovery of the load removal, with the assumption that any additional changes past this time for each load will offset each other.

A question that must also be answered is the use of superposition for old concrete where the change in age during loading will have little effect on the creep curve. Upon load removal, a similar creep curve may be generated, negating the original creep.

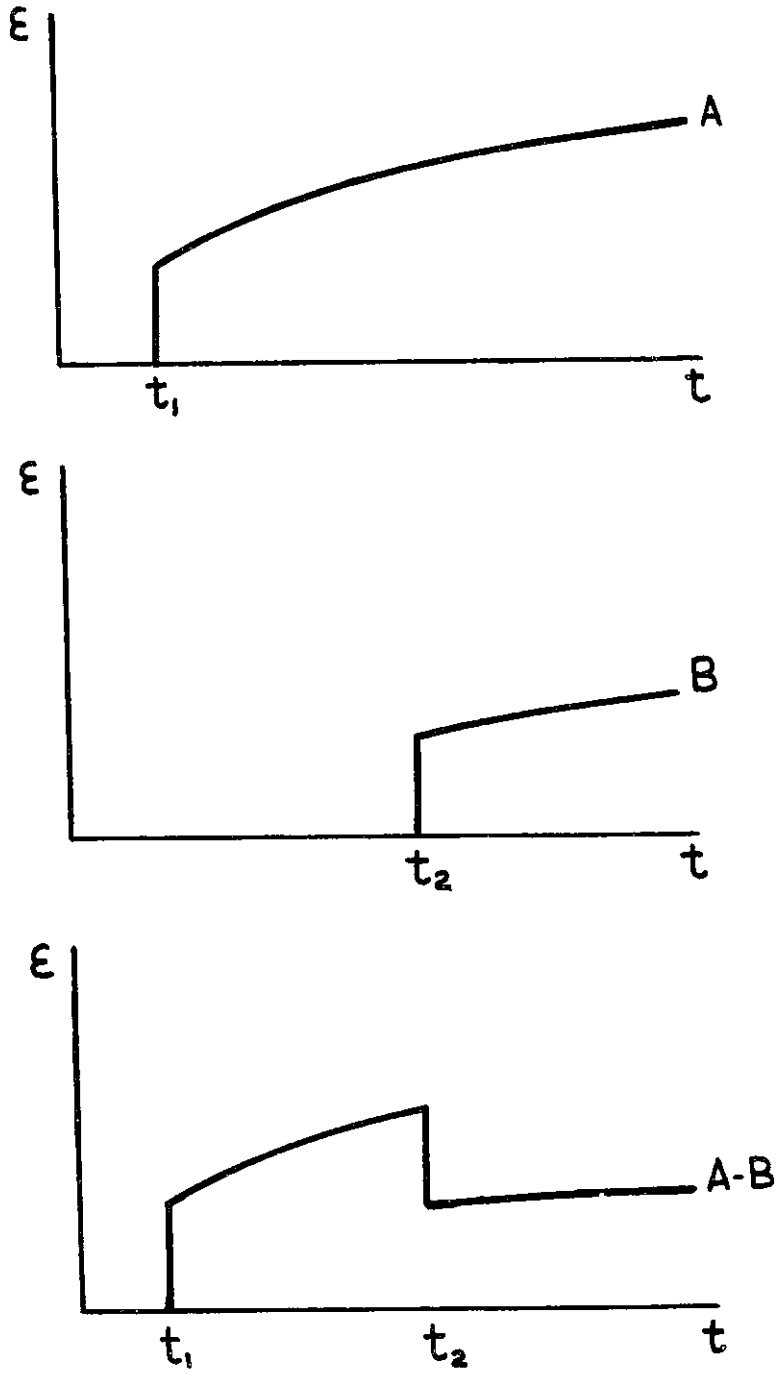

SUPERPOSITION OF CREEP

FIG. 2.11

All the preceding creep equations and solution methods have been for the uniaxial load case. With the complicated triaxial states of stress and strain in a prestressed concrete pressure vessel, there is a need to consider biaxial and triaxial creep states. This is done using a creep Poisson ratio which is generally taken as equal to the elastic value. (ref. 11, 55) Tests have shown (ref. 28) that it is possible to consider the value to remain constant throughout the life of the pressure vessel.

Triaxial creep is calculated by interrelating the triaxial principle stresses using Poisson's ratio in the creep equations:

$$\sigma = \sigma_i - \nu(\sigma_j + \sigma_k) \qquad (2.13)$$

The use of this method has been justified by comparisons with experimental results. A test performed by General Atomic (ref. 72) gave results for uniaxial and biaxial states of stress in the test specimen. A three dimensional finite element analysis using a creep equation fit to the uniaxial data shows a similar fit to the biaxial case. (fig.2.12)

The present creep theories and solution methods have been presented. The problems of creep analysis do not lie in explaining the physical phenomenon. This can be avoided by curve fitting of the creep equation curve by varying constant parameters to conform with test data.

It is important that the effects of age and temperature be included in the equation, and that they be accurately modeled. Thus, there is a need to perform extensive experimentation on the concrete to be used to construct the vessel so that an accurate creep formulation can be derived. The method of modeling creep recovery must also be extensively tested. The use of a creep equation with permanent and recoverable creep is

CREEP TEST

Fig. 2.12

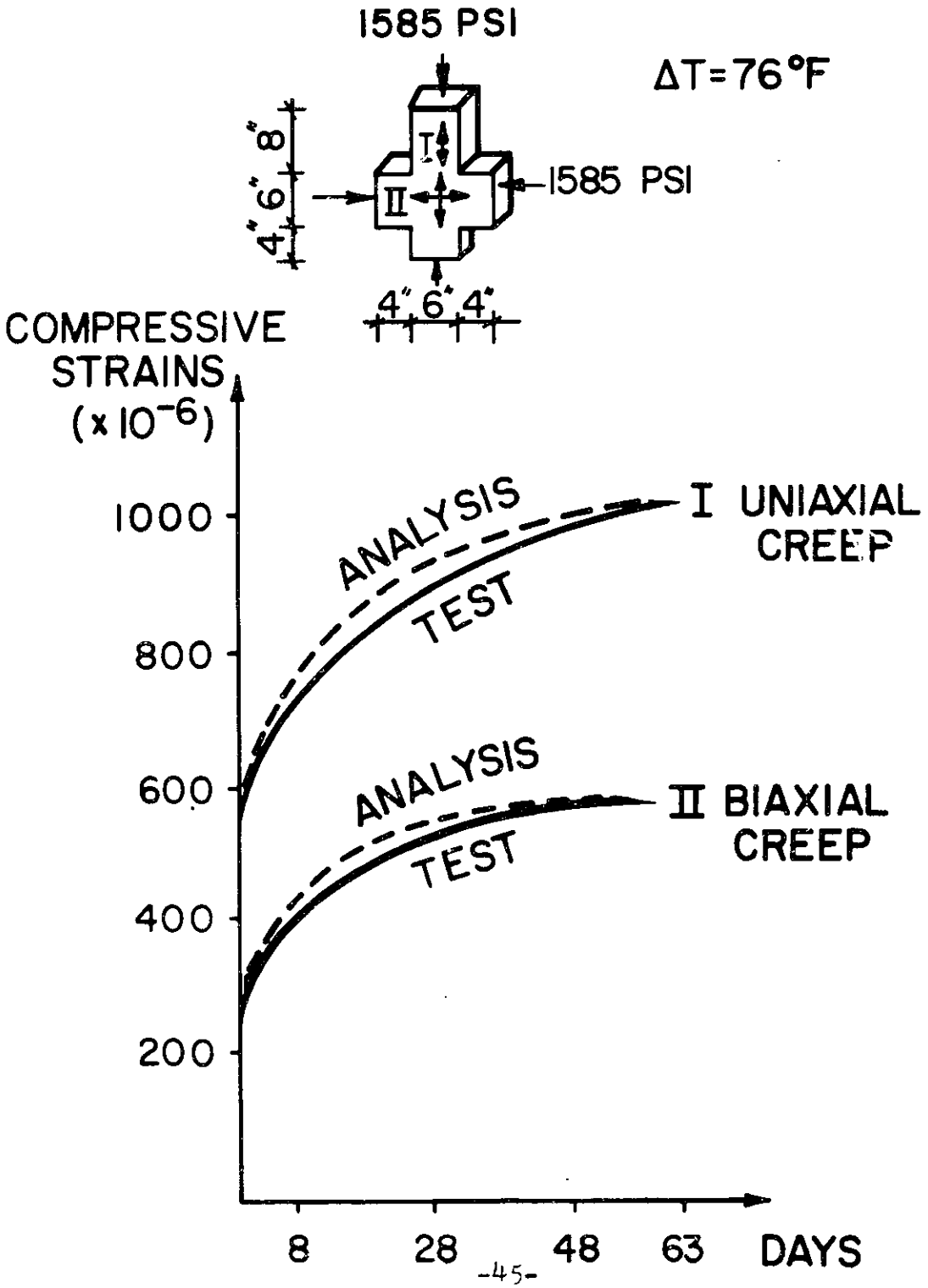

preferable if available computer storage permits memory of the extensive load history which the PCRV is subject to. The method of superposition is the simplest to adapt, but care must be taken to see that the effect of short term loading conditions which might exist during refueling can be accurately evaluated, and that errors using this method do not accumulate.

2.4 Ultimate Analysis

The structural safety of the pressure vessel depends upon its ability to maintain its load carrying capacity at load levels several times greater than the design pressure. It may be necessary, however, to limit the factor of safety in order to assure that the failure mechanism is an acceptable one.

The possible failure modes of a short thick-walled cylinder were presented by Haris et. al. (ref. 29) as being:

1) simple tension, either vertically in the walls or radially in the ends,

2) shear along a horizontal plane at the base of the head, combined with loss of circumferential prestress,

3) shear along the vertical surface where the ends meet the walls,

4) vertical bending failure at 3 hinges in the wall with circumferential prestress failure,

5) bending failure of the head with radial yield lines.

4 and 5 are the most attractive failure models,as extensive deformation preceeds rupture. Testing of pressure vessels and pressure vessel top heads has shown that failure of the side wall due to bending and failure of the top head due to either bending or shear are the only likely mechanisms.

Factors contributing to the strength of the end slab include the amount of bonded reinforcement, the presence of penetrations in the pressurized zone, penetrations in the barrel wall, concrete strength, level of hoop prestress, slab dimensions, and boundary conditions.

Circumferential prestress considerably increases the ultimate shear strength of the concrete. However, a level can be reached where additional prestress has a negligible effect on the shear strength. Also, a study (ref. 23) showed that applying the prestress over the entire depth of the top head increased the shear strength by only about 20% above specimens which have the prestress applied to the tensile zone only.

The inclusion of penetrations in the top head effects the angle of the shear plane. In all perforated end slab models the failure plane intersected the outer row of standpipes, and the ultimate pressure was reduced by 10%. The inclusion of shear connectors could, therefore, increase the ultimate strength of perforated pile caps.

One of the major factors which represents the failure mechanism of the top head is the span-to-depth ratio. Tests performed at the University of Illinois (ref. 44) on the top head showed a high rate of flexural failure. The specimens generally had relatively high span-to-depth ratios (3.3 to 5). In work performed by Langan and Garas (ref. 39) with lower ratios of less than 3, shear failure was the most prominent.

Flexural failure of the top head is characterized by cracking of the concrete in the corner between the end slab and side walls, and along radial lines in the outer face of the end slab. (figure 2.13) Wedge shaped sections which are formed rotate as rigid bodies about an axis near the outer edge of the vessel, at a level near the inside face of the

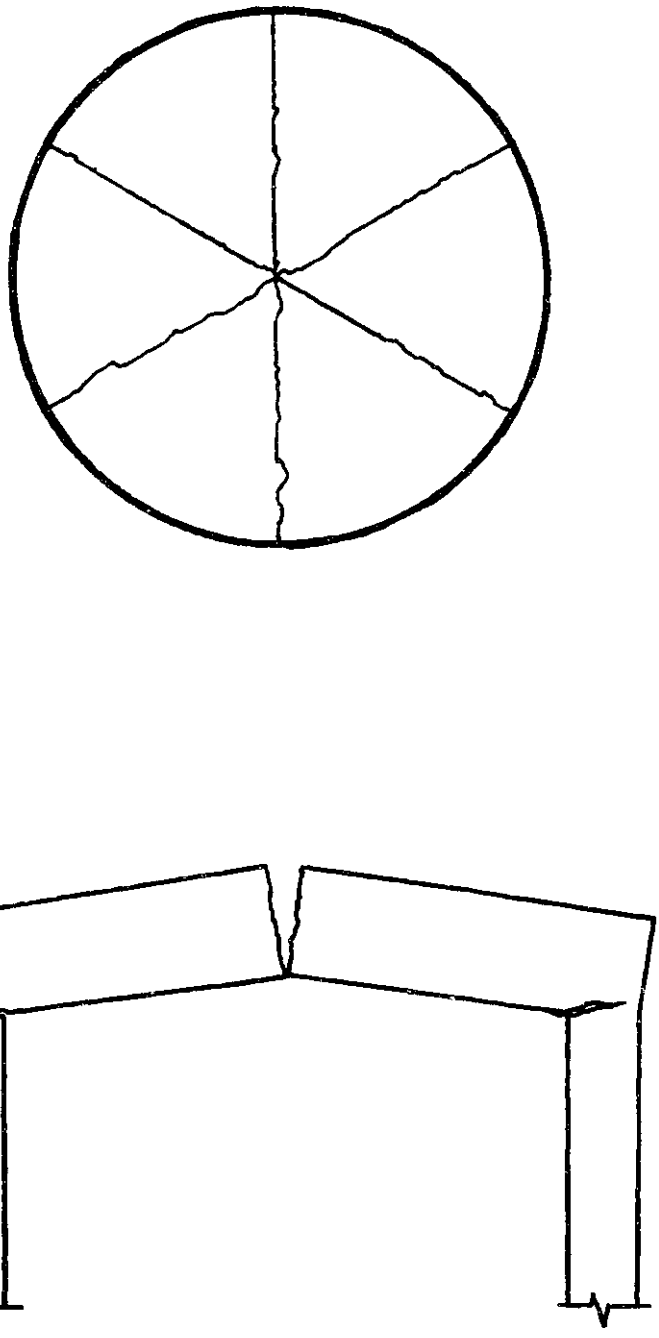

FLEXURAL FAILURE OF TOP HEAD

FIG. 2.13

slab. Failure is reached when circumferential prestressed wires break near the top of the end slab due to the rotation of the sections. Prior to failure, large deflections and surface cracks occur, giving adequate warning. However, failure occurs abruptly due to the fracture of prestressing wire.

Shear failure is represented by inclined cracks which extend from the anchorage plate to the inside of the center of the slab at about 45°. Cracks are first formed at the center of the head and then propagate in both directions. Failure occurs when the crack has extended through to the top of the head, followed by punchout of a center plug. (figure 2.14) When the crack extends downward, it will change direction until it is horizontal. As it progresses toward the center, it forms a dome which might prevent immediate failure. Shear failure will not neccessarily be brittle, depending upon what point it occurs in the flexural response of the slab.

Flexural failure of the sidewall (figure 2.15) starts with cracks extending outward from the sidewall-top head junction, and horizontal cracks at the midheight extending inward. Cracks continue to grow until hinge mechanisms are formed, and the sections act as rigid bodies. The concrete does not add any strength to the vessel at this point, and the pressure may be increased until the circumferential cables fail. Quite often there is a loss of pressure prior to this, caused by cracks in the liner at the corners.

Because of the nonlinear nature of the material properties of concrete and steel, ultimate analysis with a finite element method was not carried out for the early pressure vessels. To perform the analysis,

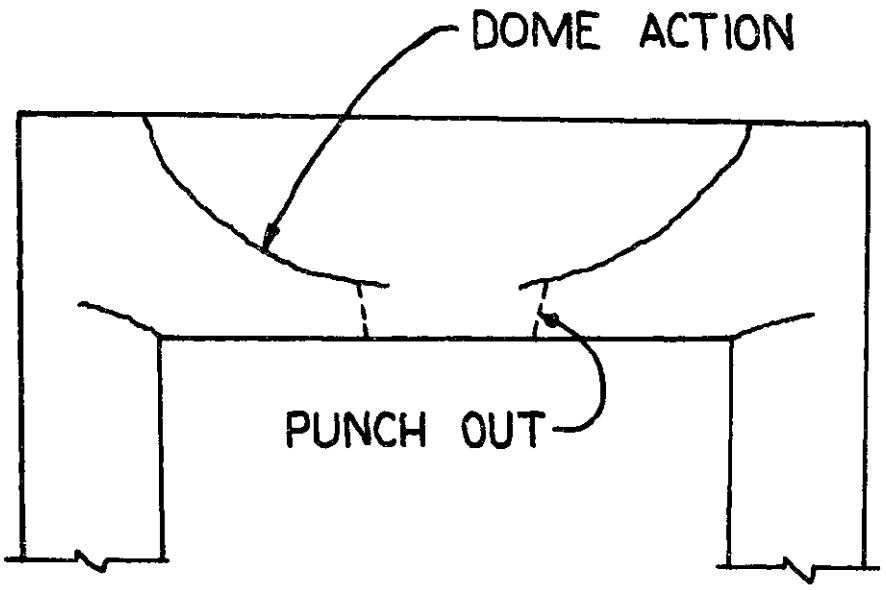

SHEAR FAILURE OF TOP HEAD

Fig. 2.14

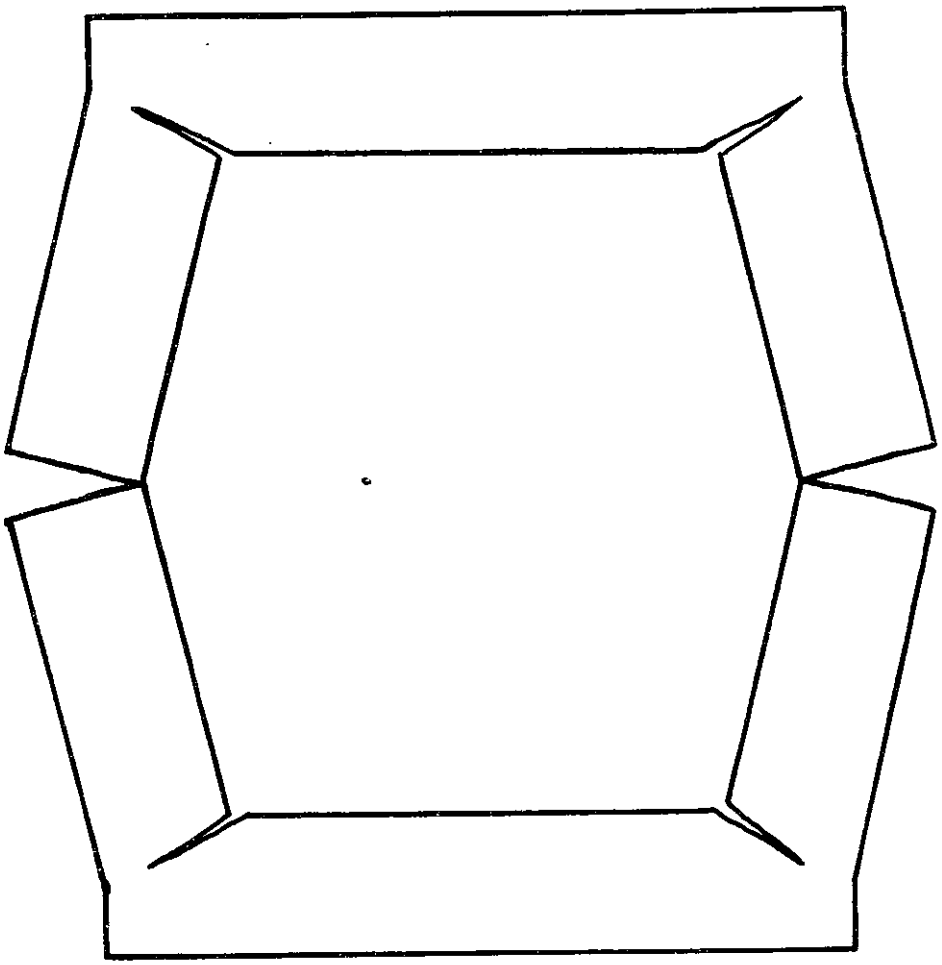

FLEXURAL FAILURE OF SIDEWALL

Fig. 2.15

failure mechanisms were assumed, and the rigid bodies analyzed to determine the minimum pressure.

In designing the Oldbury vessels, the tendon layout was selected such that a bending mode would prevail. Sections were analyzed by taking moments about the assumed hinge positions. The prestressing system used helical tendons, whose shape adds to the flexural strength of the walls.

The Wylfa vessel is spherical in shape, making it impractical to assume a traditional failure mode of a cylindrical vessel. In order to calculate the ultimate strength of the vessel several assumptions had to be made. These included: (1) The ultimate load is resisted by a membrane consisting of the three steel components. (2) The concrete does not contribute to the strength of the vessel, and the shear and bending resistance are ignored. (3) At failure, the prestressing tendons, the liner, and the bonded reinforcement all resist the load simultaneously, and all are at yield. To find the section of the vessel with the minimum ultimate load factor, the vessel was divided up into a number of ring elements. The safety factor for each ring can be determined, and the lowest value represents that of the vessel. The inclusion of an adequate percentage of bonded steel will insure a redistribution of stresses after cracking, allowing the inclusion of the liner strength in the ultimate load calculations.

The ultimate analysis of the Dungeness B vessel included analysis of the end cap for shear and flexure failure and of the sidewall for flexure. Analysis of the top head showed that the flexural failure was unlikely and that shear failure had a safety margin of 3.0 times the design pressure. An analysis of the walls using a membrane solution for an infinitely long cylinder gave a load factor of 2.5.

A similar method of analysis was used to calculate the ultimate strength of the Hartlepool pressure vessel. (ref. 40) It was assumed that a hinge was formed at the equator by the formation of a horizontal crack, and that a second crack forms near the corner. The distance of the height of the second crack above the equator was determined by finding the point at which equilibrium is satisfied by the minimum pressure. A comparison to test results from a 1/10 scale model showed the mode of failure was accurately represented by the analysis. An analysis to find the crack positions if 4 hinge points were formed resulted in verifying the assumption of only 2 hinge points.

A simplified method using the equilibrium equation of a sector of the top slab failing due to flexure was given by Paul (ref. 48) (see fig. 2.16)

$$\sigma_g = \frac{2F_h\left(aT - \frac{0.4F_h}{R_o f_{cu}}\right) + F_v D\,\frac{1-B}{\pi}}{R_i^2\left(R_o - \frac{2}{3}R_i - BD\right)} \qquad (2.14)$$

where:

F_h = the total force in the circumferential reinforcement around the end slab,

F_v = the total force in the longitudinal reinforcement.

This equation was compared to experimental results and was shown to slightly underestimate the ultimate pressure of the top heads which failed in flexure. In the same paper, an estimate of the maximum pressure causing shear failure was also given. This is based on the shear strength of the concrete at the midheight of the top head at the point where cracks first form. Comparison to results of top heads which failed in shear also were conservative. However, the failure mechanisms were known from

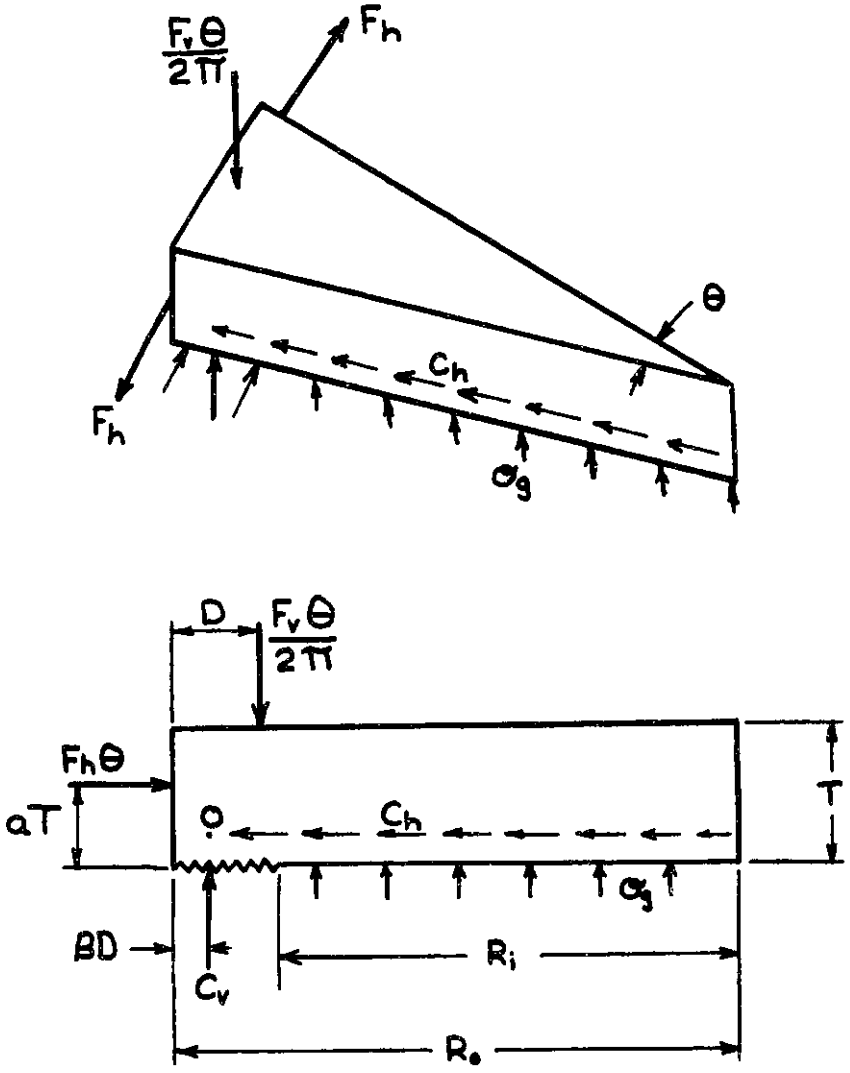

SECTOR OF TOP SLAB

FIG. 2.16

tests before the analysis was made. Comparisons of estimates of maximum pressure for flexural failure or shear failure showed that the failure modes could not be predicted. An important result revealed by the tests was that circumferential prestress failed before the strain reached the ultimate because of the strains across exterior cracks.

Another simplified method for the analysis of the walls of the pressure vessel was proposed by Koerner. (ref. 35) An equation was presented based on bending theory and a beam on elastic foundation analogy. Comparisons to tests of a model of the Fort St. Vrain pressure vessel showed the failure mechanism was well represented.

Numerical methods employed for the ultimate analysis of pressure vessels are mainly finite element models, with a limited use of dynamic relaxation. Dynamic relaxation was employed to analyze the top head closure of the Heysham vessels and gave good results as represented by Garas and Crittendon. (ref. 23)

Davidson (ref. 18) presented the use of dynamic relaxation to predict the extension of cracks in a mathematical model. The method considered separation of elements in the model along the crack by duplicating the nodes. (fig. 2.17) The extent of the crack was determined by varying the length of the doubled nodes until a minimum angle is maintained, and the doubled nodes no longer overlap. The use of this method is questionable as the amount of computer time needed is large. Also, the method assumes the direction and location of the crack, and several directions must be tried before adopting the one with the minimum pressure.

Finite element analysis is now the most frequently employed approach. The development of larger computers and non-linear material models have

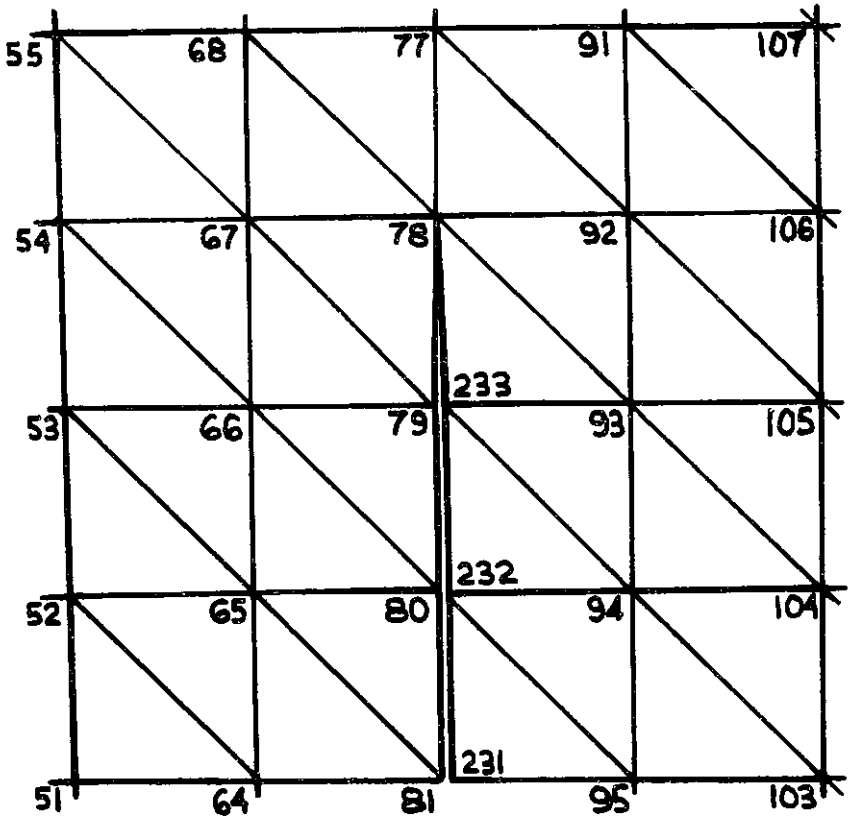

DUPLICATION OF NODES

FIG. 2.17

made this possible.

Finite element ultimate load analysis of axisymmetric pressure vessels was first attempted by Rashid. (ref. 52) The nonlinearities included were concrete cracking caused by excessive tensile stresses in the principal directions, and yielding of the steel liner according to the von Mises yield criteria and the Prandtl-Reuss flow rule. Results were compared to experimental results for a cylindrical vessel. The significance of the analysis is not that the ultimate pressure of the vessel can be predicted, but its ability to predict the deformation, cracking, and yielding of the structure. Also, severe deformation and cracking developed at much lower pressure than the ultimate.

The inclusion of nonlinear properties of concrete in compression in the axisymmetric analysis of pressure vessels was presented by several groups. Zienkiewicz et. al. (ref. 69) assumed the behavior of the principal directions was constrained to follow results from unconfined compression models. No effects of the stresses in the other principal directions on the yield strength were incorporated.

Argyris et. al. (ref. 3) included triaxial and biaxial failure criteria for concrete in tension and compression. Two tension failure criteria were considered: a) Tension cut-off which assumes failure depends on the major principle stress, and b) Mohr-Coulomb criteria, which depends on the major and minor principal stresses. Compression nonlinearities for triaxial and biaxial compression failure surfaces were also treated with the two different approaches: a) First by assuming no coupling of normal and shear stresses, and b) with an elastic-plastic formulation. Results of an axisymmetrical analysis using the tension cut-off and elastic-

plastic formulation compared to experimental results of a top closure showed fair correlation. Nonlinear material properties and finite element modeling will be described more fully later.

Analysis of other test models (ref. 36, 63) using nonlinear axisymmetric finite element methods showed their acceptability to predict the behavior of pressure vessels. The need for more advanced methods came with the design of podded boiler pressure vessels.

The development of three dimensional nonlinear finite element techniques has recently been presented by several groups.

Saugy et. al. (ref. 58) analyzed a Swiss pressure vessel for the helium cooled fast reactor of 1000 Mw capacity. The analysis included pressure and variable temperature loads, and creep. Nonlinearities included triaxial failure criteria for concrete in compression and tension. Steel components were not included in the analysis. The additional stiffness of the liner and reinforcement was modeled by increasing the yield strength in those regions. The finite element model included a 1/16 section of the top half of the pressure vessel, and one half of the sidewall cavity. Results of the analysis put the factor of safety of the vessel at about 2.0 times the design pressure. The cause for such a low value cannot be presently explained as no experimental data is available. A possible reason could be the ineffective modeling of the steel reinforcement.

A three dimensional nonlinear analysis of the G.A. HTGR including concrete and steel nonlinearities was presented by Sarne. (ref. 55) Nonlinearities included triaxial failure surfaces for tension and compression of concrete using principal stresses, and elasto-plastic analysis of

steel using the Huber-Mises yield criteria, and the flow and normality rules. The analysis used a 30° section of the vessel. Results showed the effect of overpressure, excessive temperatures, and the removal of normal operating temperature after 40 years. The importance of temperature in the analysis of the vessel was evident. The factor of safety has traditionally been based on the pressure capacity of the vessel. The inclusion of temperature and time should also be considered when determining this value.

2.5 Conclusion

Methods of analysis for prestressed concrete pressure vessels have been presented. The complex stress states in thick walled cylinders with penetrations make simplified analysis methods inconclusive in determining the ultimate strength. Use of finite element methods has made it possible to analyze the vessel for all loads it will be subjected to during its life, including time effects, and the determination of the ultimate strength, using the same analysis technique.

In analyzing the vessel for the effects of time on the stress state, it is important that the mathematical model accurately represent the actual material behavior. Material tests should be performed before making the analysis to determine properties which might affect the concrete.

1) The effect of age and temperature on recoverable creep

2) The effect of age and temperature on non-recoverable creep

3) The effect of duration of loading on non-recoverable creep.

When calculating the factor of safety of the pressure vessel, the effect of extreme temperature should be included along with the overpressure analysis. Also, the effect of load removal should be studied.

The improvement in numerical modeling techniques will assist in the development of accurate simplified analysis methods since they will lead to increased knowledge of the behavior of the vessel.

Chapter III

Nonlinear Finite Element Displacement Method

3.1 Introduction

The finite element method is generally recognized as being the most suitable numerical method for the analysis of complex structures. Two dimensional approximations such as plane strain and axisymmetric behavior are no longer acceptable for predicting the behavior of reactor vessels. Also, nonlinear material properties must be accounted for if the ultimate load is desired. The nonlinearities include:

1. Cracking of concrete
2. Non-linear stress-strain relationships of concrete in compression
3. Biaxial and triaxial states of stress
4. Yielding of reinforcing
5. Biaxial yielding of steel liners.

In the sections that follow, the finite element displacement method and the steps necessary for solution are presented. Material non-linearities which must be accounted for in the analysis are described, and the solution strategies for solving a non-linear analysis are compared.

3.2 Finite Element Displacement Method

The finite element displacement method is based on the Principle of Virtual Displacements which equates the internal work done by the stresses to the external work of the body and surface forces due to arbitrary displacements, $\delta \underline{U}$.

$$\int \underline{\sigma}^T \delta \underline{\varepsilon} \, dV = \int \underline{b}^T \delta \underline{U} \, dV + \int \underline{P}^T \delta \underline{U} \, dS \qquad (3.1)$$

In the analysis, the total domain of the structure is divided into a number of subregions known as elements. A simple displacement function is assumed for each region:

$$\{U\} = [N]\{U_N\} \tag{3.2}$$

where $\{U\}$ represents the displacements of any point in the interior of the element, and $\{U_N\}$ contains the unknown nodal displacements. Operating on (3.2), the strain-displacement relations in the region are determined:

$$\varepsilon_i = \frac{\partial U_i}{\partial X_i} = \frac{\partial (\underline{N}\,\underline{U}_N)}{\partial X_i} = \frac{\partial \underline{N}}{\partial X_i}\,\underline{U}_N = \underline{B}\,\underline{U}_N \tag{3.3}$$

where the $\underline{B}$ matrix is dependent on the geometric properties of the element. The stress-strain relations are written as:

$$\underline{\sigma} = \underline{D}(\underline{\varepsilon} - \underline{\varepsilon}_0) + \underline{\sigma}_0 \tag{3.4}$$

$\underline{\varepsilon}_0$ and $\underline{\sigma}_0$ are initial strains and stresses, and $\underline{D}$ is a material rigidity matrix.

Substituting the above expressions into (4.1) and summing over the elements yields the system's equilibrium equations.

$$\sum_{el} \underline{P}_N = \sum_{el} \left(\left(\int \underline{B}^T \underline{D}\,\underline{B}\, dV \right) \underline{U} - \int \underline{B}^T \underline{D}\,\underline{\varepsilon}_0\, dV + \int \underline{B}^T \underline{\sigma}_0\, dV - \int \underline{N}^T \underline{P}\, dV \right) \tag{3.5}$$

The element stiffness matrix is defined as:

$$\underline{K} = \int \underline{B}^T \underline{D}\,\underline{B}\, dV_{el} \tag{3.6}$$

and the equivalent element nodal forces for initial strains, initial stresses, and body and surface forces are, respectively:

$$\begin{aligned} \underset{\sim}{P}_{\varepsilon} &= +\int \underset{\sim}{B}^{T} \underset{\sim}{D} \underset{\sim}{\varepsilon}_{0}\, dV \\ \underset{\sim}{P}_{\sigma} &= -\int \underset{\sim}{B}^{T} \underset{\sim}{\sigma}_{0}\, dV \\ \underset{\sim}{P}_{p} &= +\int \underset{\sim}{N}^{T} \underset{\sim}{P}\, dV \end{aligned} \tag{3.7}$$

With this notation, (3.5) simplifies to:

$$\sum_{el} \underset{\sim}{K} \underset{\sim}{U}_{N} = \sum_{el} \underset{\sim}{P} \tag{3.8}$$

where:

$$\underset{\sim}{P} = \underset{\sim}{P}_{N} + \underset{\sim}{P}_{p} + \underset{\sim}{P}_{\varepsilon} + \underset{\sim}{P}_{\sigma} \tag{3.9}$$

This set of equations is then solved for the unknown nodal displacements, $\underset{\sim}{U}_{N}$; from which the element strains and stresses are determined.

$$\underset{\sim}{\sigma} = \underset{\sim}{D}(\underset{\sim}{\varepsilon} - \underset{\sim}{\varepsilon}_{0}) + \underset{\sim}{\sigma}_{0} = \underset{\sim}{D}\underset{\sim}{B}\underset{\sim}{U}_{N} - \underset{\sim}{D}\underset{\sim}{\varepsilon}_{0} + \underset{\sim}{\sigma}_{0} \tag{3.10}$$

The number of elements employed depends on the computer capacity, and also on the accuracy associated with the element. In general, the accuracy increases with the order of the polynomial approximations (first degree, second, etc.). Since higher order elements with straight edges cannot model accurately the irregular geometry of the structure, the introduction of isoparametric elements is necessary. In this formulation, the shape functions defining the variations of the unknown displacements are also used to define the element boundaries. (ref. 69) This allows one to approximate a boundary with a polynomial having the same degree as the displacement function.

In the isoparametric approach, the cartesian coordinates of a point are expressed in terms of dimensionless coordinates, (S_1, S_2, S_3)

whose values range from -1 to 1., and the nodal coordinates

$$\begin{Bmatrix} X \\ Y \\ Z \end{Bmatrix} = \sum_{i=1}^{n} [N_i] \begin{Bmatrix} X_i \\ Y_i \\ Z_i \end{Bmatrix} \tag{3.11}$$

$N_i = N_i(S_1, S_2, S_3)$ are interpolation functions satisfying $N_i = 1$ at node i, and equal to zero at all other nodes.

The $\underset{\sim}{B}$ matrix takes a more complicated form since it is necessary to transform derivatives to curvilinear coordinates. The steps are:

$$\begin{bmatrix} \frac{\partial N_i}{\partial S_1} \\ \frac{\partial N_i}{\partial S_2} \\ \frac{\partial N_i}{\partial S_3} \end{bmatrix} = \begin{bmatrix} \frac{\partial X}{\partial S_1} & \frac{\partial Y}{\partial S_1} & \frac{\partial Z}{\partial S_1} \\ \frac{\partial X}{\partial S_2} & \frac{\partial Y}{\partial S_2} & \frac{\partial Z}{\partial S_2} \\ \frac{\partial X}{\partial S_3} & \frac{\partial Y}{\partial S_3} & \frac{\partial Z}{\partial S_3} \end{bmatrix} \begin{bmatrix} \frac{\partial N_i}{\partial X} \\ \frac{\partial N_i}{\partial Y} \\ \frac{\partial N_i}{\partial Z} \end{bmatrix} = [J] \begin{bmatrix} \frac{\partial N_i}{\partial X} \\ \frac{\partial N_i}{\partial Y} \\ \frac{\partial N_i}{\partial Z} \end{bmatrix} \tag{3.12}$$

$$[J] = \begin{bmatrix} \frac{\partial N_1}{\partial S_1} & \frac{\partial N_2}{\partial S_1} & \cdots \\ \frac{\partial N_1}{\partial S_2} & \frac{\partial N_2}{\partial S_2} & \cdots \\ \frac{\partial N_1}{\partial S_3} & \frac{\partial N_2}{\partial S_3} & \cdots \end{bmatrix} \begin{bmatrix} X_1 & Y_1 & Z_1 \\ X_2 & Y_2 & Z_2 \\ X_3 & Y_3 & Z_3 \\ \vdots & \vdots & \vdots \end{bmatrix} \tag{3.13}$$

$$dX\, dY\, dZ = [J]\; dS_1\, dS_2\, dS_3 \tag{3.14}$$

where $\underset{\sim}{J}$ is the Jacobian for the transformation. Explicit integration is impossible and one has to resort to numerical integration techniques which are easily incorporated into the computer program. For convergence of the numerical integration to the true result, the volume integral must be

capable of being determined exactly. This imposes a restriction on the integration rule.

The optimum choice for representing concrete in the three dimensional analysis of pressure vessels is the twenty node linear strain element. (fig. 3.1) This element has one node along each edge in addition to the corner nodes, making it possible to define a quadratic curve. Artificial stresses may be introduced if the element geometry is highly distorted. Therefore, 20 node hexahedron elements reduced to tetrahedron can be used, but are not recommended for regions of interest. (ref. 55)

A doubly curved thin shell membrane quadrilateral element is employed to model steel liners and reinforcement. (fig. 3.2) The element is based on a quadratic expansion, and is compatible with the three dimensional element.

3.3 Concrete Nonlinearities

Nonlinear material properties of concrete that must be modeled in the analysis include:

1. Triaxial and biaxial states of stress
2. Non-linear uniaxial stress-strain relationships
3. Cracking of concrete
4. Crushing of concrete
5. Effect of temperature on Young's modulus.

The multi-axial state of stress present in concrete pressure vessels makes modeling of a concrete failure surface under triaxial conditions necessary. Most failure surfaces used for concrete are based on the octahedral normal and shear stresses:

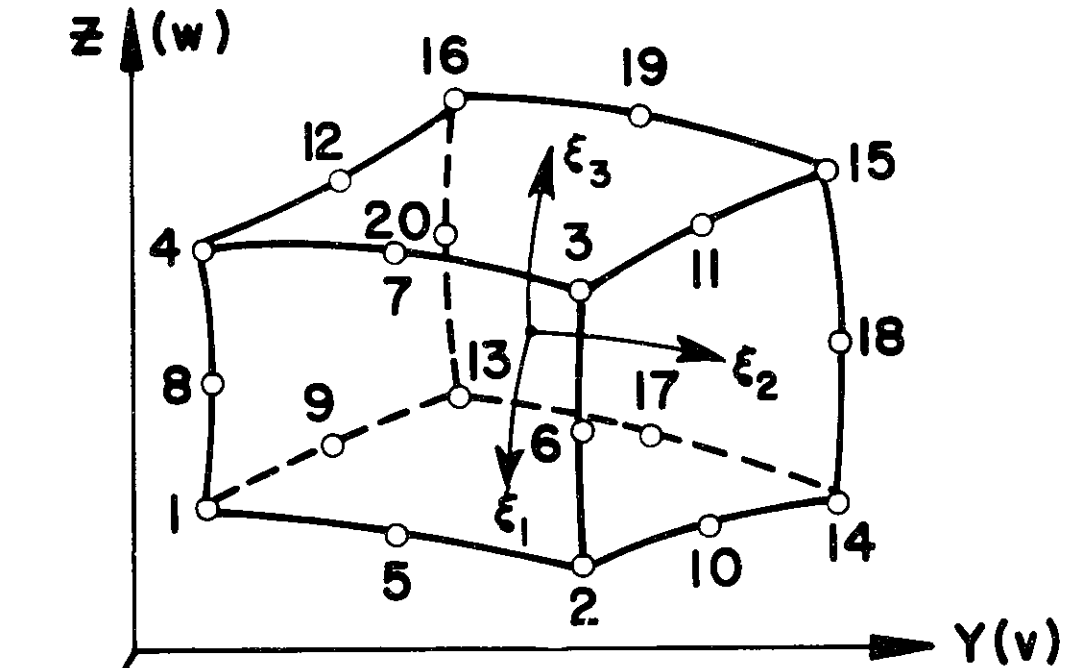

INTERPOLATION FUNCTIONS:

CORNER NODES – 1,2,3,4,13,14,15,16

$$N_i = 1/8\,(1+\xi_1\xi_i)(1+\xi_2\xi_i)(1+\xi_3\xi_i)(\xi_1\xi_i+\xi_2\xi_i+\xi_3\xi_i-2)$$

MIDSIDE – 5,7,17,19 ($\xi_2 = 0$)

$$N_i = 1/4(1-\xi_2^2)(1+\xi_1\xi_i)(1+\xi_3\xi_i)$$

MIDSIDE – 6,8,18,20 ($\xi_3 = 0$)

$$N_i = 1/4(1-\xi_3^2)(1+\xi_1\xi_i)(1+\xi_2\xi_i)$$

MIDSIDE – 9,10,11,12 ($\xi_1 = 0$)

$$N_i = 1/4(1-\xi_1^2)(1+\xi_2\xi_i)(1+\xi_3\xi_i)$$

Fig. 3.1 3D SOLID ELEMENT

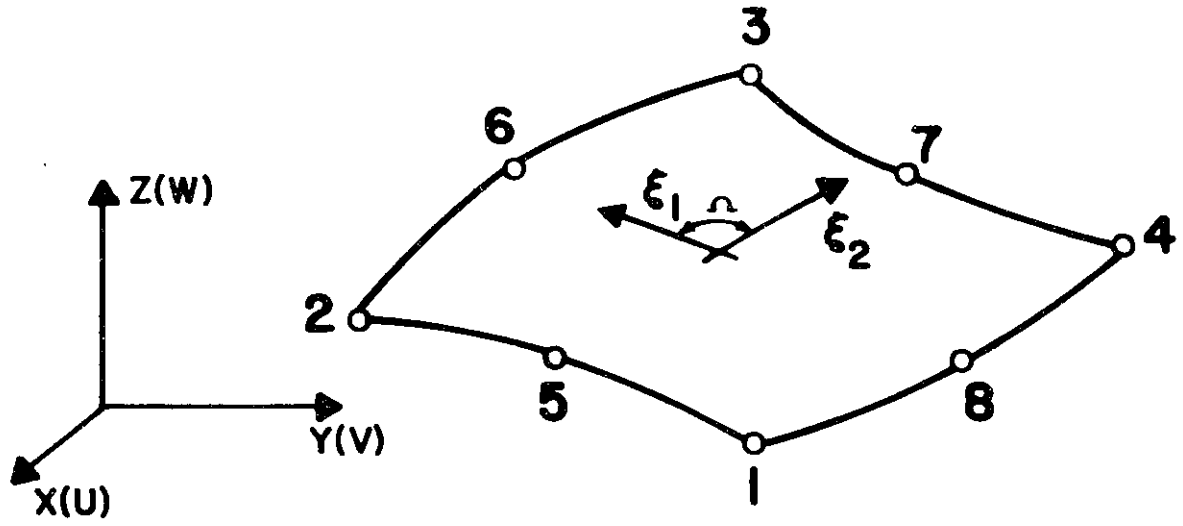

$$\begin{Bmatrix} X \\ Y \\ Z \end{Bmatrix} = \underset{\sim}{N}^T(\xi_1,\xi_2) \begin{Bmatrix} \underset{\sim}{X}_n \\ \underset{\sim}{Y}_n \\ \underset{\sim}{Z}_n \end{Bmatrix}$$

$$\begin{Bmatrix} U \\ V \\ W \end{Bmatrix} = \underset{\sim}{N}^T(\xi_1,\xi_2) \begin{Bmatrix} \underset{\sim}{U}_n \\ \underset{\sim}{V}_n \\ \underset{\sim}{W}_n \end{Bmatrix}$$

INTERPOLATION FUNCTIONS:

$$N_1 = -1/4\,(1-\xi_1)(1-\xi_2)(\xi_1+\xi_2+1) \qquad N_5 = 1/2\,(1-\xi_1^2)(1-\xi_2)$$

$$N_2 = 1/4\,(1+\xi_1)(1-\xi_2)(\xi_1-\xi_2-1) \qquad N_6 = 1/2\,(1+\xi_1)(1-\xi_2^2)$$

$$N_3 = 1/4\,(1+\xi_1)(1+\xi_2)(\xi_1+\xi_2-1) \qquad N_7 = 1/2\,(1-\xi_1^2)(1+\xi_2)$$

$$N_4 = -1/4\,(1-\xi_1)(1+\xi_2)(\xi_1-\xi_2+1) \qquad N_8 = 1/2\,(1-\xi_1)(1-\xi_2^2)$$

MEMBRANE SHELL ELEMENT

FIG. 3.2

$$\sigma_o = \frac{1}{3}(\sigma_1 + \sigma_2 + \sigma_3)$$

$$\tau_o = \frac{1}{3}\left((\sigma_1-\sigma_2)^2+(\sigma_2-\sigma_3)^2+(\sigma_3-\sigma_1)^2\right)^{\frac{1}{2}} \qquad (3.15)$$

where $\sigma_1, \sigma_2, \sigma_3$ are the three principal stresses. The stress measures, σ_o and τ_o, can be interpreted as the hydrostatic and deviotoric stresses, respectively. Basically the triaxial failure surface is a cone with curved meridians and a non-circular base section with its axis along the line $\sigma_1 = \sigma_2 = \sigma_3$. (fig. 3.3) If the three principal stresses are equal the concrete can theoretically withstand unlimited compression.

Four criteria for the selection of the mathematical model of the failure surface are: (ref. 65)

1. Close fit of experimental data
2. Simple identification of nodal parameters from standard test data
3. Smoothness -- continuous surface with continuously varying tangent planes
4. Convexity -- monotonically curved surface with no inflexion points.

Experimental results indicate that the failure surface depends on the hydrostatic as well as the deviatoric stress. In addition, in the tensile region, the surface should include a tension cut-off criteria. Simple identification permits defining the failure surface by a small number of parameters, such as the uniaxial tensile strength, the uniaxial compressive strength, and the biaxial compressive strength. Also, the failure surface should encompass other simple failure envelopes for specific modal parameters, such as the biaxial failure curve. (fig. 3.4)

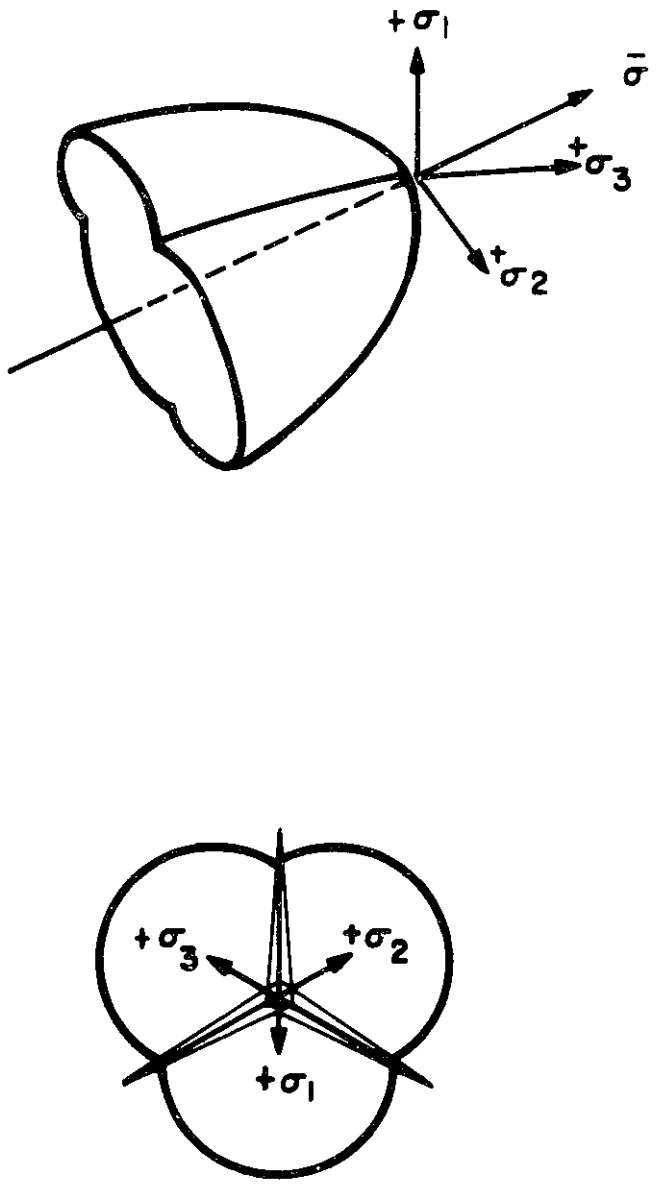

TRIAXIAL COMPRESSIVE STRESSES
FAILURE SURFACE

Fig. 3.3

BIAXIAL STATE OF STRESSES
FAILURE CRITERION

FIG. 3.4

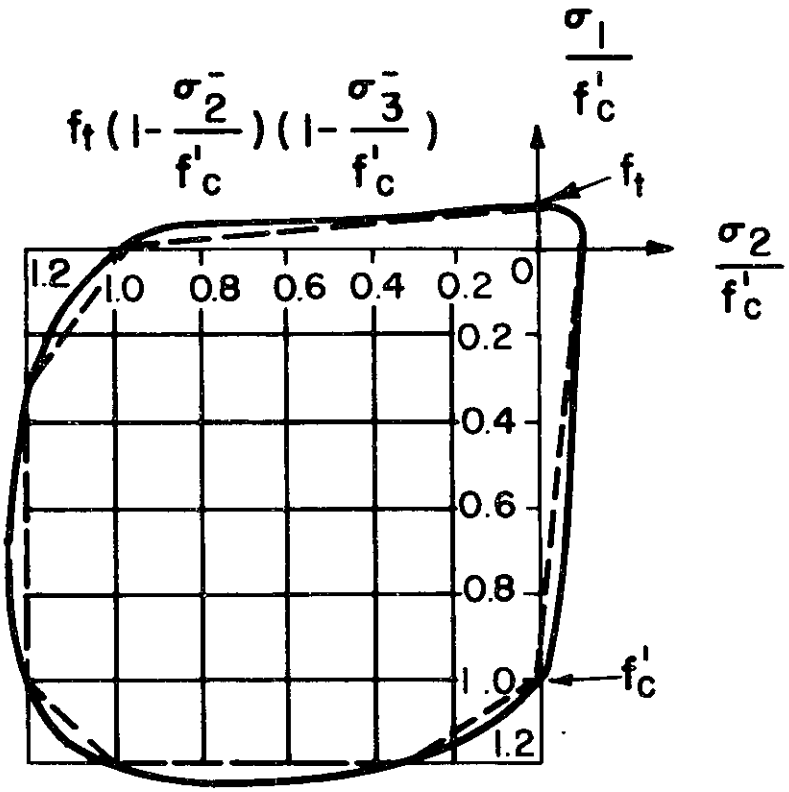

Continuity is important from a computational viewpoint as a single description of the failure surface is very convenient. Convexity, which leads to stable material behavior is assured if there are no inflection points and $\frac{r_1}{r_2} > \frac{1}{2}$ for the elliptical surface. (fig. 3.5) A three parameter model will be of the form:

$$\gamma_0 + \sqrt{2}\,\frac{1-a}{1+a}\,\sigma_0 - \frac{2\sqrt{2}}{3}\,\frac{a}{1+a}\,f_c' = 0 \qquad \sigma_1, \sigma_2, \text{OR } \sigma_3 > 0$$

$$\gamma_0 + \sqrt{2}\,\frac{B-1}{2B-1}\,\sigma_0 - \frac{\sqrt{2}}{3}\,\frac{B}{2B-1}\,f_c' = 0 \qquad \sigma_1, \sigma_2, \sigma_3 < 0 \qquad (3.16)$$

where a is the ratio of the uniaxial tensile strength to the uniaxial compression strength, and B is the ratio of biaxial to uniaxial compression strength.

A more widely used criterion for states of stress with one or more tensile values is the Mohr-Coulomb criterion with tension cut-off (fig. 3.6) which differentiates between tensile cracking and shear sliding. The maximum tensile stress condition forms a tetrahedral surface which is intersected by the hexahedral pyramid of the Mohr-Coulomb criterion. The Mohr-Coulomb surface can also be represented by Mohr circle. (fig. 3.7)

Failure under triaxial tension is considered to occur when the major principal tension exceeds the uniaxial tensile strength. This single parameter model is sometimes expressed in terms of maximum tensile strain, but this is considerably more restrictive in tension-compression quadratic. (ref. 3). When a crack is formed, it is in the plane perpendicular to the principal direction. It will remain open if the strain is positive in the fixed principal direction.

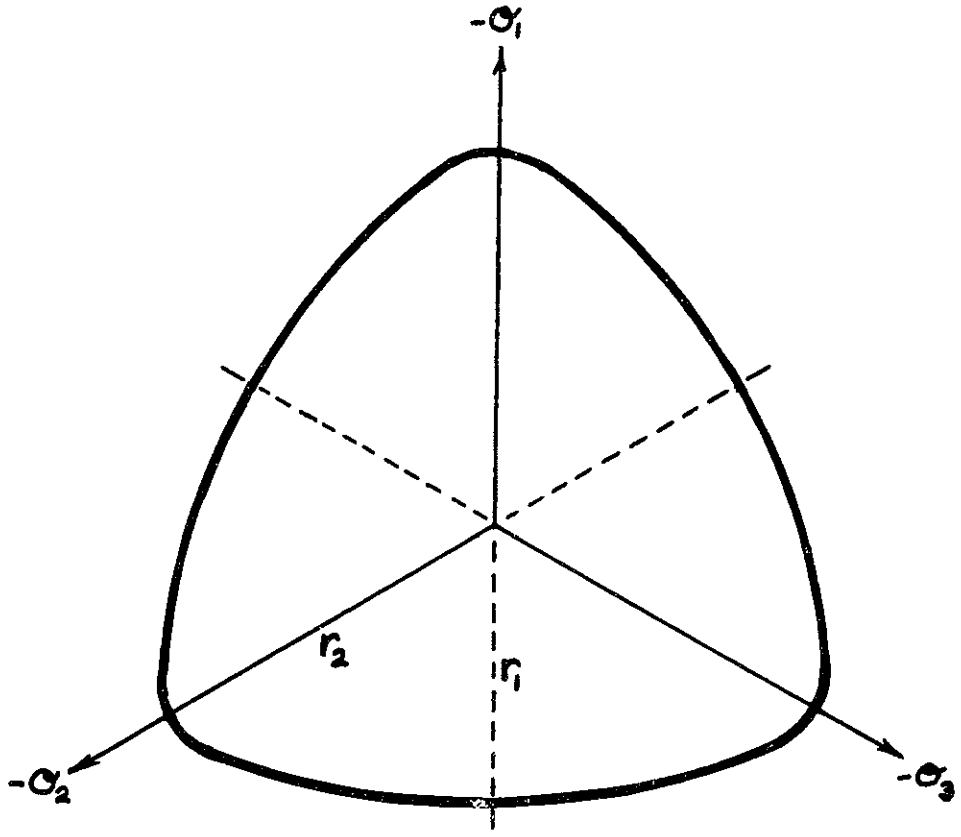

CONVEXITY OF FAILURE SURFACE

FIG. 3.5

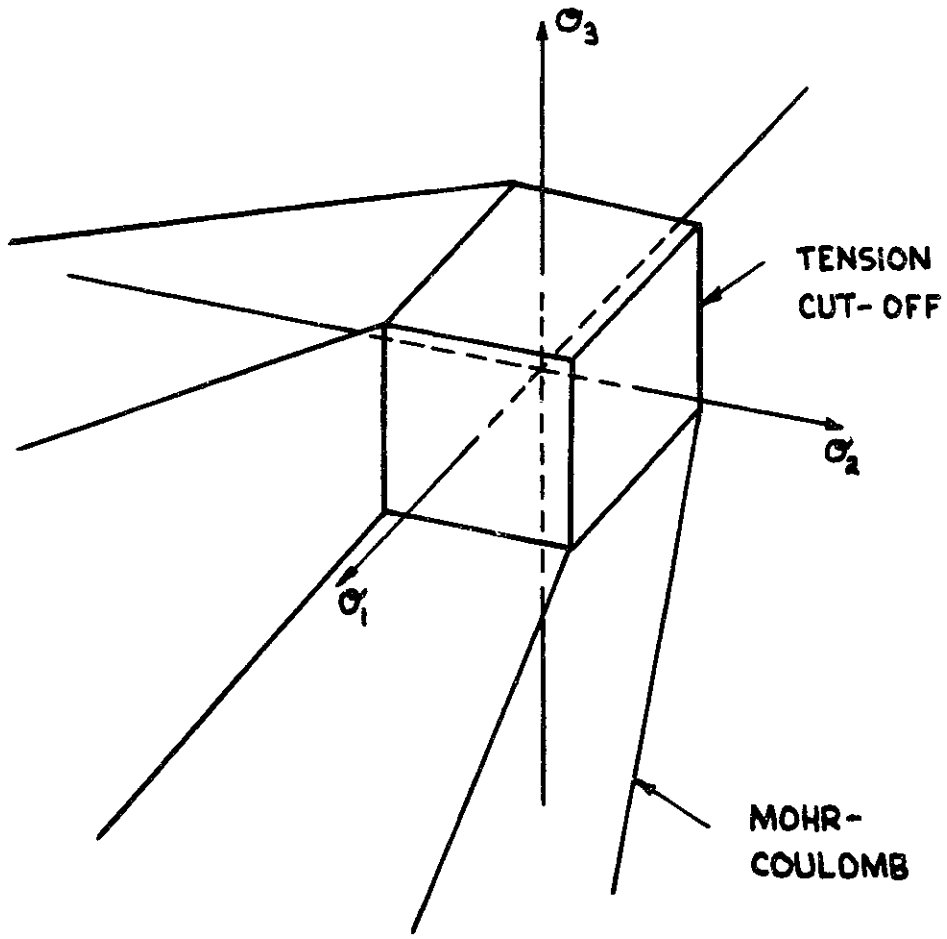

MOHR-COULOMB CRITERION WITH TENSION CUT- OFF

FIG. 3.6

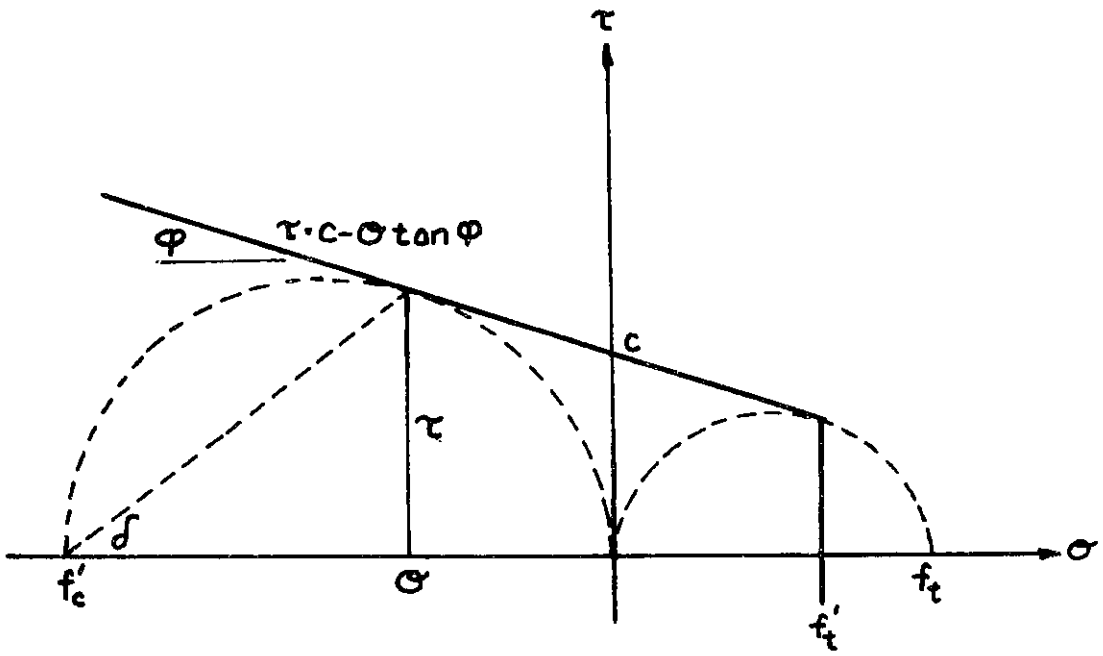

MOHR CIRCLE REPRESENTATION

FIG. 3.7

Failure due to the Mohr-Coulomb criteria is a shear type failure, and cracks will form at an angle, δ, along which sliding occurs. (fig. 3.8) This is a two parameter model of the form:

$$f(\sigma_1,\sigma_3) = \frac{\sigma_1}{f_t'} + \frac{\sigma_3}{f_c'} - 1 \qquad (3.17)$$

which holds for the case of one compressive stress. (fig. 3.9) An alternative representation is a constraint condition for normal and shear stresses at the plane of failure:

$$\tau = C - \sigma \tan \varphi \qquad (3.18)$$

The internal cohesion, c, and the angle of friction, φ, are related to the uniaxial compressive strength, f_c', and the fictitious tensile strength, f_t',:

$$f_c' = 2C \cdot \cos\varphi / (1 - \sin\varphi)$$
$$f_t' = 2C \cdot \cos\varphi / (1 + \sin\varphi) \qquad (3.19)$$

A three parameter model used for the case of two compressive stresses is:

$$\frac{\sigma_1}{f_t'} = \left(1 - \frac{\sigma_2}{f_c'}\right)\left(1 - \frac{\sigma_3}{f_c'}\right) \qquad (3.20)$$

However, a form without the reduction to the fictitious tensile stress was used by Sarne. (ref. 55) (fig. 3.10)

An alternative to finding the slip planes of the concrete is to assume the concrete to be cracked perpendicular to the direction of the principal stress violating the Mohr-Coulomb criteria. (ref. 11,55) Though

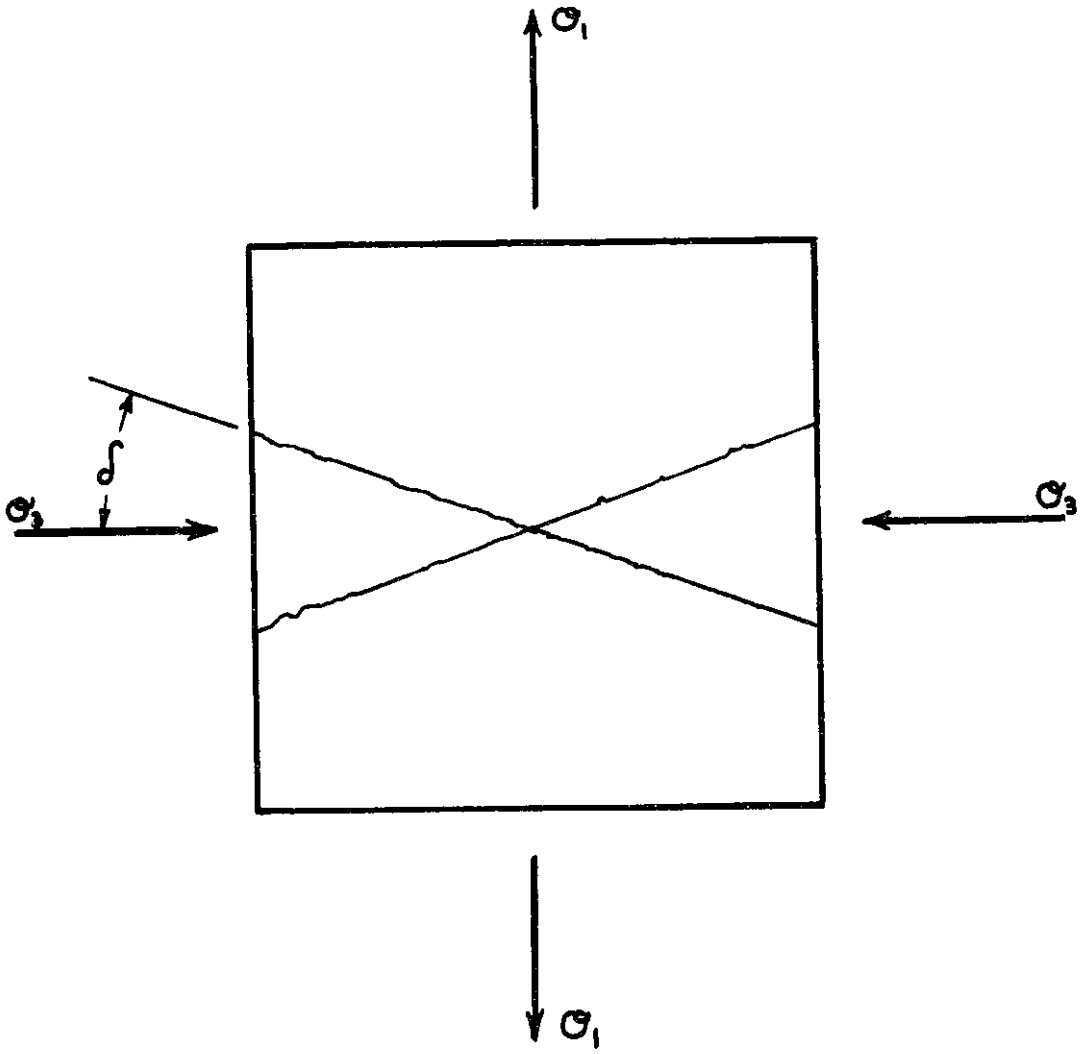

CRACKS DUE TO SHEAR FAILURE

FIG. 3.8

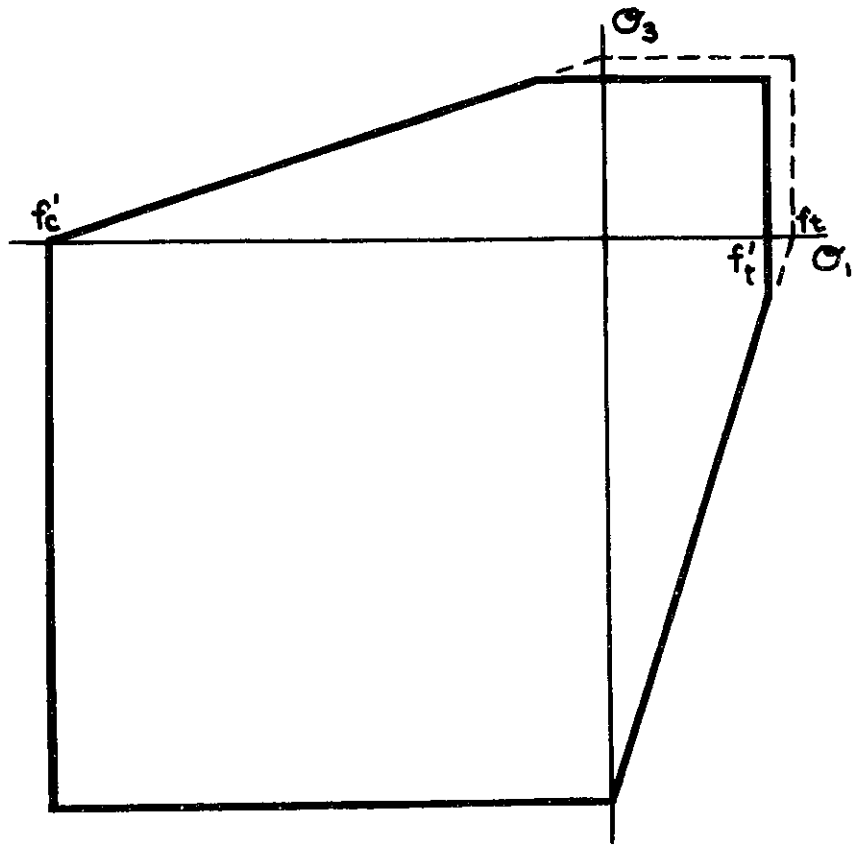

FIG. 3.9

TWO PARAMETER MODEL

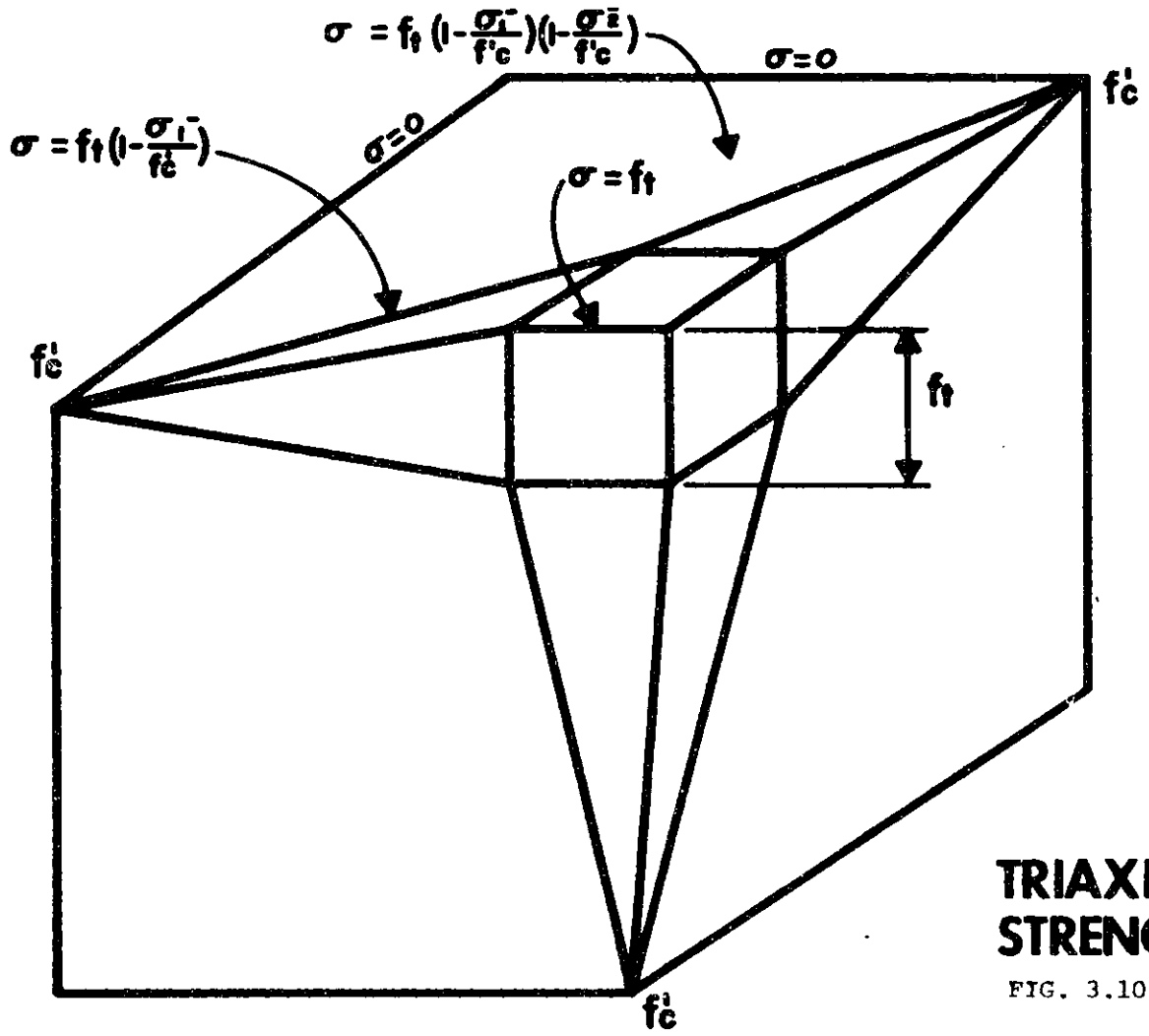

TRIAXIAL TENSILE STRENGTH

FIG. 3.10

this will not give the exact crack direction for shear slippage, it will give a reduction of stiffness in the correct direction.

Two methods have been presented to determine if concrete has failed in compression. One uses a bilinear stress-strain relation assuming perfectly plastic behavior. Failure occurs when the state of stress falls outside the yield surface, and the von Mises flow-rule is used to expand the surface. (ref. 3,4,11,65) This approach is similar to the plastic deformation theory of metals, and will be explained in section 3.4. A second method assumed independence of the principal stresses (ref.55) in which the failure surface is used only to find the ultimate strength in the direction in question. From this new value of f_c', a nonlinear uniaxial stress-strain relationship is determined, and failure, or crushing, occurs if the ultimate stress is less than the calculated value.

There is little experimental data justifying either of these two methods. Also, it is known that frictional materials do not obey the normality rule which must be used in the first method, i.e., the elastic-plastic formulation.

Another nonlinear property of concrete which must be incorporated into the analysis is the stress-strain relationship in compression. It starts with a linear portion which gradually deviates until the tanget is horizontal. Beyond this point the curve descends to the point of failure. (fig. 3.11) In the curve shown by Saenz (ref. 55), the descending portion has been specified by a straight line, although a cubic equation is sometimes used. Because the exact state of strain is known, it is possible to use an incremental secant modulus in the rigidity matrix when determining the state of stress.

CONCRETE STRESS-STRAIN RELATIONSHIP

Fig. 3.11

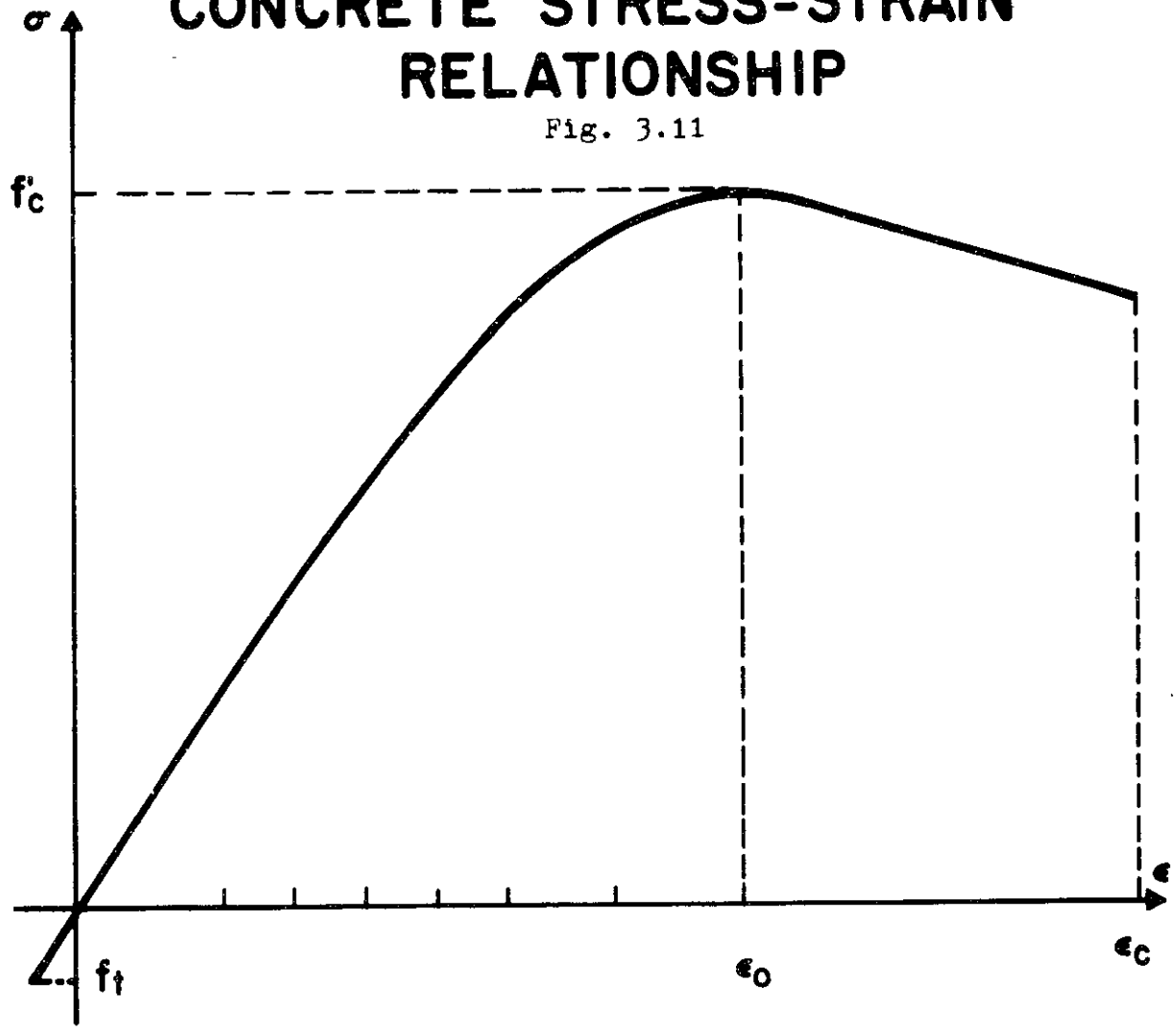

$$f = E\epsilon \left[1 + (3E_0/E - 2)(\epsilon/\epsilon_0) + (1 - 2E_0/E)(\epsilon/\epsilon_0)^2\right]$$

WHERE: f, ϵ CONCRETE STRESS AND STRAIN, RESPECTIVELY

ϵ_0 ULTIMATE STRAIN $= (31.5 - \sqrt[4]{f'c}) * \sqrt[4]{f'c} * 10^{-3}$

E INITIAL YOUNG'S MODULUS

E_0 SECANT MODULUS AT THE ULTIMATE STRESS (f'_c/ϵ_0)

Young's modulus, E, of concrete is also a function of temperature, decreasing with increasing temperatures. A relationship proposed by Gross (ref. 26) considers E to be a function of the stress-strength ratio (s) of the concrete as well as the temperature:

$$
\begin{aligned}
T_u &= 1000(1.0-S)+20 && 0.66 \le S \le 1.0 \\
T_u &= 219\,(0.66-S)+350 && 0.2 \le S \le 0.66 \\
T_u &= 1340(0.2-S)+425 && 0.02 \le S \le 0.2 \\
A &= (T_u-20)^{\frac{1}{2}} \\
\frac{E(T°C)}{E(20°C)} &= A(T_u-T)^{\frac{1}{2}}
\end{aligned}
\tag{3.21}
$$

Other properties of concrete which vary with either temperature or time include Poisson's ratio, and the coefficient of thermal expansion. (ref. 11) However, the variations are usually small and because of the little knowledge as to their behavior, are usually considered to be constant.

3.4 Nonlinear Properties of Steel

The nonlinear property of steel which must be considered in the pressure vessel analysis is the tensile or compression yielding of the liner under a biaxial state of stress. Yielding of the reinforcing is caused by uniaxial failure and will be used for illustration.

A reasonable approximation of the stress-strain curve is shown in fig. 3.12. It is a bilinear curve with $E_2 \ll E_1$. If $E_2 = 0$, the material is called elastic-perfectly plastic. For stresses greater than σ_y the material is said to be plastic. When unloading occurs, the path will follow the initial modulus, E_1, until failure is reached in the opposite direction.

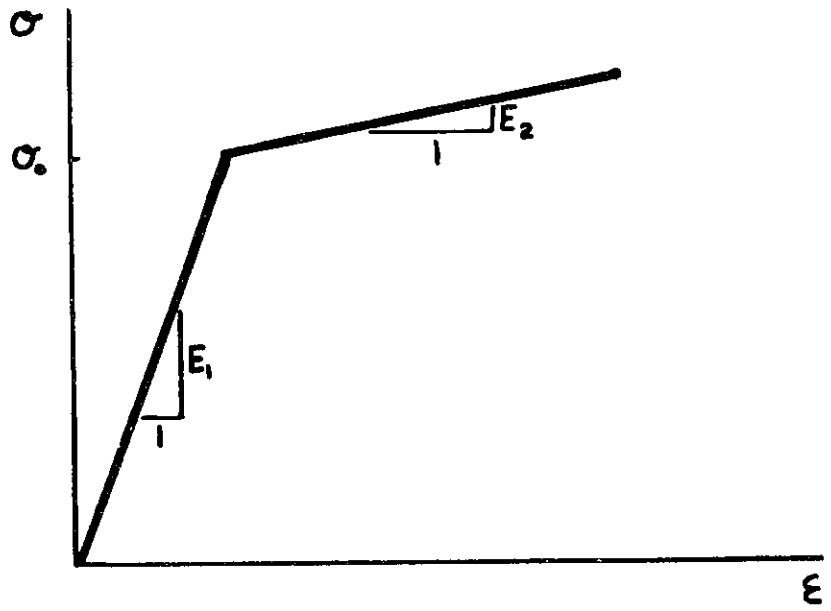

BILINEAR STRESS-STRAIN CURVE

FIG. 3.12

The yield stress under the reversed load will generally be less than the original yield stress as indicated in Figure 3.13. To simplify the analysis, this effect (attributed to Bauschinger) is neglected. For biaxial or triaxial stress states, an equivalent effective uniaxial stress, $\bar{\sigma}$, which is a function of the stress components, is introduced.

$$\bar{\sigma} = f(\sigma_{11}, \sigma_{22}, \ldots, \sigma_{12}, \ldots) \tag{3.22}$$

Numerous forms for the yield function, f, have been proposed, but the two most frequently employed are:

von Mises

$$f = \bar{\sigma} = \left\{\tfrac{1}{2}\left[(\sigma_1-\sigma_2)^2+(\sigma_2-\sigma_3)^2+(\sigma_3-\sigma_1)^2\right]^{\frac{1}{2}}\right\} \tag{3.23}$$

Tresca

$$\bar{\sigma} = \sigma_{max} - \sigma_{min} \tag{3.24}$$

Von Mises assumes that yielding occurs when the second invariant of the deviatoric stress tensor exceeds $\bar{\sigma}$. This is equivalent to saying yielding begins when the internal energy of distortion, or the octahedral shear stress, exceeds a certain value. (ref. 31) The Tresca yield condition is also referred to as the maximum shear stress criterion. The von Mises criterion agrees better with experimental data and is analytically more tractable.

Along with the effective stress, $\bar{\sigma}$, an effective uniaxial plastic strain, $\bar{\varepsilon}_p$, is defined such that the incremental plastic work done by the stress components is equal to $\bar{\sigma} d\bar{\varepsilon}_p$.

$$\sigma_{11}\, d\varepsilon^p_{11} + \sigma_{22}\, d\varepsilon^p_{22} + \ldots + \sigma_{12}\, d\gamma^p_{12} + \ldots = \bar{\sigma}\, d\bar{\varepsilon}_p \tag{3.25}$$

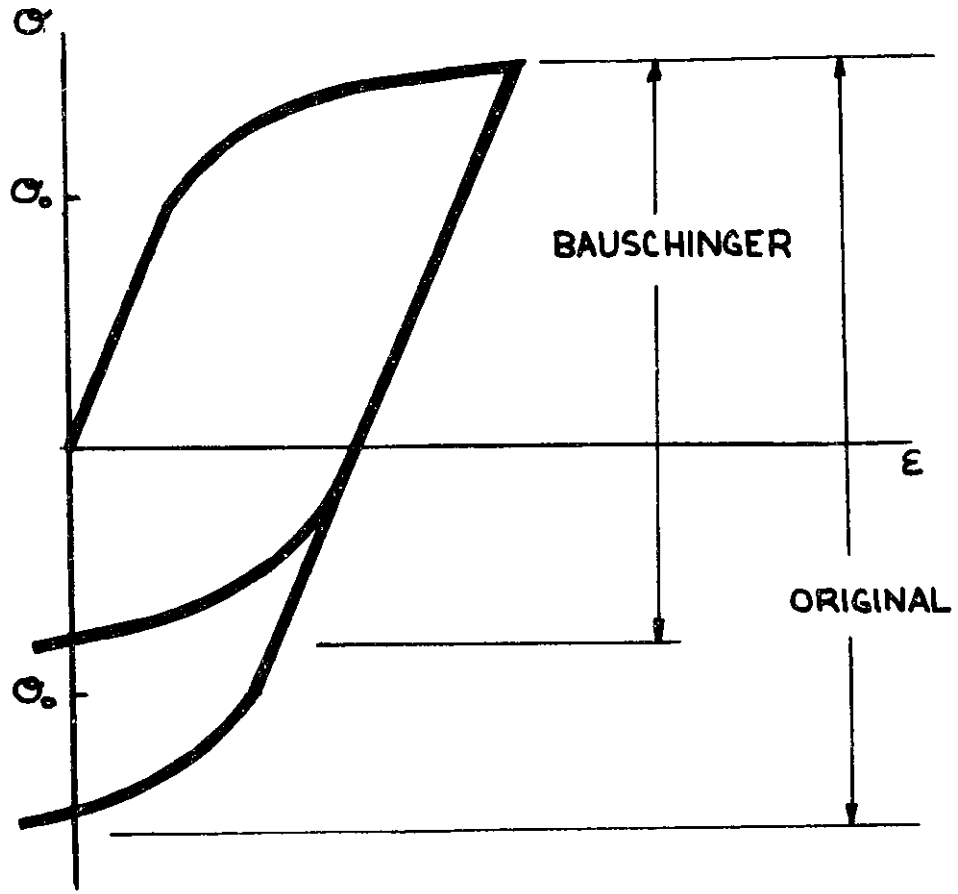

BAUSCHINGER EFFECT

FIG. 3.13

Two approaches to determining the state of stress for a given strain state are the deformation theory introduced by Hencky and incremental theory. In the deformation theory, the plastic secant modulus, E_p^s, is introduced, (fig. 3.14) and Poisson's ratio, ν_p, is taken as one half giving no volumetric strains. Since E_p^s is a function of stress, the solution will require iteration. The plastic stress-strain relations are:

$$\varepsilon_x^p = \frac{1}{E_p^s}\left(\sigma_x - \tfrac{1}{2}(\sigma_y + \sigma_z)\right)$$
$$\vdots$$
$$\gamma_{xy}^p = \frac{1}{G_p^s}\tau_{xy} = \frac{3}{E_p^s}\tau_{xy} \qquad (3.26)$$
$$\vdots$$

Since the strain increment is specified, our problem is reversed. Using matrix formulation, the plastic and elastic strains are:

$$\underset{\sim}{\varepsilon}_p = \underset{\sim}{C}_p\,\underset{\sim}{\sigma}$$
$$\underset{\sim}{\varepsilon}_e = \underset{\sim}{C}_e\,\underset{\sim}{\sigma} \qquad (3.27)$$

Adding gives:

$$\underset{\sim}{\varepsilon} = \underset{\sim}{\varepsilon}_e + \underset{\sim}{\varepsilon}_p = (\underset{\sim}{C}_e + \underset{\sim}{C}_p)\,\underset{\sim}{\sigma} \qquad (3.28)$$

from which the unknown stress, $\underset{\sim}{\sigma}$, can be found:

$$\underset{\sim}{\sigma} = (\underset{\sim}{C}_e + \underset{\sim}{C}_p)^{-1}\underset{\sim}{\varepsilon} = \underset{\sim}{D}^s\underset{\sim}{\varepsilon} \qquad (3.29)$$

The deformation theory is not widely used as it is a path independent procedure which will give acceptable results if the stresses are monotonically increasing.

Incremental plasticity theory, is a path dependent process which assumes the response is specified by an initial yield condition, a hardening rule, and a flow rule. The initial yield condition specifies the

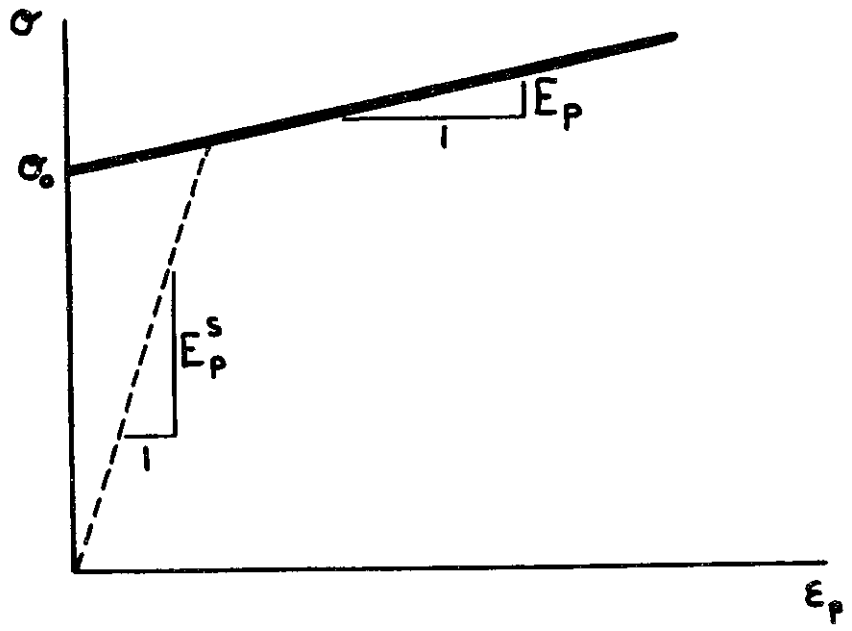

PLASTIC SECANT MODULUS

FIG. 3.14

state of stress for which plastic deformation first occurs, while the flow rule allows for the determination of plastic strain increments at each point in the loading history. It is expressed as:

$$d\underset{\sim}{\varepsilon}^{p} = d\varepsilon_{ij}^{p} = C\frac{\partial f}{\partial \sigma_{ij}} = C\,\underset{\sim}{F}_{\sigma} \tag{3.30}$$

where:

$d\varepsilon_{ij}^{p}$ = plastic strain increment

C = variable parameter

$\frac{\partial f}{\partial \sigma_{ij}}$ = gradient of the yield criterion, f

The hardening rule provides for the modification of the yield surface during plastic flow. Hardening rules available include isotropic hardening, kinematic hardening, the Mroz model, the mechanical sublayer model, the slip theory of Batdoric and Budiansky.

Isotropic hardening states that during plastic flow the yield surface expands uniformly, maintaining its original shape and orientation. (fig. 3.15). The equivalent uniaxial stress, $\bar{\sigma}$, and the equivalent uniaxial plastic strain, $\bar{\varepsilon}^{p}$, follow the uniaxial stress-plastic strain curve.

$$d\bar{\varepsilon}^{p} = \frac{1}{E_{t}^{p}}\,d\bar{\sigma} \tag{3.31}$$

where E_{t}^{p} is the plastic tangent modulus and

$$\bar{\varepsilon}^{p} = \left(\frac{2}{9}\left\{(d\varepsilon_{1}^{p}-d\varepsilon_{2}^{p})^{2}+(d\varepsilon_{2}^{p}-d\varepsilon_{3}^{p})^{2}+(d\varepsilon_{3}^{p}-d\varepsilon_{1}^{p})^{2}\right\}\right)^{\frac{1}{2}} \tag{3.32}$$

During yielding the total strain increment is:

$$d\underset{\sim}{\varepsilon} = d\underset{\sim}{\varepsilon}^{e} + d\underset{\sim}{\varepsilon}^{p} \tag{3.33}$$

and, using the elastic rigidity matrix, the stress increment is:

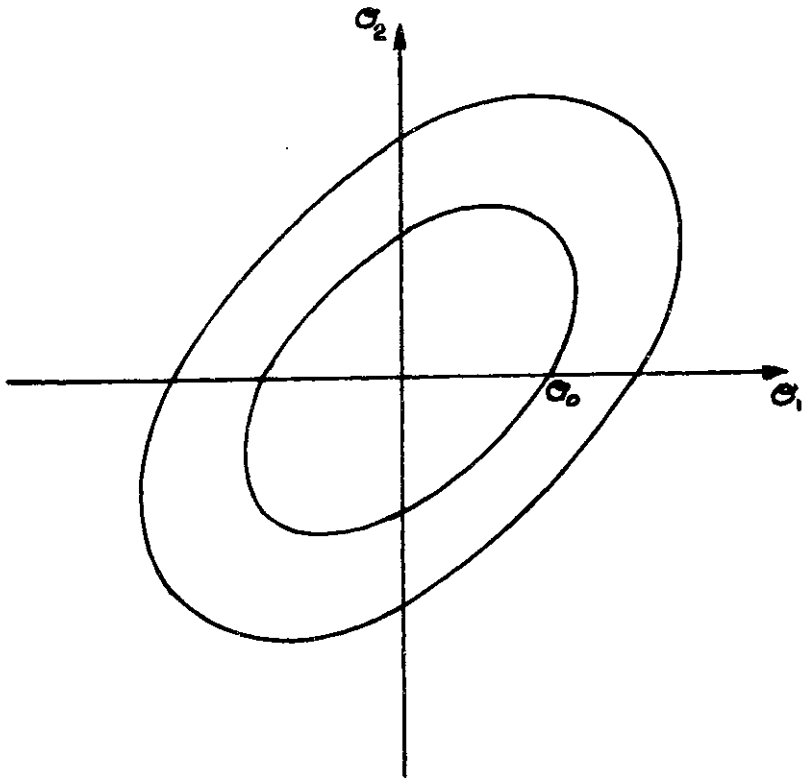

EXPANSION OF YIELD SURFACE

FIG. 3.15

$$d\underset{\sim}{\sigma} = \underset{\sim}{D}^{e}\left(d\underset{\sim}{\varepsilon} - d\underset{\sim}{\varepsilon}^{p}\right) \tag{3.34}$$

Substituting the flow rule (3.30) into the incremental plastic work equation, and replacing $d\underset{\sim}{\sigma}$ by the equivalent stress-strain relation:

$$d\bar{\varepsilon}^{p} = \frac{1}{\underset{\sim}{E}_{T}}\, \underset{\sim}{F}_{\sigma}^{T}\, d\underset{\sim}{\sigma} \tag{3.35}$$

gives:

$$d\bar{\varepsilon}_{p} = \frac{\underset{\sim}{F}_{\sigma}^{T}\, \underset{\sim}{D}^{e}\, d\underset{\sim}{\varepsilon}}{\underset{\sim}{E}_{T}^{p} + \underset{\sim}{F}_{\sigma}^{T}\, \underset{\sim}{D}^{e}\, \underset{\sim}{F}_{\sigma}} \tag{3.36}$$

Finally, substituting into the incremental stress equation yields:

$$d\underset{\sim}{\sigma} = \left[\underset{\sim}{D}^{e} - \frac{\underset{\sim}{D}^{e}\, \underset{\sim}{F}_{\sigma}\, \underset{\sim}{F}_{\sigma}^{T}\, \underset{\sim}{D}^{e}}{\underset{\sim}{E}_{T}^{p} + \underset{\sim}{F}_{\sigma}\, \underset{\sim}{D}^{e}\, \underset{\sim}{F}_{\sigma}}\right] d\underset{\sim}{\varepsilon} = \underset{\sim}{D}^{ep}\, d\underset{\sim}{\varepsilon} \tag{3.37}$$

$\underset{\sim}{D}^{ep}$ is the elastic-plastic rigidity matrix which takes the place of the elastic rigidity matrix when yielding begins.

The steps of the elastic-plastic solution after the load increment is applied are: (ref. 55)

1. Calculate additional strains and stresses $(\Delta\underset{\sim}{\varepsilon}_{1}, \Delta\underset{\sim}{\sigma}_{1})$
2. Check total stresses for yielding $(\underset{\sim}{\sigma} = \underset{\sim}{\sigma}_{0} + \Delta\underset{\sim}{\sigma}_{1})$

If plastic:

3. Calculate $\underset{\sim}{D}^{ep}$ from the total stresses
4. If yielding has occurred before, new stresses are calculated:

$$\Delta\underset{\sim}{\sigma}_{2} = \underset{\sim}{D}^{ep}\, \Delta\underset{\sim}{\varepsilon}_{1}$$

If yielding started during the current cycle the rigidity matrix is taken as:

$$\underset{\sim}{D}_m = m\underset{\sim}{D}^e + (1-m)\underset{\sim}{D}^{ep} \tag{3.38}$$

Where m is the portion of load increment that caused the first yield and the stress is computed with:

$$\Delta\underset{\sim}{\sigma}_2 = \underset{\sim}{D}_m \Delta\underset{\sim}{\varepsilon}_1 \tag{3.39}$$

5. Current stresses are: $\underset{\sim}{\sigma} = \underset{\sim}{\sigma}_0 + \Delta\underset{\sim}{\sigma}_2$

6. The unbalanced stresses are:

$$\underset{\sim}{\sigma}' = (\Delta\underset{\sim}{\sigma}_1 - \Delta\underset{\sim}{\sigma}_2)\Theta \tag{3.40}$$

(Θ will be defined when solution strategies are explained)

7. The unbalanced load vector is:

$$\underset{\sim}{P}' = \int \underset{\sim}{B}\,\underset{\sim}{\sigma}'\, dV \tag{3.41}$$

and the new stiffness matrix is:

$$\underset{\sim}{K} = \int \underset{\sim}{B}^T \underset{\sim}{D}^{ep} \underset{\sim}{B}\, dV \tag{3.42}$$

3.5 Nonlinear Solution Strategies

There are several solution strategies to analyze nonlinear structural behavior, by using either incremental or iterative linear procedures. The simplest and best known iterative procedure is the Euler-Cauchy method (fig.3.16) which is represented by

$$\begin{aligned} \underset{\sim}{K}_N \Delta\underset{\sim}{U}_N &= \Delta\underset{\sim}{P} \\ \underset{\sim}{U}_{N+1} &= \underset{\sim}{U}_N + \Delta\underset{\sim}{U}_N \end{aligned} \tag{3.43}$$

where K_n is the tangent stiffness matrix.

INCREMENTAL TANGENT STIFFNESS METHOD

FIG. 3.16

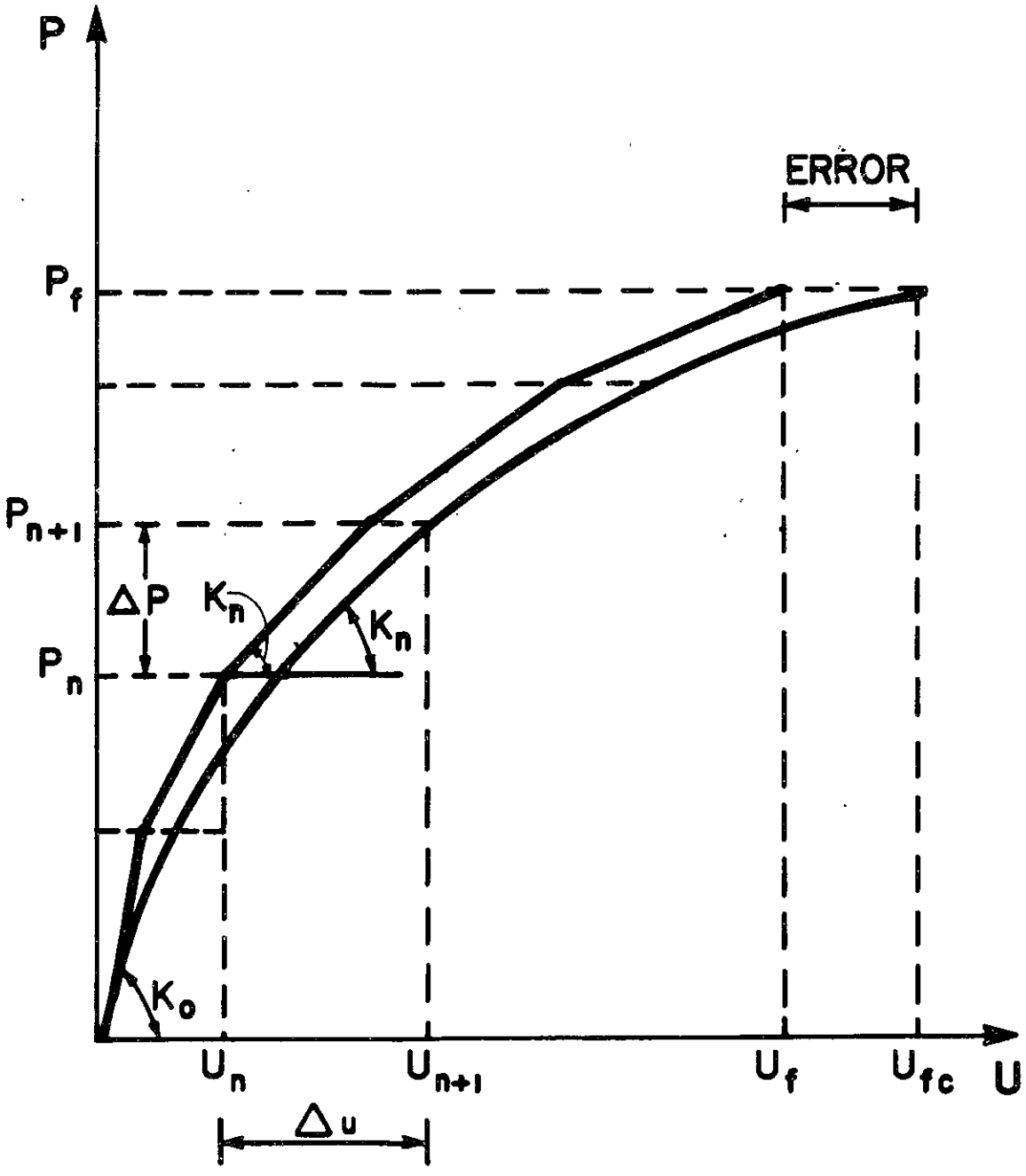

Computation provides one solution per load step,and no iteration is made. The error is accumulated at each step, and will become large if small load steps are not used.

In iterative schemes, the structure is solved several times for the same load increment. Convergence is achieved by reducing the unbalanced load, P_u, where:

$$\underset{\sim}{P}_u = \int \underset{\sim}{B}^T (\underset{\sim}{\sigma} - \underset{\sim}{\sigma}^*)\, dV \tag{3.44}$$

σ = assumed stresses calculated using the rigidity at the beginning of the cycle

σ^* = actual stresses for calculated displacements

At the end of each iteration, a new tangent stiffness matrix is generated:

$$\underset{\sim}{K}_i = \int \underset{\sim}{B}^T \underset{\sim}{D}_i \underset{\sim}{B}\, dV \tag{3.45}$$

which is used to analyze the structure for the unbalanced load, P_u. This is the Newton-Raphson solution procedure, and can be formulated as:

$$\underset{\sim}{U} = \underset{\sim}{K}_0^{-1} \underset{\sim}{P} + \Sigma \underset{\sim}{K}_i^{-1} \underset{\sim}{P}_{u_i} \tag{3.46}$$

To save computational time, the modified Newton-Raphson method which uses the initial stiffness of the structure for each iteration can be applied: (fig. 3.17)

$$\underset{\sim}{U} = \underset{\sim}{K}_0^{-1} \underset{\sim}{P} + \Sigma \underset{\sim}{K}_0^{-1} \underset{\sim}{P}_{u_i} \tag{3.47}$$

The variable stiffness method will use less iterations, but will take more time in calculating each new stiffness matrix.

A more general solution procedure presented by Connor and Sarne (ref. 17) is based on the Crank-Nicholsen numerical integration scheme

VARIBLE STIFFNESS METHOD

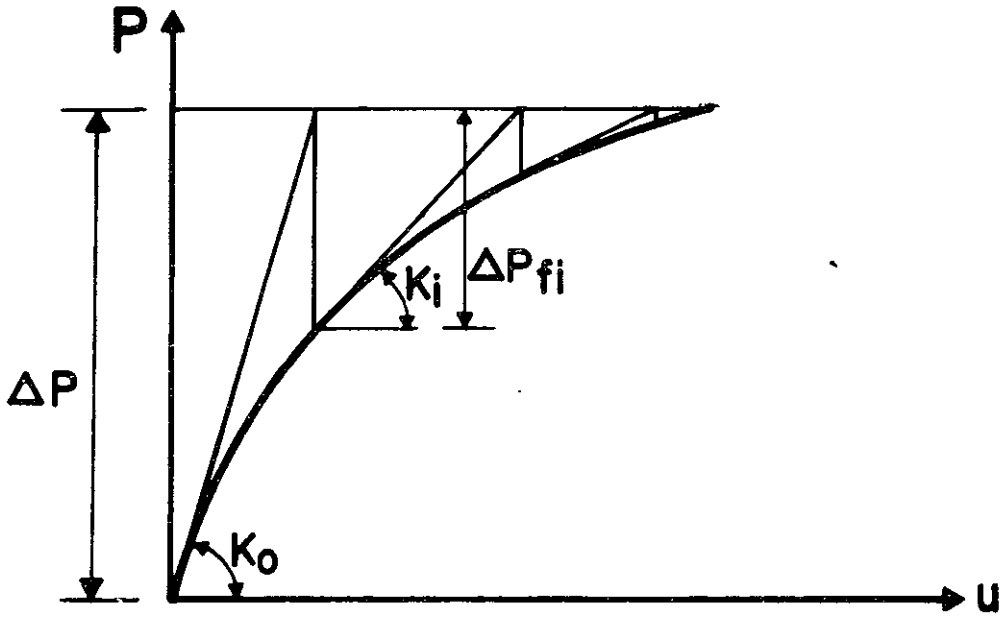

CONSTANT STIFFNESS METHOD

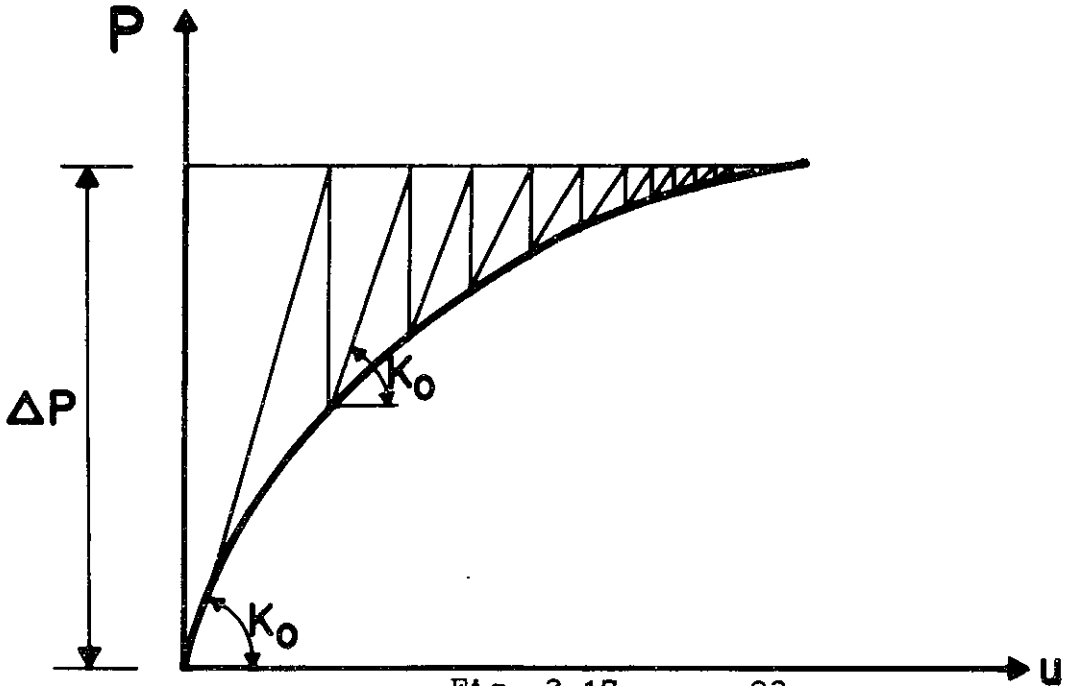

Fig. 3.17

which approximates the stress increment by:

$$\Delta \underset{\sim}{\sigma}_N = \underset{\sim}{\sigma}_{N+1} - \underset{\sim}{\sigma}_N = [\theta \underset{\sim}{D}_N + (1-\theta) D_{N+1}] \Delta \underset{\sim}{\varepsilon} + (ER) \Delta \varepsilon \tag{3.48}$$

where ER is the truncation error. The unbalanced load vector, $\underset{\sim}{P}_u$, becomes:

$$\underset{\sim}{P}_u = \int B^T ((1-\theta) \underset{\sim}{D}_N - (1-\theta) \underset{\sim}{D}_{N+1}) \Delta \underset{\sim}{\varepsilon}_N \tag{3.49}$$

For $\theta = 1$, the scheme coincides with the Euler method with no unbalanced load vector, and $\theta = 0$ is equivalent to the backward difference method where:

$$\Delta \underset{\sim}{\sigma}_N = \underset{\sim}{D}_{N+1} \Delta \underset{\sim}{\varepsilon}_N \tag{3.50}$$

The optimum choice of θ is found by looking at the truncation error, for which a minimum is obtained by setting $\theta = 1/2$. Thus, the stress increment is:

$$\Delta \underset{\sim}{\sigma}_N = (\tfrac{1}{2} \underset{\sim}{D}_N + \tfrac{1}{2} \underset{\sim}{D}_{N+1}) \Delta \underset{\sim}{\varepsilon}_N \tag{3.51}$$

and the unbalanced load vector is:

$$\underset{\sim}{P}_u = \int \underset{\sim}{B}^T (\tfrac{1}{2} \underset{\sim}{D}_N - \tfrac{1}{2} \underset{\sim}{D}_{N+1}) \Delta \underset{\sim}{\varepsilon}_N \tag{3.52}$$

The error resulting from an iterative method depends on the convergence criteria selected. Available indicators are the unbalanced load vector and incremental displacements. Comparing incremental displacements to total displacements can lead to premature convergence as is shown by the load-displacement curve of Wight's beam. (ref. 55) (fig. 3.18) Also, the possible effect of applying too large a load step is seen.

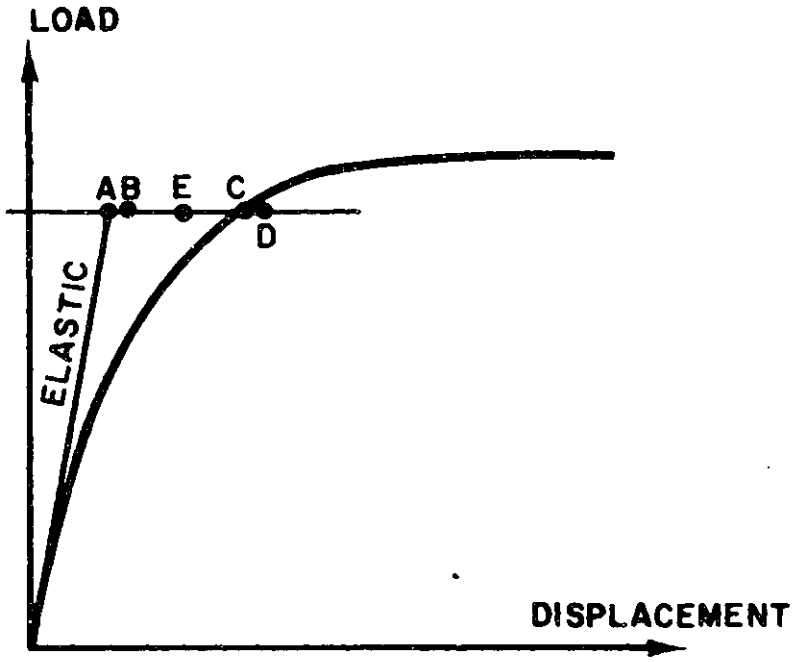

A ELASTIC SOLUTION

B ONE STEP-ITERATION WITH ELASTIC STIFFNESS

C INCREMENTAL SOLUTION-ITERATION WITH UPDATED STIFFNESS

D ONE STEP-ITERATION WITH UPDATED STIFFNESS

E INCREMENTAL SOLUTION - ITERATION WITH CONSTANT STIFFNESS

DEFLECTION OF WIGHT'S BEAM

FIG. 3.19

3.6 Steps of a Nonlinear Finite Element Analysis

At this point, the steps in performing a nonlinear finite element analysis are listed. The analysis will use an iterative solution strategy with variable tangent stiffness. This description holds for each step in the load sequence.

1. Calculate the stiffness matrix:

$$\underset{\sim}{K} = \int \underset{\sim}{B}^T \underset{\sim}{D}_o \underset{\sim}{B} \, dV \tag{3.53}$$

on the element level, and then assembled to the structural stiffness matrix. In each element, the stiffness of each integration point is calculated in the principal directions, rotated to the global coordinate frame, and then, using numerical integration, the element stiffness if found.

$$\underset{\sim}{K}_e = \sum_{i=1}^{n} \underset{\sim}{B}_i^T \underset{\sim}{D}_{oi} \underset{\sim}{B}_i * WF_i \tag{3.54}$$

n is the number of integration points in the element and WF is the weight factor of each integration point.

2. Calculate the load vector:

$$\underset{\sim}{P} = \underset{\sim}{P}_N + \underset{\sim}{P}_\varepsilon + \underset{\sim}{P}_\theta + \underset{\sim}{P}_P + \underset{\sim}{P}_U \tag{3.55}$$

where $\underset{\sim}{P}_U$ is the unbalanced load of the previous step. This is also done at the element level and assembled to the structural load vector.

3. Solved for the incremental unknown nodal displacements, $\Delta \underset{\sim}{U}_N$:

$$\underset{\sim}{K} \Delta \underset{\sim}{U}_N = \underset{\sim}{P} \tag{3.56}$$

The solution is performed using Gauss elimination techniques which triangularizes $\underset{\sim}{K}$. $\Delta \underset{\sim}{U}_N$ is then calculated by back substitution.

4. Calculate the incremental strains at the integration points in each element from the incremental displacements, $\Delta \underset{\sim}{U}_N$:

$$\Delta \underset{\sim}{\varepsilon} = \underset{\sim}{B}\, \Delta \underset{\sim}{U}_N \tag{3.57}$$

5. The exact incremental stresses for the given strain state are then calculated:

$$\Delta \underset{\sim}{\sigma}^* = \underset{\sim}{D}_1 \Delta \underset{\sim}{\varepsilon} \tag{3.58}$$

For concrete, D_1 is the secant rigidity matrix.

6. Yielding is checked. If yielding occurs, the new stresses are calculated:

$$\Delta \sigma^* = \underset{\sim}{D}_2 \Delta \underset{\sim}{\varepsilon} \tag{3.59}$$

7. The unbalanced load vector is calculated:

$$\underset{\sim}{P}_U = \int \underset{\sim}{B}^T \underset{\sim}{D}_3 (\Delta \underset{\sim}{\sigma} - \Delta \underset{\sim}{\sigma}^*)\, dV \tag{3.60}$$

where:

$$\Delta \underset{\sim}{\sigma} = \underset{\sim}{D}_0 \Delta \underset{\sim}{\varepsilon}$$

$\underset{\sim}{D}_0$ is the initial tangent rigidity at the beginning of the cycle, and $\underset{\sim}{D}_3$ is the new value.

8. Convergence is then checked. If the solution has converged (reached equilibrium) and there are more load steps, steps 1 - 8 are repeated. If the solution hasn't converged, steps 1 - 8 are then repeated where for step 2 only the unbalanced load vector is applied.

Chapter IV

Analysis of Prestressed Concrete Pressure Vessels Using the Nonlinear Finite Element Displacement Method

4.1 Introduction

The nonlinear finite element analysis of the pressure vessel shown in fig. 1.4 will now be described. Of particular interest are the assumptions introduced in constructing the finite element model, the nonlinear material properties, and the load sequence which simulates the expected life of the structure for normal and abnormal conditions. The different models considered in the analysis and some results are shown. This presentation is focused more on describing the steps in the analysis of a pressure vessel than on attempting to display results.

4.2 The Pressure Vessel

The pressure vessel, shown in fig. 4.1, is a podded boiler vessel with nine circular cavities spread around the periphery of the reactor. The six steam generator cavities extend the full height of the vessel, and are symmetrically placed, while the three which house the auxiliary cooling equipment, lie between two generators, and are placed at 120° to one another. All the openings are connected to the core cavity by two cross ducts.

Prestressing is achieved by vertical and circumferential cables. The vertical system is comprised of 456 unbonded cables extending the full height of the vessel, 96 of which continue through to the base of the mat. The circumferential prestressing consists of wire strand wound around the external surface, and is assumed to be bonded to the vessel by the radial

Ⓐ REACTOR CAVITY
Ⓑ STEAM GENERATOR CAVITY
Ⓒ AUX. COOLING LOOP CAVITY

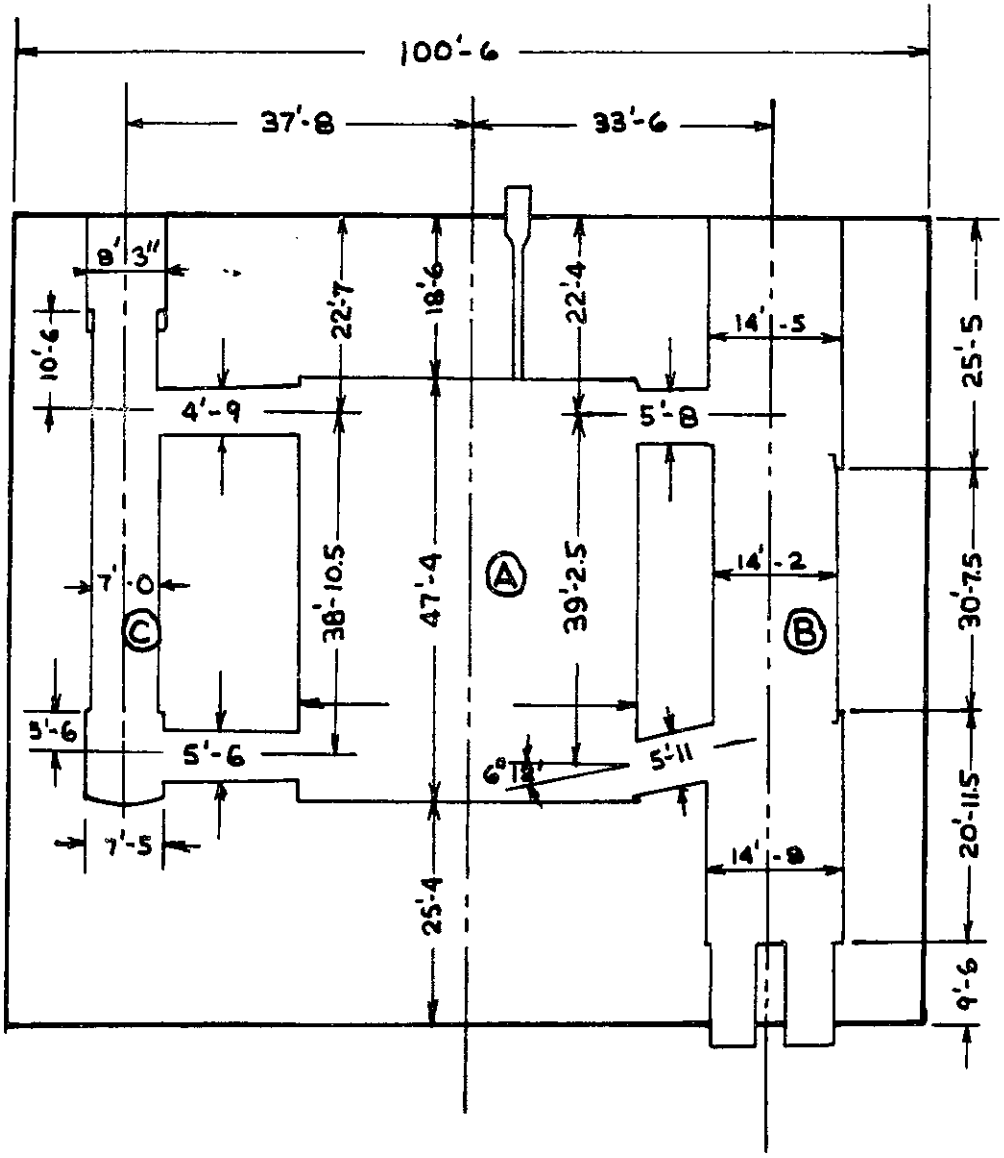

DIMENSIONS OF PRESSURE VESSEL

FIG. 4.1

pressure.

Bonded reinforcing steel is placed near the interior and exterior concrete surfaces of the vessel, around the prestressing tendon anchor plates, and through the top head standpipe region. All the vessel cavities are lined with a gas-tight steel liner with thickness varying from 3/4 inch in the core cavity to 1/2 in the auxiliary cooling loop cavity.

4.3 Finite Element Modeling

The initial finite element model consists of a 30° section defined by radials passing through an auxiliary cooling loop cavity and an adjacent steam generator. (fig. 4.2) The model extends to the bottom of the mat below the support, where it is assumed to be fixed in the vertical direction. Symmetry is introduced by constraining the circumferential displacement at nodes in the radial boundary planes. Concrete is modeled with the 20 node brick element described earlier. There are fifteen integration points located symmetrically throughout the element volume. Nonlinearities are checked at each integration point, which allows simulation of partial cracking, and the use of reasonably large elements.

Elements for the standpipe region have reduced Young's modulus, E, varying according to the equation presented by Harrop et al. (ref. 30) A more refined model of this area including the penetrations (fig. 4.3) has its external boundary at the top head-side wall junction. The boundary conditions are obtained from results for the main 30° model. The crossducts connecting the cavities of the steam generators and auxiliary cooling loops to that of the core were ignored in the original model, but are included in more refined models of the top and bottom corners of the core

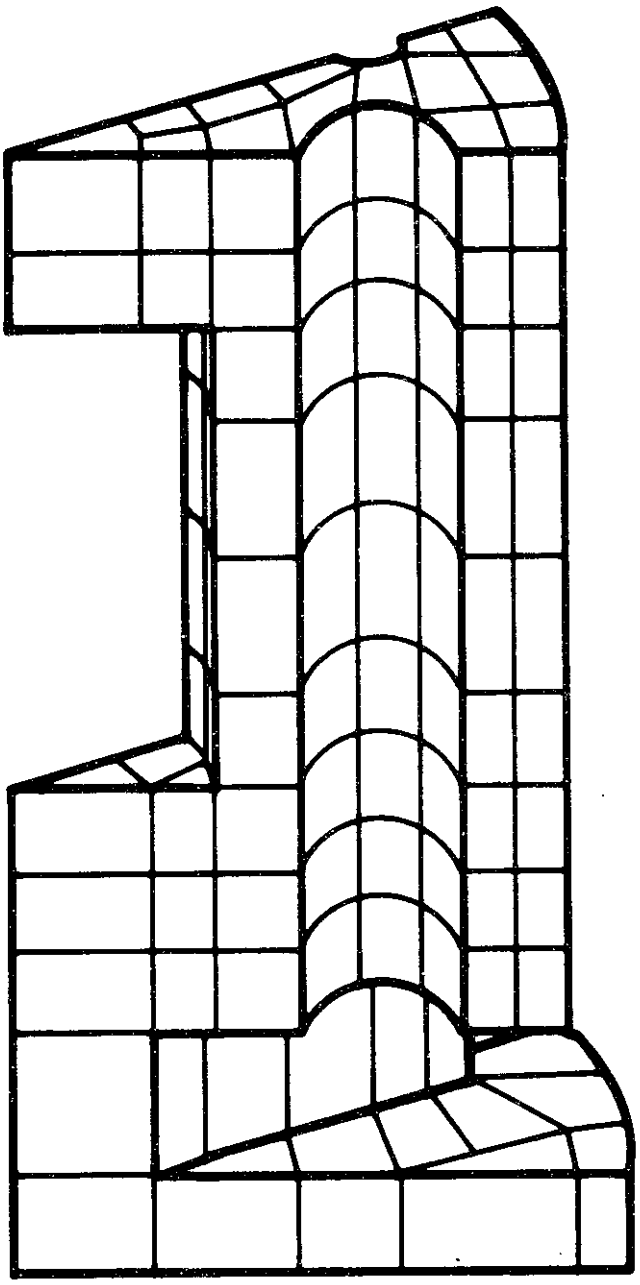

3-D FINITE ELEMENT MODEL
OF PRESTRESSED CONCRETE
REACTOR VESSEL

Fig. 4.2

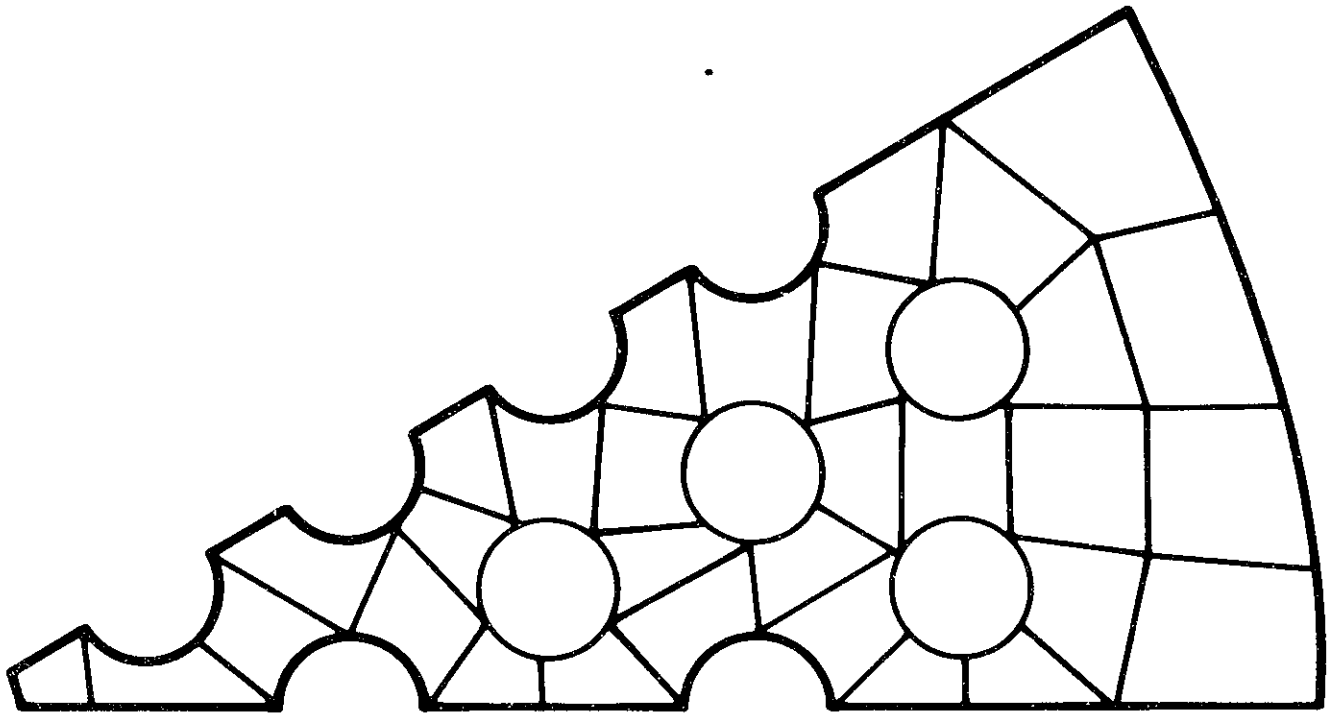

FIG. 4.3

PCRV TOP HEAD FINITE ELEMENT MODEL

cavity. (fig. 4.4, 4.5)

Steel reinforcement and liner are modeled with an 8 node membrane element having nine Gauss integration points. To ensure interelement compatibility, the membrane elements must be placed on the sides of the brick elements, and this necessitates lumping the reinforcement at the faces of the concrete elements. The triangular pattern between the standpipes is modeled by equivalent plate elements with modified Young's modulus and Poisson ratio. (ref. 7) The calculations are based on strain energy formulations, and will not give exact results if nonlinearities occur. However, results are expected to be better than for other modeling techniques available, and yielding is not considered to be a problem in this area except under the most extreme conditions.

No additional stiffness is given to the model due to the prestressing system, but variation of the prestress force due to expansion and contraction of the cable is included. Because the cable forces must be applied at the nodes of the elements, it was necessary to develop an acceptable method for grouping the distributed cable forces at nodes. The method selected (fig. 4.6) calculated the equivalent stress distribution for all the cables which were anchored within the element, which was then divided into four nodal forces applied at the midnodes of the element face. Due to differences at the top and bottom head modeling, an average force was applied to the equivalent cables. This permitted the calculation of an accurate estimate of prestress loss because the total force in the equivalent cables was equal to the actual cable force of the vessel. To correct the load distribution on the top and bottom faces, a system of self-equilibrating nodal forces was applied. Relaxation of prestress

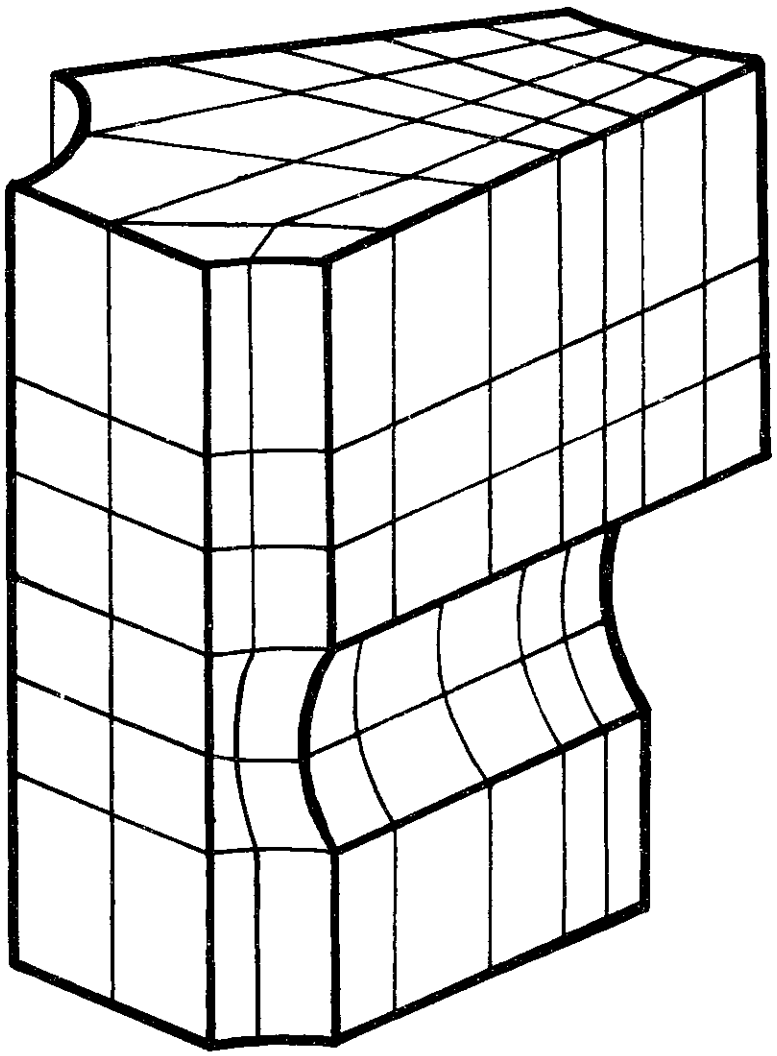

FINITE ELEMENT MODEL OF CORE CAVITY TOP CORNER

FIG. 4.4

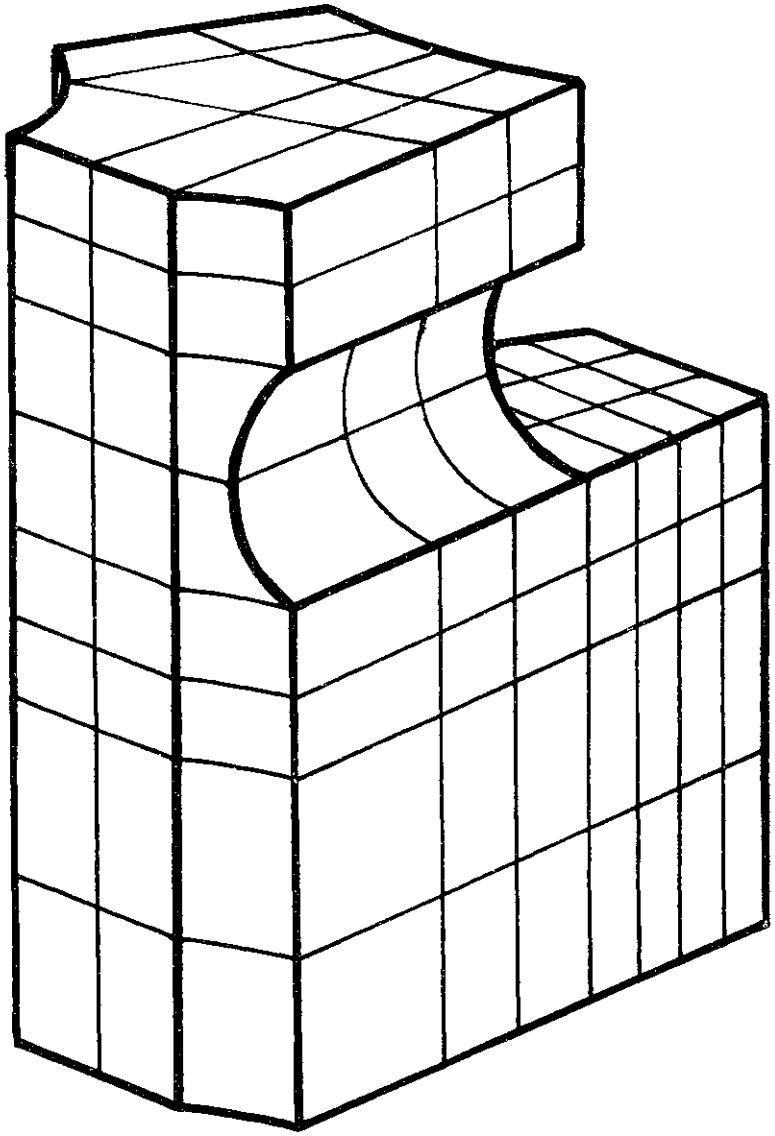

FINITE ELEMENT MODEL OF CORE CAVITY BOTTOM CORNER

FIG. 4.5

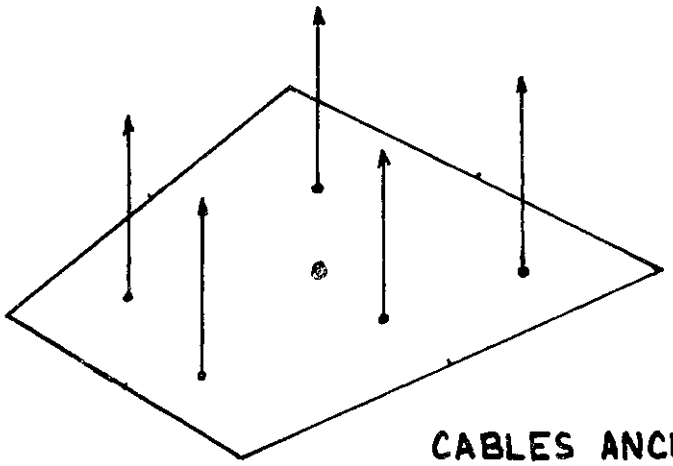

CABLES ANCHORED IN ELEMENT

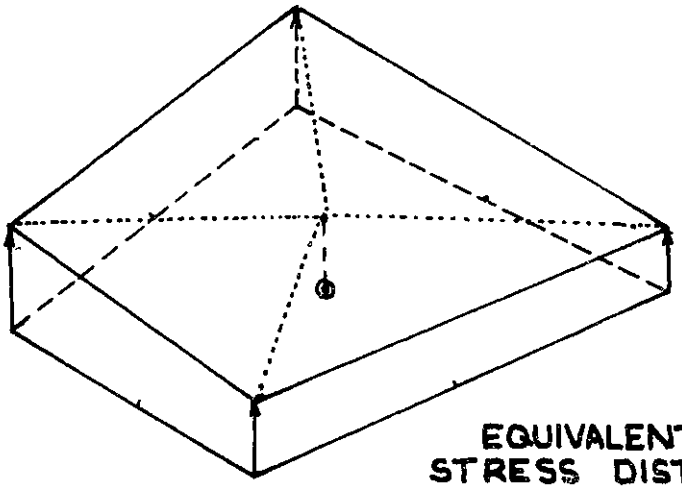

EQUIVALENT STRESS DISTRIBUTION

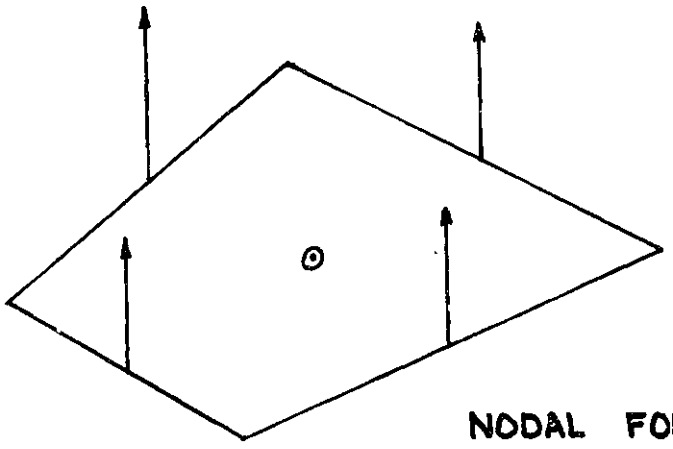

NODAL FORCES

Fig. 4.6 MODELING OF PRESTRESS CABLES

cables during the life of the vessel was calculated with the expression for strain presented by Cahill et al. (ref. 14):

$$\Delta\varepsilon = \frac{a\,t^m}{m} + b \tag{4.1}$$

where a, b, and m are functions of the cable temperature and t is the life of the vessel in hours.

Additional finite element models to be considered in the analysis include a refined model of the support of the PCRV (fig. 4.7) and models of the steampipe area at the bottom of the steam generator cavity, and the concrete plug at the top.

A study was performed to see how accurate the results of a model of the top half of the pressure vessel would be. Comparisons were made with the complete 30° model for the following load cases: initial prestress and dead load; one year after prestress; twice the maximum cavity pressure after one year; and an abnormal temperature and pressure after one year. Results shown for two cases (fig. 4.8-4.11) indicate that a coarse model of the top half of the pressure vessel will give a representative picture of the behavior and could be used to study modes of failure. However, to obtain results which can be used as boundary conditions in more refined models, a full size is suggested.

4.4 Loadings

The loading sequence for the model (fig. 4.12) was chosen to simulate the actual life of the normal vessel. This included prestressing, pressure test, start up, operating conditions, and annual shut down for refueling. As each load was applied, the effect of creep was also calculated. Abnormal, severe, and extreme loading combinations the vessel must be

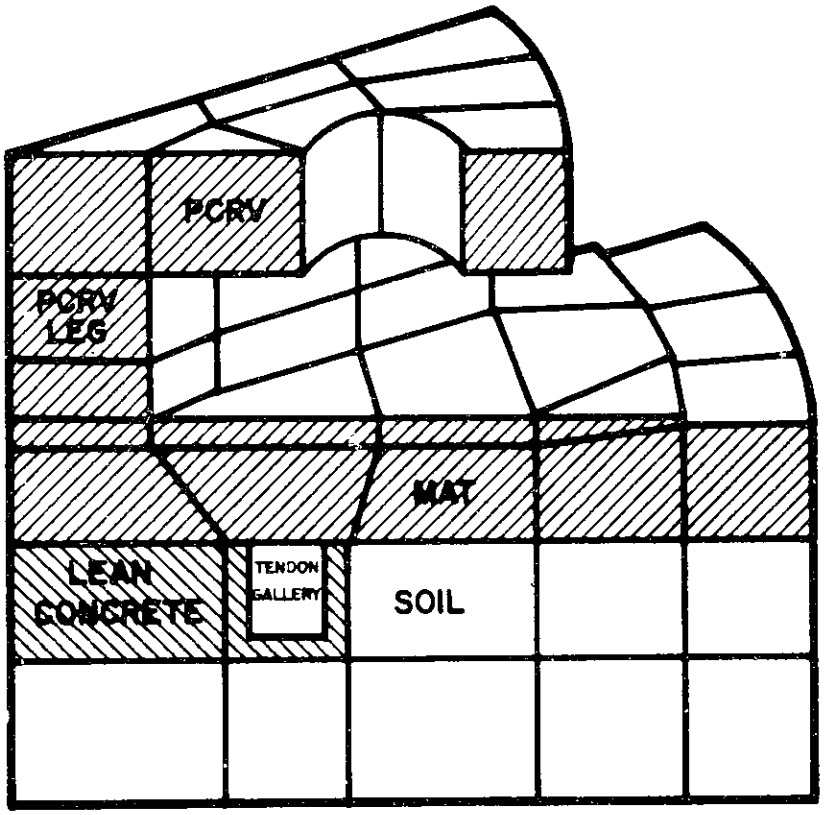

PCRV LEG
FINITE ELEMENT MODEL

Fig. 4.7

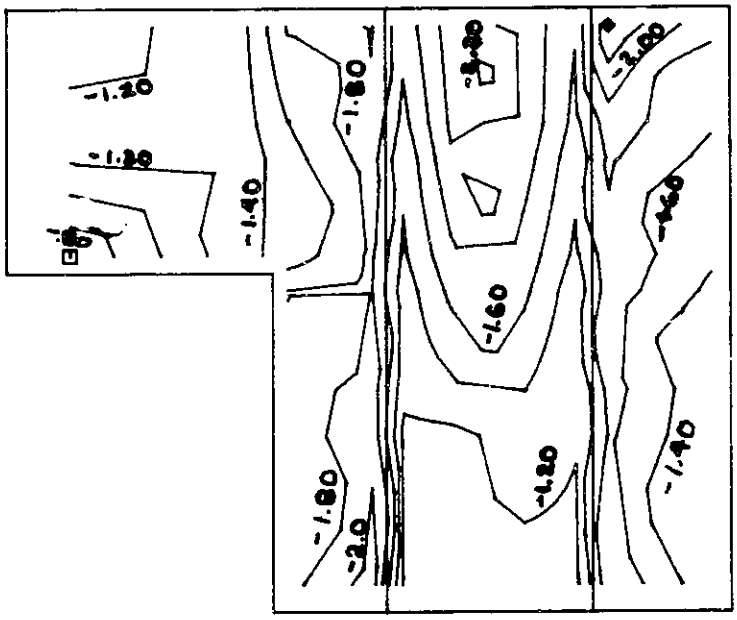

STRESSES- PRESTRESS (HALF MODEL)

FIG. 4.8

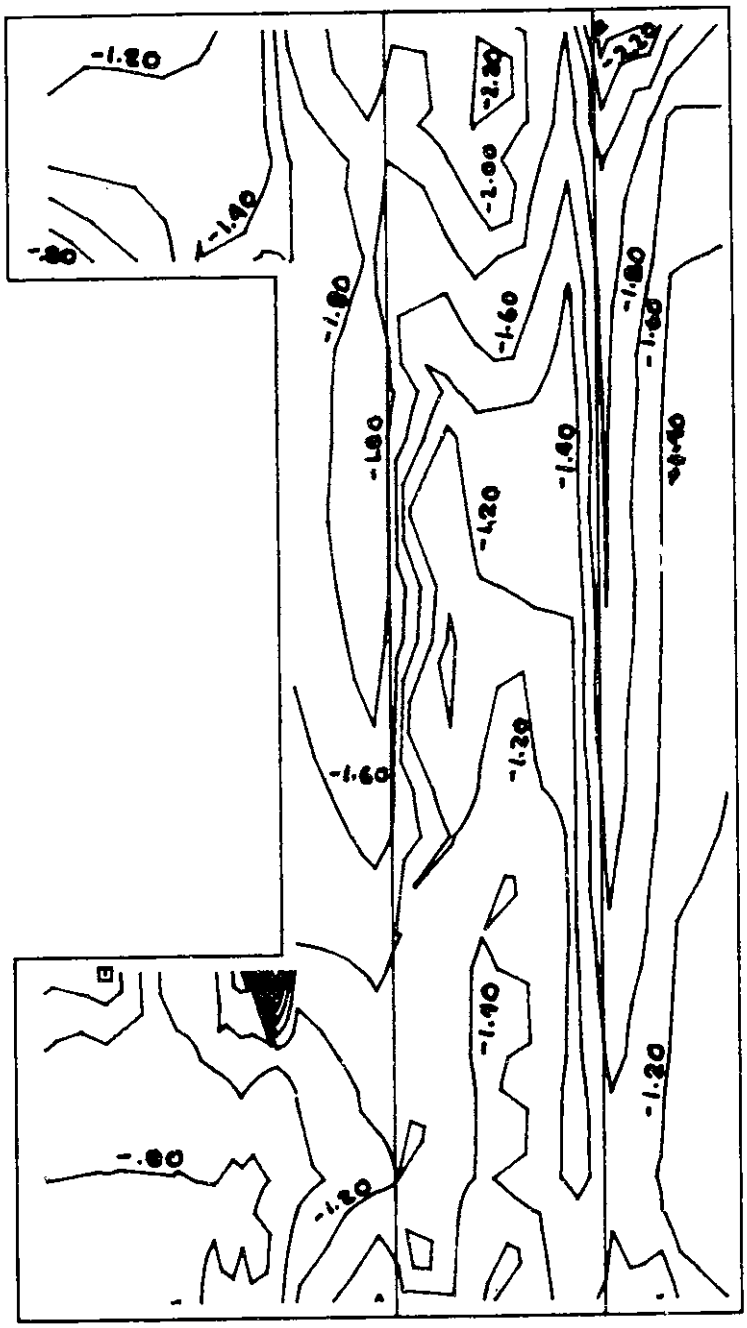

STRESSES - PRESTRESS (FULL MODEL)

FIG. 4.9

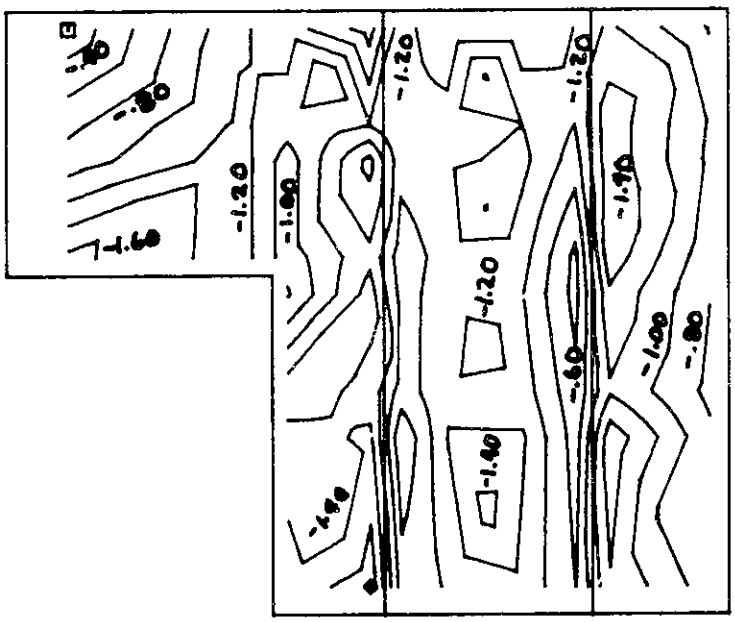

STRESSES - 2 × MCP (HALF MODEL)

FIG. 4.10

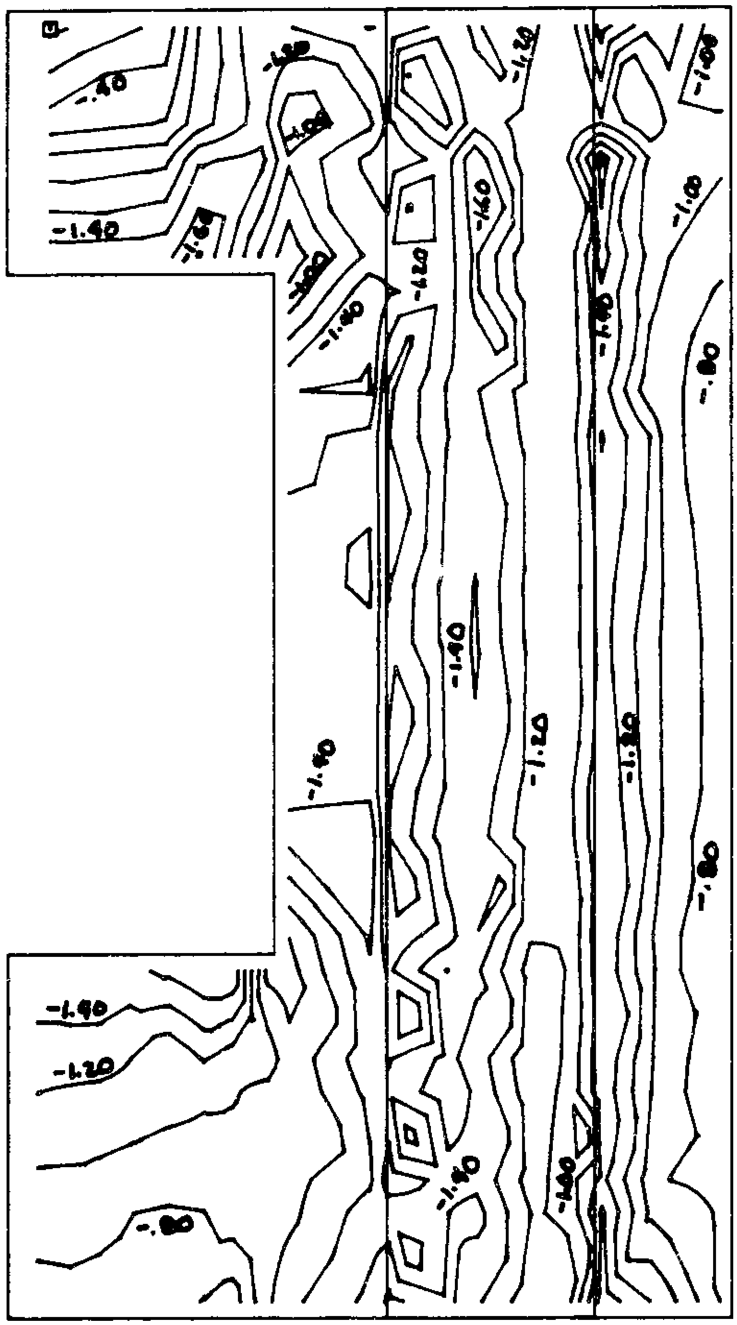

STRESSES- 2 × MCP (FULL MODEL)

FIG. 4.11

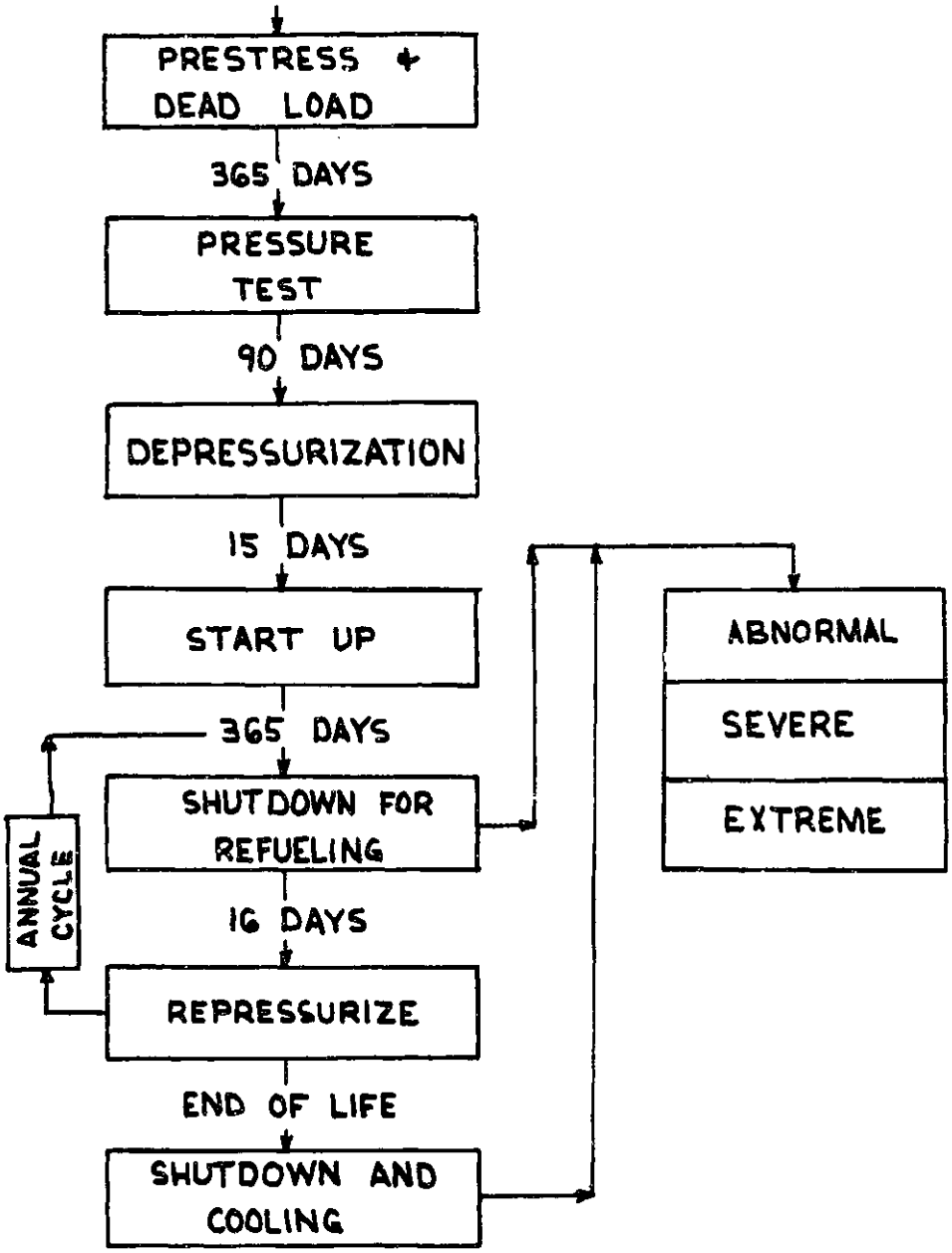

LOAD SEQUENCE

FIG. 4.12

able to withstand are applied after one year and at the end of the vessel's expected life.

4.5 Results

Results are shown for a vertical section through the steam generator cavity, and a horizontal section at the midheight of the sidewall. Plots include contours of the maximum negative principal stresses calculated at the integration points, and nodal displacements. (fig. 4.13-4.19) Additional results for several abnormal cases and overpressure are presented by Sarne. (ref. 55)

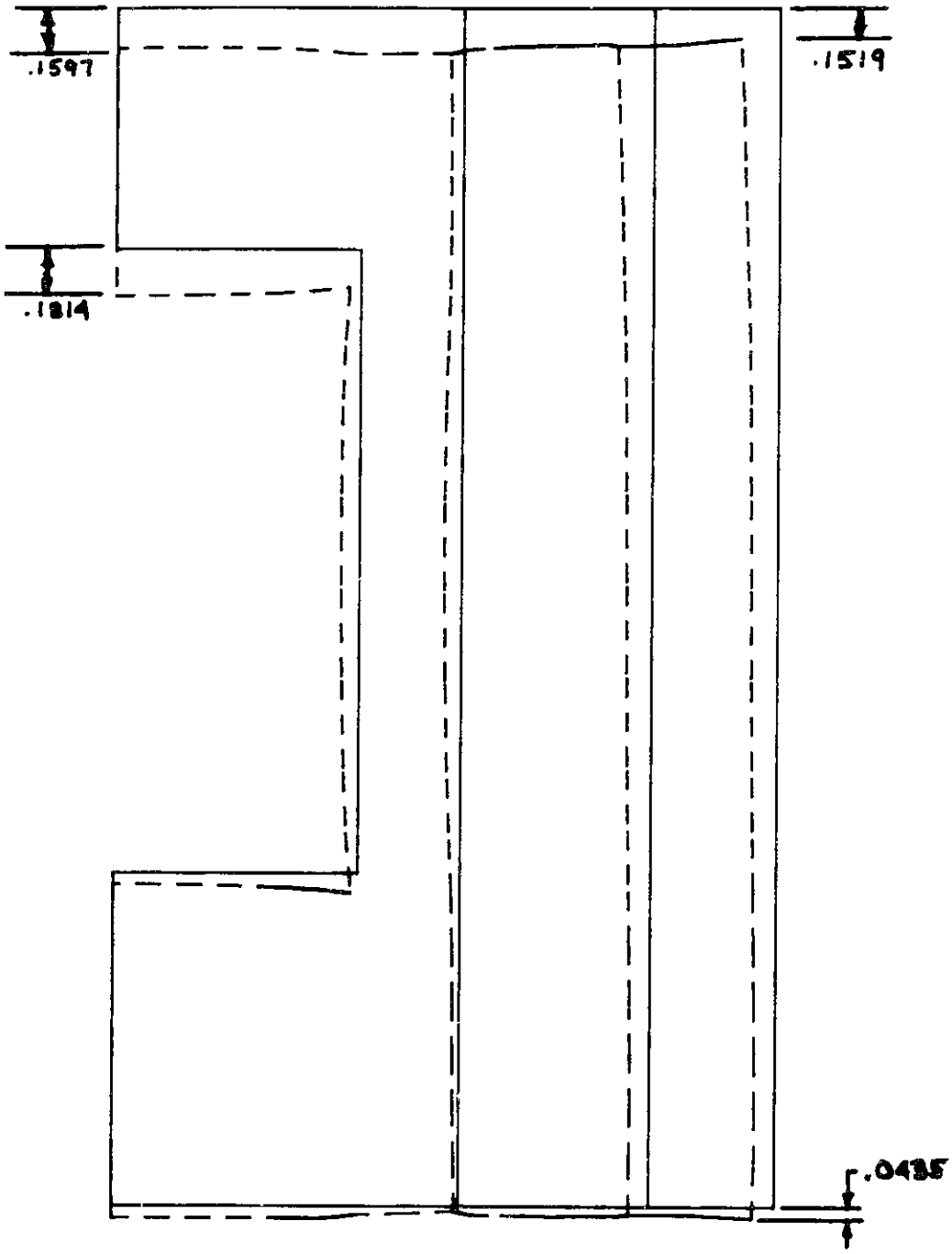

DISPLACEMENTS- PRESTRESS + DEAD LOAD

FIG. 4.13

DISPLACEMENTS - PRESTRESS + DEAD LOAD

FIG. 4.14

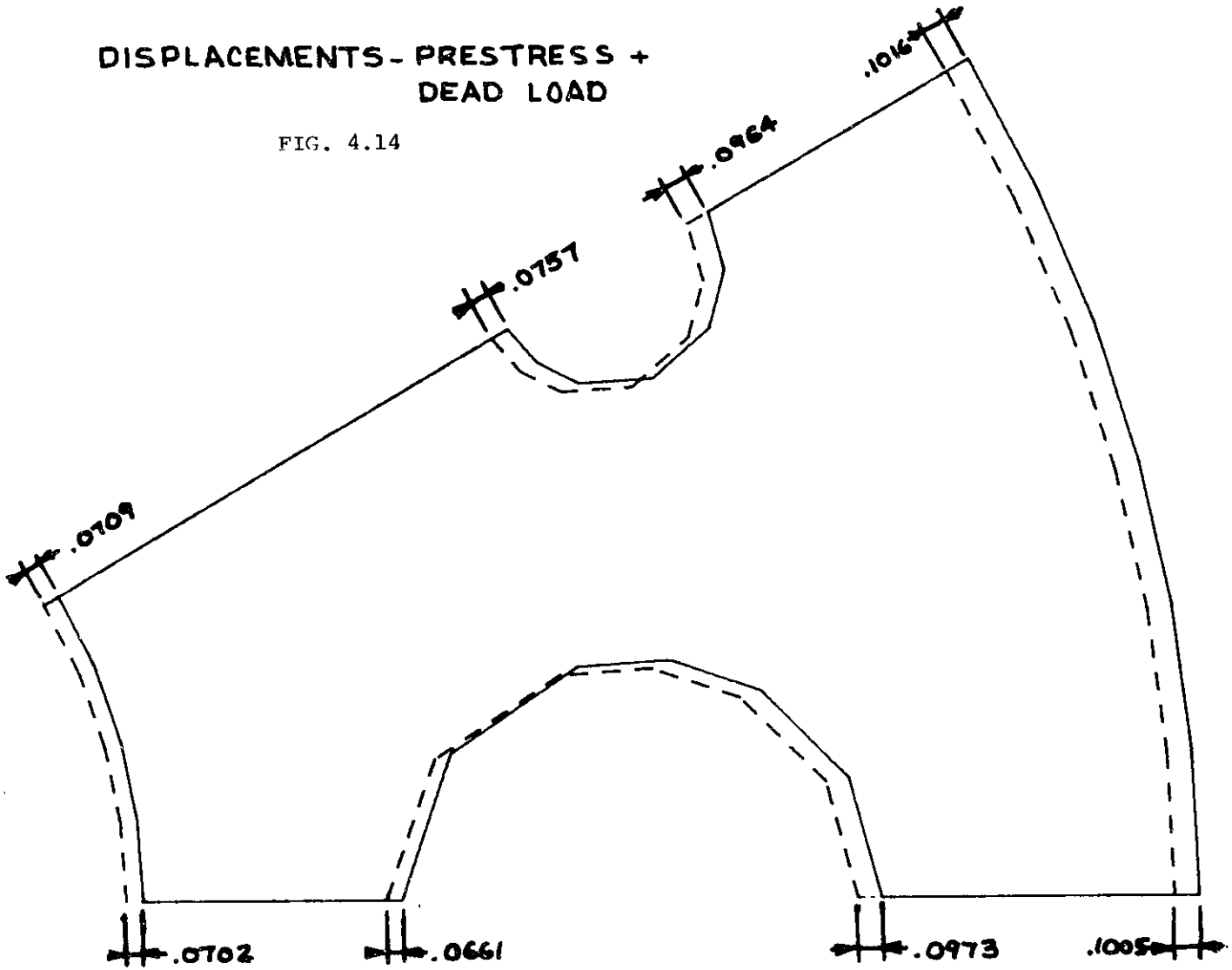

STRESSES - PRESTRESS + DEAD LOAD

FIG. 4.15

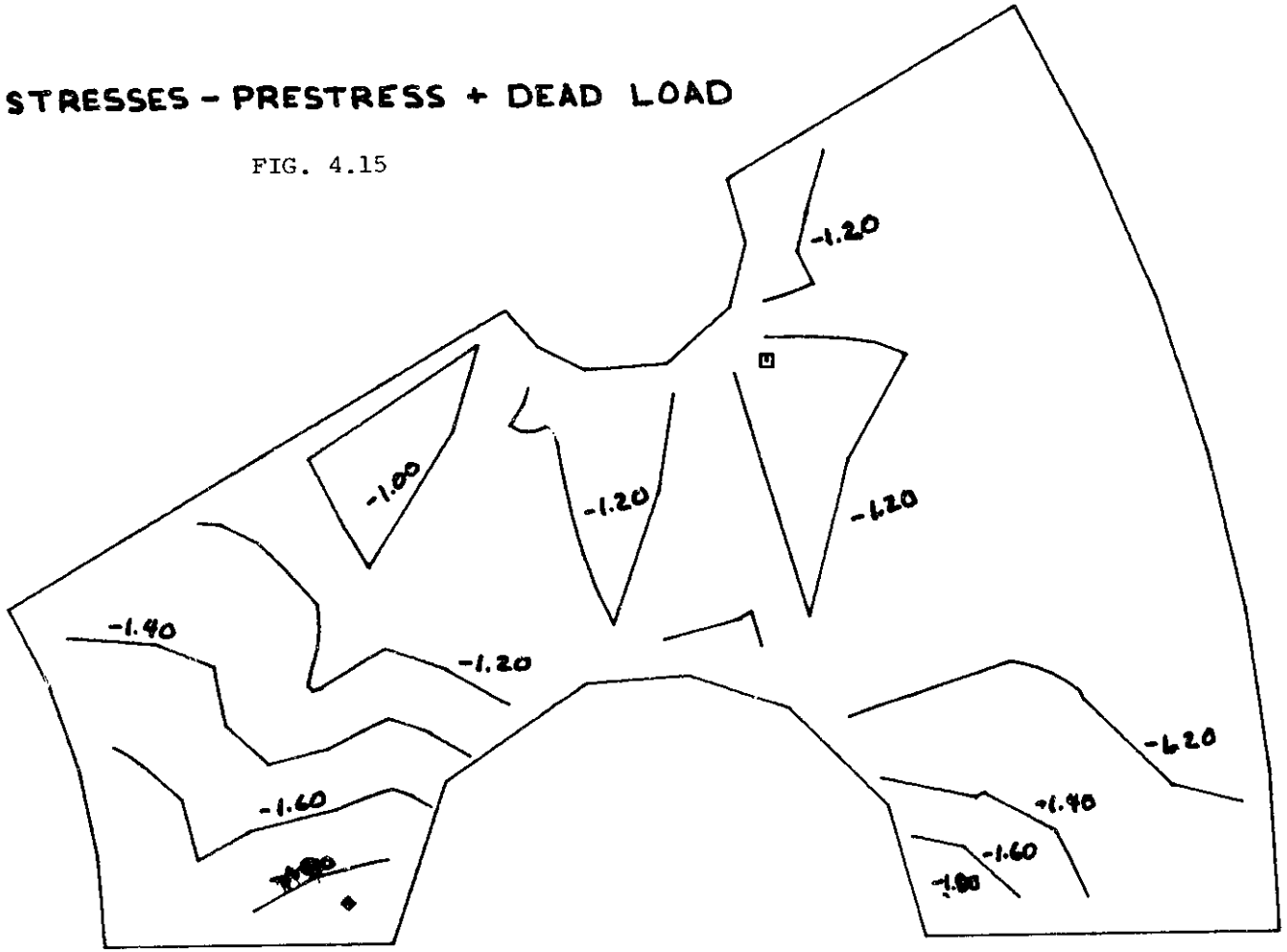

DISPLACEMENTS - ONE YEAR AFTER PRESTRESS

FIG. 4.16

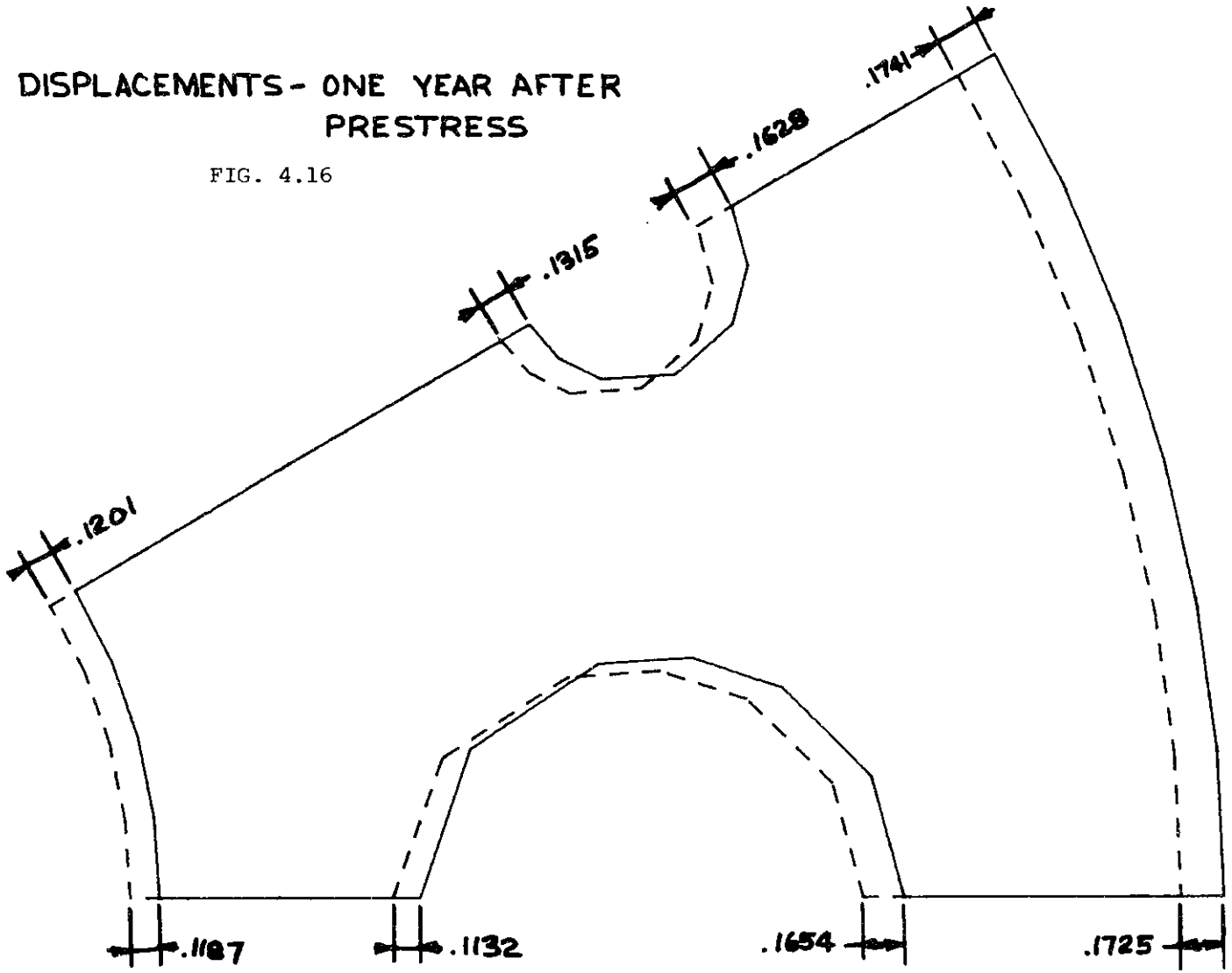

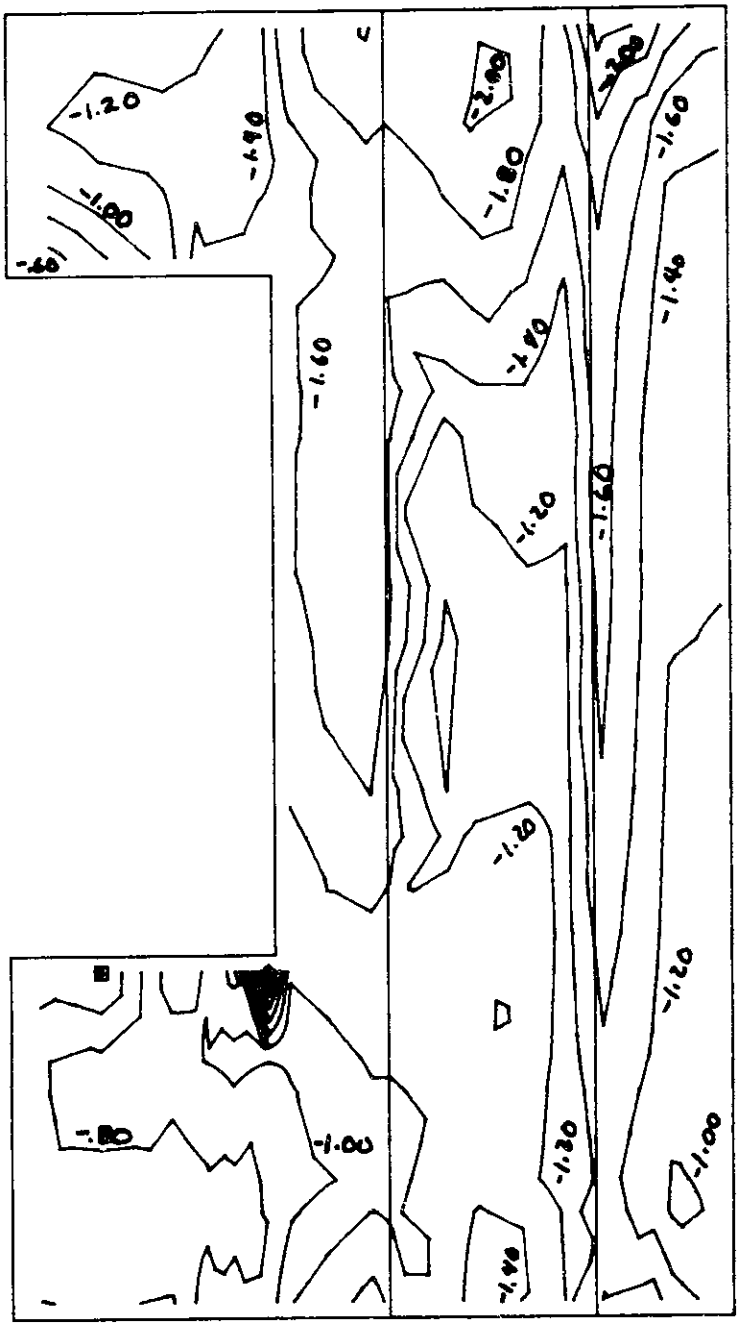

STRESSES- ONE YEAR AFTER PRESTRESS

FIG. 4.17

STRESSES- ONE YEAR AFTER PRESTRESS

FIG. 4.18

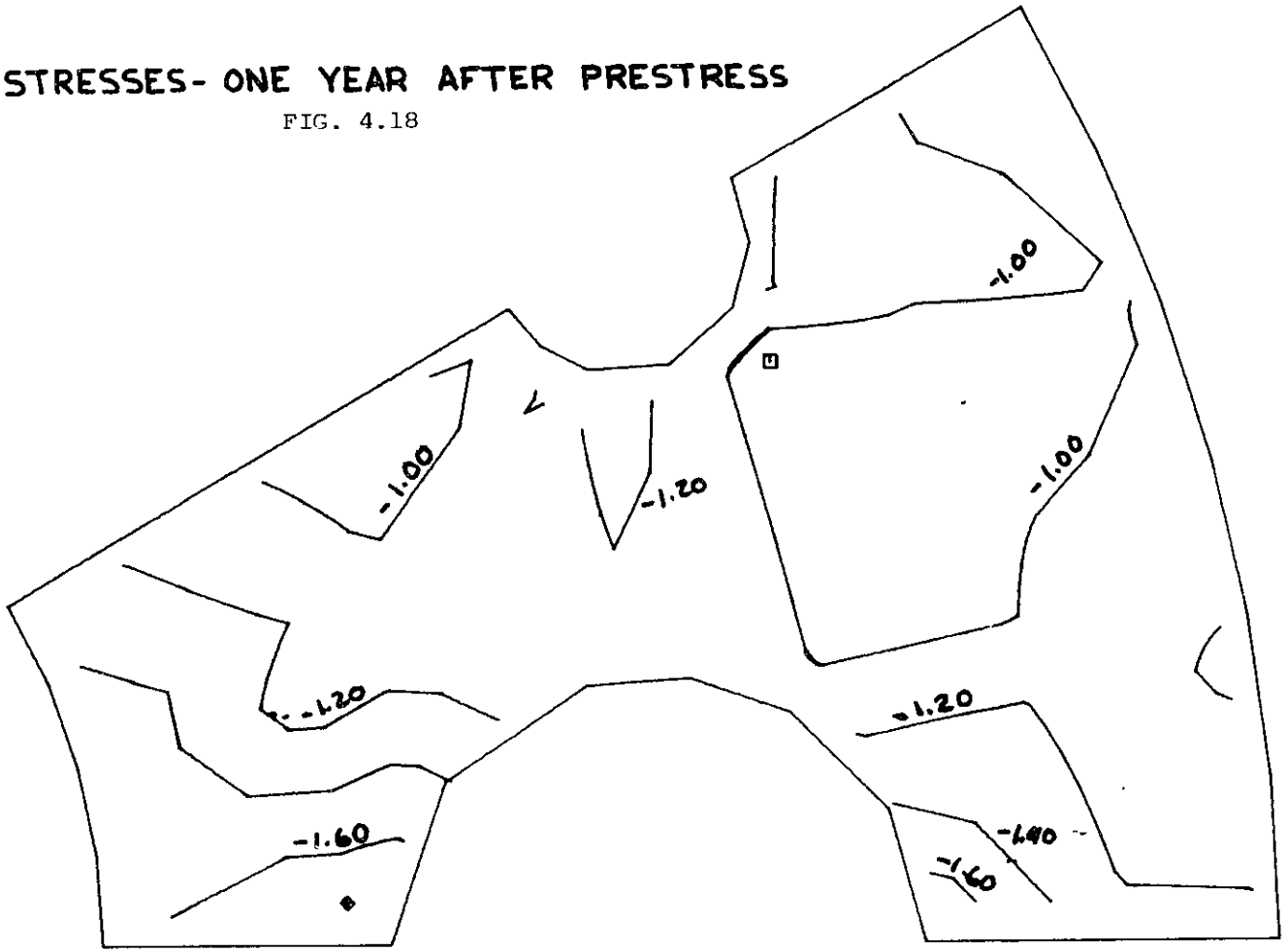

STRESSES- 2 × MCP

FIG. 4.19

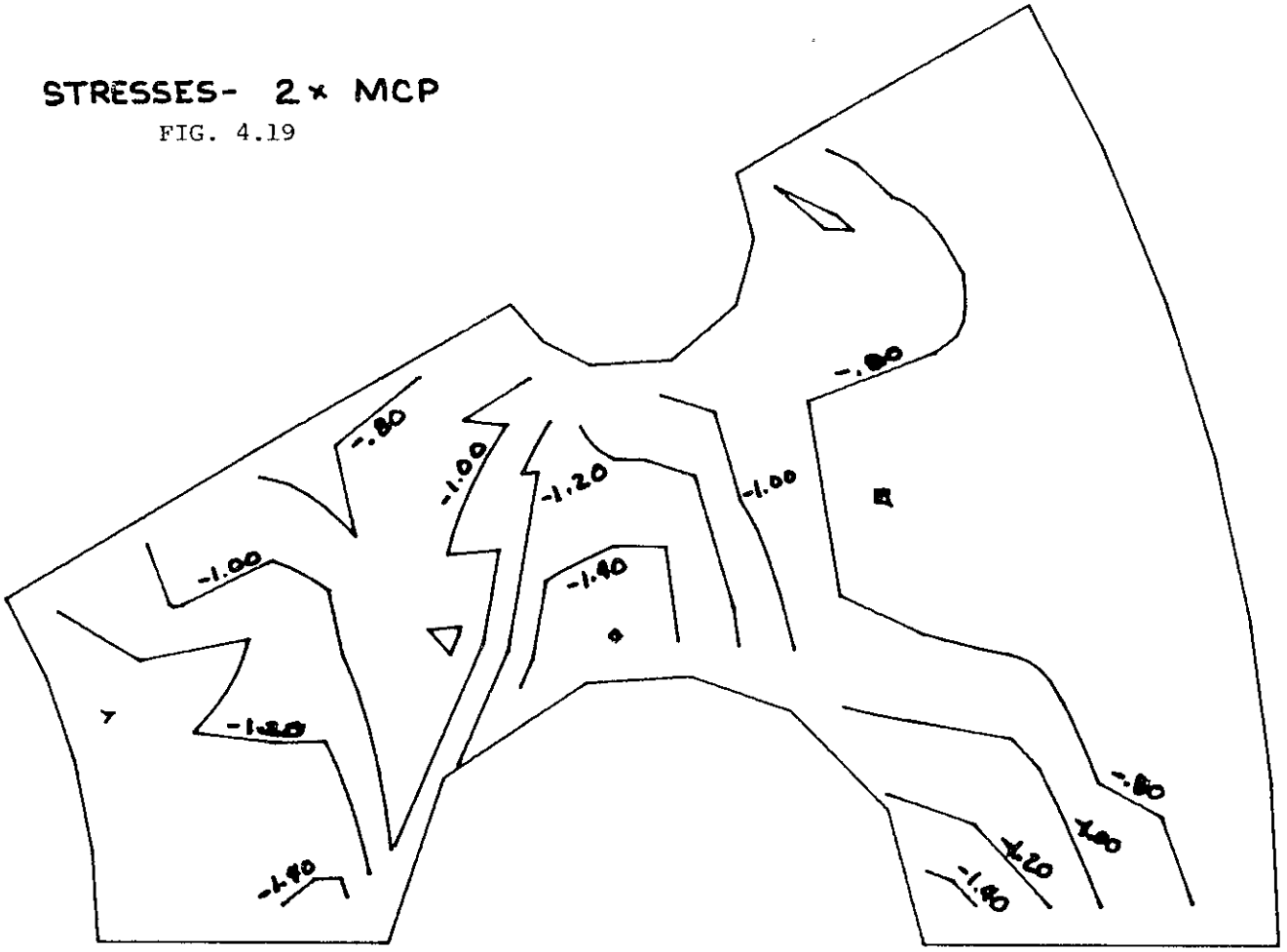

Chapter V

Conclusion

The high temperature gas cooled reactor with a prestressed concrete pressure vessel is the most recent nuclear system to evolve. Its many advantages over conventional types more than justifies the development. These vary from higher efficiency with lower operating cost to less pollution of the environment. One major disadvantage which must be evaluated before choosing this system is the high initial cost associated with it.

Pressure vessel configurations have progressed from the initial steel cylinders to the podded boiler prestressed concrete vessels of today. Analysis of the earlier vessels required simpler techniques because of their axisymmetric nature. Two dimensional finite element methods were capable of giving accurate results for the elastic conditions, but it was still necessary to use approximate techniques in determining the overpressure capacity.

The development of three dimensional mathematical methods has extended the analysis capability for nonaxisymmetric structures. Improved modeling of material properties and extensive testing of scale models have greatly increased the understanding of the behavior of the concrete pressure vessel.

At this time, the engineer is limited in improving the analysis and design of pressure vessels by the accuracy in modeling material behavior, the manpower and computer costs incurred in the analysis, and the size of available computers. Improvements in these areas will not only permit more

refined analyses using nonlinear finite element methods, but should also lead to simplified techniques for preliminary analysis.

References

[1] Argyris, J.H.; Buck, K.E.; and Scharpf, P.W. Linear Methods of Structural Analysis", First Structural Mechanics in Technology (SMIRT) Conference, 1971. Paper M2/1.

[2] Argyris, J.H.; Buck, K.E.; and Scharpf, P.W. "Nonlinear Methods of Structural Analysis", First SMIRT Conference, 1971. Paper M2/2.

[3] Argyris, J.H., et al. "Recent Developments in the Finite Element Analysis of Prestressed Concrete Reactor Vessels", University of Stuttgart, 1973.

[4] Argyris, J.H., et al. "Finite Element Ultimate Load Analysis of Three Dimensional Concrete Structure", University of Stuttgard, 1974.

[5] Argyris, J.H.; Pister, K.S.; and William, K.J. "Thermomechanical Creep of Aging Concrete -- A Unified Approach", University of Stuttgard, 1974.

[6] Barrett, N.T.; and Davidson, I., "Design Philosophy and Safety", Conference on PCPV, London, 1967. Paper #6.

[7] Brebbia, C.A.; and Connor, J.J. "Fundamentals of Finite Element Techniques, Butterworths, London, 1973.

[8] Boyer, U.S.; et al. "Fulton Station HTGR" Nuclear Engineering International, August, 1974.

[9] Brown, A.H.; and Darton, A.J. "The Oldbury Vessels", Conference on PCPV, London, 1967, Paper #1.

[10] Browne, R.D., "Properties of Concrete in Reactor Vessels", Conference on PCPV, London, 1967. Paper #13.

[11] Browne, R.D.; and Blundell, R. "The Behavior of Concrete in Prestressed Concrete Pressure Vessels", First SMIRT Conference, 1971. Paper H1/1.

[12] Brown, R.D.; Smith, J.R.; and Bamforth, P. "The Performance of the Wylfa Nuclear Pressure Vessel During Commissioning in Relation to Design Analysis, Second SMIRT Conference, 1973. Paper H4/4.

[13] Burrow, R.E.D.; and Crowder, R. "The Analysis of Prestressed Concrete Pressure Vessels with Wire Wound Prestress", Second SMIRT Conference, 1973. Paper H3/3.

[14] Cahill, T.; and Branch, G.O. "Long Term Relaxation Behavior of Stabilized Prestressing Wires and Strands", Conference on PCPV, London, 1967. Paper #19.

[15] Carlton, D.; Smith, J.R.; and Bellwood, G.N. "Prestressing and Proofpressure Testing of the Wylfa Prestressed Concrete Pressure Vessels and Comparison of Measured Data with Predicted Performance", First SMIRT Conference, 1971. Paper H4/2.

[16] Carmichael, G.D.T. "The Application of Three Dimensional Finite Elements to the Analysis of Podded Boiler Type Prestressed Concrete Pressure Vessels", Nuclear Engineering and Design, 16, 1971.

[17] Connor, J.J.; and Sarne, Y. "Lecture Notes on Finite Element Analysis of Physically Nonlinear Systems", International Symposium on Discrete Methods in Engineering, Milan, 1974.

[18] Davidson, I. "Theoretical and Experimental Modes of Behavior of Cylindrical Model Prestressed Concrete Pressure Vessels when Pressurized to Failure Hydraulically and Pneumatically", First SMIRT Conference, 1971. Paper H5/1.

[19] DerDecken, C.B. Von; and Schulten, R. "High Temperature Gas Cooled Reactor Development and its Mechanica-Structural Requirements and Problems, First SMIRT Conference, 1971. Paper B0/3.

[20] Eadie, E.McD. "The Behavior of the Oldbury No. 1 Reactor Pressure Vessel During Prestressing and Proof PressureTest," Nuclear Engineering and Design 5, 1967.

[21] Finigan, A. "Ultimate Analysis of the Dungeness B Vessel, Conference on PCPV, London, 1967. Paper #31.

[22] Fluge, F.; Gausol, E.; and Lenschow, R. "Inelastic Behavior and Failure Modes of Prestressed Concrete Vessels", Second SMIRT Conference, 1973. Paper H2/4.

[23] Garas, F.K.; and Crittenden, G.M. "The Problems in Designing for Complex Stress States in Prestressed Concrete Pressure Vessels with Particular Reference to Cylindrical End Slabs and Closures", Second SMIRT Conference, 1973. Paper H3/4.

[24] Gratton, C.P. "International Developments in Alternative Coolant Fast Breeder Reactors", American Power Conference, Chicago, IL, 1972.

[25] Greenbaum, G.A.; and Rubinstein, M.F. "Creep Analysis of Axisymmetric Bodies Using Finite Elements", Nuclear Engineering and Design 7, 1958.

[26] Gross, H. "On High Temperature Creep of Concrete", Second SMIRT Conference, 1973. Paper H6/5.

[27] Gulf Oil Corporation, "HTGR Highpoints", 1972.

[28] Hannant, D.J., "Strain Behavior of Concrete up to 95°C Under Compressive Stresses", Conference on PCPV, London, 1967. Paper #17.

[29] Harris, A.J.; and Hav, J.D. "Rupture Design of the Oldbury Vessels", Conference on PCPV, London, 1967. Paper #29.

[30] Harrop, J.; and Abdul-Wahab, H.M.S. "The Rigidity of Perforated Concrete Scabs", Nuclear Engineering and Design, 6, 1967.

[31] Hunsaker, B.; et al. "A Comparison of Current Work-Hardening Models Used in the Analysis of Plastic Deformations", Texas A & M University, 1973.

[32] Irving, J.; and Carmichael, G.D.T. "The Assessment of Bounds on Stresses in Prestressed Concrete Reactor Pressure Vessels, Second SMIRT Conference, 1973. Paper H3/2.

[33] Jaeger, T.A. "Discussion on Design and Structural Analysis of Prestressed Concrete Reactor Pressure Vessels",M.I.T., 1974.

[34] Kesler, L.E. "Control of Shrinkage, Creep, and Temperature Volume Changes Through Variations of Material Properties", International Conference on Planning and Design of Tall Buildings, Pennsylvania, 1972.

[35] Koerner, R.J., "A Simplified Overpressure Analysis of the Walls of a Cylindrical Pressure Vessel", Nuclear Engineering and Deseign, 14, 1970.

[36] Kuroda, T.; et al. "Pressure Tests of a 1/10 TH Scale Model", Journal of Japan Prestressed Concrete Engineering Association, 1974.

[37] Kuroda, T.; et al. "Experimental and Theoretical Study on a 1/10 TH Scale Model PCPV", Second SMIRT Conference, 1973. Paper H4/1.

[38] Lamiral, G.; et al. "Pressure Vessels for Electricite de France Nucluer Power Station", Conference on PCPV, London, 1967. Paper #4.

[39] Langan, D.; and Garas, F.K. "Behavior of End Slabs in Cylindrical Prestressed Concrete Pressure Vessels with Wire Wound Prestress, Second SMIRT Conference, 1973. Paper H3/4.

[40] Langan, D.; O'Flynn, M.; and Welch, A.K. "The Design of Pod Boiler Pressure Vessels with Particular Regerence to Hartlepool Nuclear Power Station, First SMIRT Conference, 1971. Paper H4/4.

[41] Lenschow, R. "An Investigation on a Prestressed Concrete Reactor Vessel Under Internal Gas Pressure -- Mode of Rupture", First SMIRT Conference, 1971, Paper H5/7.

[42] Lewis, D.J.; Bye, G.P.; and Crisp, R.J. "Longterm Thermal Creep Effects in Pressure Vessels", Conference on PCPV, London 1967, Paper #32.

[43] Lewis, D.J.; Irving, J.; and Carmichael, G.D.T. "Advances in the Analysis of Prestressed Concrete Pressure Vessels, First SMIRT Conference, 1971. Paper H3/1.

[44] Mikkola, J.J. and Schnobrich, W.C. "Material Behavior Characteristics for Reinforced Concrete Shells Stressed Beyond the Elastic Range", University of Illi-oi, 1970.

[45] Miller, D.R. and Landis, J.W. "The G.A. High Temperature Gas Cooled Reactor -- A General Discussion", Power Institute, Nuclear Power Workshop, California Polytechnic State University, San Luis Obispo, California, March, 1974.

[46] Neville, A.M. "Theories of Creep in Concrete, ACI, V. 27, No. 1, September, 1955.

[47] Page, R.W. and Read, D.T. "High Temperature Gas Cooled Reactor Development outside the United States -- A Consultant's View", American Power Conference, Chicago, IL, May 1973.

[48] Paul, S.L. "Structural Behavior of Prestressed Concrete Reactor Vessels", Proceedings ASCE Structural Division, July, 1971.

[49] Popov, E.P. "Introduction to Mechanics of Solids", Prentice-Hall, Inc., 1968.

[50] Rashid, Y.R., Rockenhauser,E.P."Pressure Vessel Analysis by Finite Element Techniques", Conference on PCPV, London, 1967, Paper #37.

[51] Rashid, Y.R. "Structural Analysis of Prestressed Concrete Reactor Vessels -- Atate of the Art", General Atomic, 1968.

[52] Rashid, Y.R. "Analysis of Axisymmetric Composite Structures by the Finite Element Method", Nuclear Engineering and Design, 3, 1966.

[53] Rashid, Y.R. "Ultimate Strength Analysis of Prestressed Concrete Pressure Vessels, Nuclear Engineering and Design, 7, 1968.

[54] Rockenhauser; Eszterger, E.P.; and Northrup, J.E. "Design Criteria for Prestressed Concrete Nuclear Reactor Vessels", General Atomic, 1968.

[55] Sarne, Y. "Material Nonlinear Time Dependent Three Dimensional Finite Element Analysis for Reinforced and Prestressed Concrete Structures", Ph.D. Thesis, M.I.T., 1974.

[56] Sarne, Y. "Applications of the Finite Element Technique to R/C Nuclear Containment Design", Master's Thesis, M.I.T., 1972.

[57] Saugy, B.; and Zimmerman, T.H. "The Finite Element Method Applied to Massive Heterogeneous Structures, Second SMIRT Conference, 1973. Paper H2/5.

[58] Saugy, B.; Zimmerman, T.H.; and Hussain, M. "Three Dimensional Rupture Analysis of a Prestressed Concrete Pressure Vessel Including Creep", First SMIRT Conference, 1971. Paper H3/5.

[59] Stefanov, G.D.; Yu, C.W.; and England, G.E. "Two Dimensional Time-Dependent Analysis of Perforated End Caps for Nuclear Reactor Pressure Vessels by the Finite Element Method", First SMIRT Conference, 1971. Paper H3/5.

[60] Stone & Webster Engineering Corp. "High Temperature Gas-Cooled Reactor, Basic Power Plant Systems", Boston, 1974.

[61] Taylor, R.W. "The Wylfa Vessels", Conference on PCPV, London, 1967. Paper #1.

[62] Thorp, D.E. "Elastic Analysis of the Dungeness B Vessel",Conference on PCPV, London, 1967. Paper #36.

[63] Tsuboi, Y.; et al. "Gypsum Concrete Models for Failure Tests of PCPV", First SMIRT Conference, 1971. Paper H5/9.

[64] Warner, P.C. "The Dungeness B Vessels", Conference on PCPV, London, 1967, Paper #3.

[65] William, K.J. and Warnke, E.P. "Constitutive Model for the Triaxial Behavior of Concrete, University of Stuttgart, 1974.

[66] Zbirohowski-Koslia, K. and Carlton, D. "Analysis of Vessel Structures with Particular Reference to Wylfa", Conference on PCPV, London, 1967. Paper #30.

[67] Zeller, A.Z. and Crump, A.R. "Mathematical and Computer Techniques Used in the Oldbury Vessels" Conference on PCPV, London, 1967. Paper #28.

[68] Zienkiewicz, O.C. "Analysis of Visco-Elastic Behavior of Concrete Structures with Particular Reference to Thermal Stresses", ACI Proceedings, V. 50, No. 4, 1961.

[69] Zienkiewicz , O.C.; et al. "Finite Element Methods in the Analysis of Reactor Vessels, First SMIRT Conference, 1971. Paper M5/1.

[70] Zienkiewicz , O.C.; Watson, M.; and Cheung, Y.K. "Stress Analysis By the Finite Element Method -- Thermal Effects", Conference on PCPV, London, 1967. Paper #35.

[71] Zienkiewicz , O.C.; Watson, M.; and King, I.P. "A Numerical Method of Visco-Elastic Stress Analysis",Int. J. Mech. Sci., V. 10, 1968.

[72] Ft. St. Vrain Nuclear Generating Station, "Final Safety Analysis Report

List of Figures